Exploring the Dark Universe with Cosmic Microwave Background and Optical Data

A Dissertation presented

by

Mathew Syriac Madhavacheril

to

The Graduate School
in Partial Fulfillment of the
Requirements for the Degree of

Doctor of Philosophy

in

Physics

Stony Brook University

August 2016

Stony Brook University

The Graduate School

Mathew Syriac Madhavacheril

We, the dissertation committee for the above candidate for the
Doctor of Philosophy degree, hereby recommend
acceptance of this dissertation

Neelima Sehgal - Dissertation Advisor
Assistant Professor, Department of Physics and Astronomy, Stony Brook University

Alan Calder - Chairperson of Defense
Associate Professor, Department of Physics and Astronomy, Stony Brook University

Fred Walter
Professor, Department of Physics and Astronomy

Patrick Meade
Associate Professor, C.N. Yang Institute for Theoretical Physics, Stony Brook University

Nikhil Padmanabhan
Associate Professor, Department of Physics, Yale University

This dissertation is accepted by the Graduate School

Charles Taber
Dean of the Graduate School

Abstract of the Dissertation

Exploring the Dark Universe with Cosmic Microwave Background and Optical Data

by

Mathew Syriac Madhavacheril

Doctor of Philosophy

in

Physics

Stony Brook University

2016

Over the past two decades, a standard cosmological model has emerged that supports the picture of an expanding Universe dominated by dark matter and dark energy. Understanding the nature of the dark Universe is a major open problem in cosmology. The work described in this dissertation advances our understanding of the dark Universe by first constraining the properties of dark matter through the effect of annihilations on the cosmic microwave background (CMB), and then by mapping dark matter via gravitational lensing as a way of constraining dark energy. By making the first measurement of gravitational lensing of the CMB by dark matter halos and the first measurement of the ratio of this signal to the lensing signal from optical data, this dissertation develops new techniques to map dark matter and constrain the properties of dark energy.

We first investigate the particle properties of dark matter by examining its effect on fluctuations in the CMB, thereby setting the tightest constraints on the annihi-

lation cross-section and mass of dark matter particles from the CMB. The rest of the thesis focuses on gravitational lensing, the phenomenon by which photons from a background source are deflected by the gravitational interaction with intervening matter as the photons travel to us. We explore how dark matter can be mapped by measuring the lensing distortions in shapes of galaxies, and develop a general formalism for unbiased estimators particularly suitable for measurements of correlation functions when the lensing distortion varies across the sky. Next, using CMB maps from the Atacama Cosmology Telescope, we make the first measurement of lensing of the CMB by dark matter halos. This detection opens up a new way of measuring masses of dark matter halos, a crucial step in constraining dark energy through its effect on the growth of structure over cosmic time. Dark energy also affects the expansion history of the Universe and leaves an imprint on the relationship between cosmic distances and redshifts. For our final chapter, we perform the first measurement that compares the lensing signal of dark matter halos using sources at two very different distances, the CMB (redshift ~ 1000) and background galaxies (redshift ~ 1), thus obtaining a purely geometric distance ratio that can be used to constrain dark energy.

For PVT

Contents

Acknowledgments

> People assume that time is a strict progression of cause to effect, but actually — from a non-linear, non-subjective viewpoint — it's more like a big ball of wibbly-wobbly... timey-wimey... stuff.
>
> *The Doctor*

In the big ball of wibbly-wobbliness that is our strange Universe, I've had the pleasure of meeting some wonderful people who made this dissertation possible and helped me grow as a person while it was being written.

I want to thank Joe and Lindsey for being the closest I had to family in this country. Life here in Stony Brook wouldn't haven't been the same without Abhi, Mike, Zoya, Naveen, Bertus and Nush, and all the fiery political discussions and arguments; they know how I like a good argument. Rahul, Missy, Mel and Max made the Astro offices a bright and fun place to work and put up with my caffeine-fueled weirdness. I'm grateful to all of them.

I am especially grateful to my dissertation advisor, Neelima Sehgal, from whom I learned the most. She kept me on my toes and taught me to balance being creative with being practical. Every meeting I've had with Anže Slosar left me more knowledgeable, more productive and more excited about cosmology than before. I also owe a great deal to Alexander van Engelen who I was lucky to have around in Stony Brook when I was just starting out and learning the ropes in cosmology.

Some of the happiest memories I have from my childhood are of my father patiently explaining to me, as best as he understood it, how a computer works, or what makes up the solar system. He is singularly responsible for sparking in me my desire to understand and explore the world we live in. I am immensely grateful to my parents for having supported what is otherwise an unconventional career path for where I come from, and to my brother and sister for keeping me motivated.

This dissertation is dedicated to the memory of my high school physics teacher, P.V. Thomas, who passed away earlier this year. His students affectionately called him PVT after the thermodynamic variables he taught us about. PVT's passion for physics was contagious, and he pushed me to consider a career in research, a decision I've never regretted since.

Publications

1. H. Miyatake, M. Madhavacheril, N. Sehgal, A. Slosar, D. Spergel, B. Sherwin, A. van Engelen **"Measurement of a Cosmographic Distance Ratio with Galaxy and CMB Lensing"**, submitted to Physical Review Letters, arXiv:1605.05337

2. M. Madhavacheril, N. Sehgal for the ACT Collaboration, **"Evidence of Lensing of the Cosmic Microwave Background by Dark Matter Halos"**, Physical Review Letters (2015), doi:10.1103 / PhysRevLett.114.151302, arxiv:1411.7999

3. M. Madhavacheril, P. McDonald, N. Sehgal, A. Slosar, **"Building Unbiased Estimators from Non-Gaussian Likelihoods with Application to Shear Estimation"**, Journal of Cosmology and Astroparticle Phys ics (2014), doi:10.1088/1475-7516/2015/01/022, arxiv:1407.1906

4. M. Madhavacheril, N. Sehgal, T. Slatyer, **"Current Dark Matter Annihilation Constraints from CMB and Low-Redshift Data"**, Physical Review D (2014), doi:10.1103/PhysRevD.89.103508, arxiv:1310.3815

Chapter 1

Introduction

Increasingly precise observations over the last few decades show that ordinary matter comprises only about 5% of the energy density of the Universe. Non-baryonic 'dark matter' that does not interact through the electromagnetic force is required to explain a variety of observations including galaxy rotation curves [1–3], X-ray emission from hot gas in galaxy clusters [4, 5], gravitational lensing distortions around galaxy clusters [6], and acoustic peaks in the power spectrum of the cosmic microwave background (CMB) [7, 8]. In addition, distance-redshift measurements using Type Ia supernovae indicate that the expansion of the Universe is accelerating [9, 10], requiring a substantial 'dark energy' component [11], a fact that was subsequently corroborated through combinations of measurements of the CMB power spectra and the abundance of galaxy clusters [12]. The CMB alone, as measured today, provides the strongest evidence for dark matter from the ratio of the second and third acoustic peaks. In addition, the CMB alone provides evidence for dark energy when both the primary power spectrum and CMB lensing signal are combined [13]. A standard model of cosmology that includes dark energy through a cosmological constant Λ and cold dark matter (CDM) has emerged, and is supported by an array of concordant cosmological data-sets that include the CMB and its secondary observables [14], large-scale structure measurements through the distribution of galaxies [15], weak lensing measurements of the distortions in the shapes of galaxies [16] and cosmic distance ladder measurements utilizing Type Ia supernovae [17]. However, the concordance model does not yet tell us what the particle nature of dark matter is and leaves open many possible explanations of the acceleration of the Universe beyond a cosmological constant, such as quintessence models [18] or modifications of General Relativity [19]. Identifying the precise nature of dark matter and dark energy are two of the most important open problems in cosmology today.

The Cosmic Microwave Background

Two valuable tools for learning about the dark Universe are the CMB, and optical measurements of galaxies. The CMB consists of photons that for the most part have not interacted with matter since the epoch of recombination, when the Universe had cooled enough for protons and electrons to form neutral atoms [20]. The first measurements [21, 22] of this 2.7 Kelvin background confirmed the hot, dense past predicted in the model of an expanding Universe. Subsequent measurements of the black-body spectrum and anisotropies in the CMB temperature at a level of 1 part in 10^5 by the COBE satellite [23, 24] provided a snapshot of the fluctuations in the distribution of radiation when the Universe was 380,000 years old.

The power spectrum of the CMB temperature fluctuations (which characterizes the amplitude of the fluctuations as a function of scale) has since then been measured to unprecedented accuracy by the WMAP [25] and Planck [26] satellites, ground-based experiments including the Atacama Cosmology Telescope (ACT) [27] and the South Pole Telescope (SPT) [28], and various balloon-borne experiments (e.g., [29, 30]). These measurements strongly indicate that the early Universe went through an inflationary epoch that seeded nearly scale-invariant Gaussian random fluctuations in the matter distribution. The fact that the third peak in the acoustic oscillations of the CMB power spectrum is of comparable height to the second peak indicates that a large fraction of the matter density consists of highly non-relativistic 'cold' dark matter (CDM) that does not interact with itself or other particles other than through the gravitational force. Tight constraints have been obtained on the properties of the primordial fluctuations, the curvature of the Universe, and the fraction of energy density in baryons and CDM through these measurements. The CMB is polarized at the few-micro-Kelvin level because of Thomson scattering of photons off free electrons [31]; measurements of the corresponding polarization anisotropies and temperature-polarization correlation [25, 26, 32–34] are crucial for removing the degeneracy of the temperature power spectrum with the reionization history of the Universe and improving the precision on cosmological parameters [35].

Probing Dark Matter Properties with the CMB

It is possible to use the CMB temperature and polarization power spectra to probe the physics of dark matter particles beyond the standard CDM picture. The dominant paradigm for the particle nature of dark matter is that it consists of weakly interacting massive particles (WIMPs) [36]. At high temperatures and early times, the self-annihilation rate of dark matter particles is much greater than the expansion rate keeping their annihilations in equilibrium. If annihilations indefinitely continued to be in equilibrium, the abundance of dark matter particles would be suppressed exponentially. However, as the Universe expands and cools, annihilations become much less efficient; the time between annihilations becomes comparable to the Hubble time effectively causing the dark matter abundance to 'freeze-out'. The relic abundance that is left behind depends on the annihilation cross-section. It is a fact that the cross-section required for the relic abundance of dark matter to match what is observed today (around 30% of the total energy density) is roughly what would be expected for particles with mass of order 100 GeV interacting through the weak nuclear force [37]. For this reason, there is great interest in detecting WIMPs as possible dark matter candidates through collider experiments like the Large Hadron Collider (e.g., [38]), through direct detection of scattering of WIMPs off heavy nuclei [39–42] and indirect detection through Standard Model products of dark matter annihilation in regions of high dark matter density such as the galactic center [43–45] or dwarf galaxies [46, 47]. Previous studies [48–52] have shown that dark matter annihilating at redshifts of around 1000 injects energy into the plasma and modifies recombination physics so as to have observable consequences in the CMB power spectra: a suppression of power in temperature and polarization fluctuations at small scales and an enhancement of power in polarization fluctuations at large scales. This allows the CMB to be used as a powerful complementary indirect detection probe of the particle nature of dark matter. The CMB also has the advantage of being free of uncertainties such as astrophysical backgrounds of high-energy particles or the local distribution of dark matter. In Chapter II, we examine the effect that annihilating dark matter would have on the physics of recombination and how this modifies the power spectrum of CMB temperature and polarization. We study the improvement in constraining power that can be obtained by measuring large-scale polarization of the CMB and set the tightest constraints on annihilating dark matter from Planck 2013 temperature, WMAP, ACT and SPT data, and several low-redshift datasets.

CMB Secondaries for Growth of Structure Measurements

The CMB also contains several 'secondary' signals (on top of the primordial anisotropy signal) that in combination with other probes can be used to understand the nature of dark energy and differentiate it from possible modifications of General Relativity. As the Universe expands, fluctuations in the matter distribution grow as matter collapses under gravity (see [53]). On their journey from the surface of last scattering to us, CMB photons occasionally interact with baryonic matter or get deflected by the gravitational pull of dark matter along the line of sight and thus pick up information about the evolution of matter fluctuations. Two important CMB secondary signals are the thermal Sunyaev-Zeldovich (tSZ) effect [54] and gravitational lensing of the CMB [55].

The tSZ effect is the frequency shift of CMB photons that inverse-Compton scatter off hot ionized gas located in galaxy clusters. This locally distorts the blackbody spectrum of the CMB photons leading to a frequency-dependent signal in CMB maps at the location of galaxy clusters. The tSZ signal is thus useful for identifying the locations of massive galaxy clusters in a way that is independent of redshift, making it the best method for detecting high-redshift galaxy clusters. Since galaxy clusters are among the largest structures in the Universe, the abundance of clusters as a function of redshift (or cosmic time) gives us a direct handle on the growth of matter fluctuations on large scales. Non-standard dark energy models with an equation of state different from $p = -\rho$ will have an identifiable effect on the growth rate measured this way.

It is also possible that the observed cosmic acceleration is due to a modification of General Relativity, rather than a dark energy component affecting the background expansion. If this were the case, growth of structure measurements could yield cosmological parameters which disagree with those inferred from expansion probes such as supernovae and baryon acoustic oscillations (BAO) [56]. Measuring the growth of structure is therefore a critical complement to expansion rate probes of dark energy.

CMB photons are also deflected as they pass through the curved spacetime around matter along the line of sight. Numerous measurements of this CMB 'gravitational lensing' effect have been made, first in cross-correlation [57] and subsequently internally by ACT [58], SPT [59, 60], Planck [61, 62], PolarBear [63] and BICEP [64]. The lensing maps made for these results measure the projected matter density over a very broad range of redshifts peaking at $z \sim 2$ and are sensitive to the large-scale distribution of matter. Only very recently have CMB experiments reached the resolution and sensitivity to yield lensing maps sensitive to the dark matter halos hosting galaxy groups and clusters, with first measurements presented by ACTPol (work included in this thesis) [65], SPT [66] and Planck [67]. These high resolution measurements provide a way of measuring the dark matter mass associated with galaxy clusters detected via the tSZ effect. While galaxy lensing, discussed below, can also be used for measuring masses of clusters, CMB lensing provides a complementary measurement at low and intermediate redshifts, and will be indispensable for high-redshift clusters which simply do not have enough background galaxies for a useful mass estimate. CMB lensing also has different systematic effects than galaxy lensing, allowing for robust measurements when taken in combination. This would yield a powerful growth of structure measurement. In Chapter IV, we analyze data from the ACTPol experiment and present the first measurement of CMB lensing by dark matter halos, opening up this new method of measuring the masses of dark matter halos.

Galaxy Shear for Growth of Structure Measurements

The distribution and properties of galaxies also contain a wealth of information about the dark Universe. The positions of galaxies trace the distribution of dark matter since both baryons and CDM populate the same gravitational potentials. However, since galaxies form preferentially at the peaks of the dark matter distribution, an estimate of the total dark matter distribution made solely using galaxy positions is inherently biased. Gravitational lensing of galaxies provides a way to measure the true matter distribution. Light from background galaxies is deflected as it travels through the gravitational potential of foreground matter. The typical deflections are small; for example, for a typical elliptical galaxy and cosmological line of sight, the ellipticity is 'sheared' by around 2%. Because of the wide dispersion in the intrinsic ellipticities of galaxies, galaxy shear can only be measured statistically over ensembles of galaxies. This optical 'weak lensing' effect was first detected [68, 69] as a tangential alignment of galaxies behind massive clusters; a method actively used now for measuring the masses of galaxy clusters discussed earlier. Measuring 'cosmic shear', the correlations induced in shapes of galaxies by large-scale structure in blind fields, is more challenging, but has the potential for mapping out dark matter with great precision due to the large number of galaxies available. First measurements of cosmic shear [70–73] have been improved upon by dedicated optical imaging surveys such as CFHTLens [74] and DES [75] and new results are expected from DES, HSC [76], KiDS [77] and RCSLens [78]. Future surveys like LSST [79], Euclid [80] and WFIRST [81] expect to image of order a billion objects across a large fraction of the sky. At this level of statistical precision, control of systematic errors becomes of paramount importance. Because the galaxy ellipticity is related to the quadrople moments of an image, and the moments are a non-linear function of the intensity of a galaxy image, noise in the image can bias the inferred shear [82]. Galaxies, of course, are never perfectly intrinsically elliptical, so any attempt at reducing the shearing effect into a finite set of numbers (in the simplest case, two ellipticity parameters) will introduce a model bias [83]. Selection effects (for example, rejection of blended objects [84]) also introduce additional bias. Mitigating these biases through analytical techniques (e.g., [85]), calibration against simulations [86], and calibration using cross-correlations with CMB lensing maps [87–90] are all active areas of research.

In Chapter III, we focus on the estimation of galaxy shears. We develop a general formalism for unbiased shear estimators particularly suitable for measurements of correlation functions when the lensing shear varies across the sky.

Lensing Cross-correlations for Expansion Rate Measurements

Combining the information in CMB lensing and galaxy surveys through cross-correlations opens up multiple new avenues for constraining dark energy. The wide redshift kernel of the CMB lensing signal allows one to cross-correlate with tracers both at low and high ($z > 1$) redshifts making it especially suitable for mapping out dark matter as a function of cosmic time. While measurements involving foreground galaxy densities alone depend on an unknown galaxy bias, this dependence can be eliminated by combining CMB lensing with galaxy lensing, where both sources of background light are being lensed by the same dark matter distribution around dark matter halos.

These cross-correlations can be used to measure the expansion history, instead of mapping the dark matter distribution to measure growth. The magnitude of the lensing signal depends on the distances to the lens and the source. By comparing the lensing signal from the same set of dark matter halos for two different sources, one can extract a purely geometric distance ratio that strongly constrains cosmological parameters that affect the expansion history, like the dark energy equation of state, without being affected by systematics of modeling of the lensing matter distribution [91–93]. If the CMB is used as one of the background light sources, the sensitivity to dark energy parameters is maximal because of the long cosmic lever arm generated between the CMB at $z \sim 1000$ and galaxy shear at $z \sim 1$. While previous measurements have only used galaxy shears for such cosmographic distance ratios, in Chapter V, we present the first measurement of the ratio of the galaxy lensing signal to the CMB lensing signal where both have been lensed by the same dark matter halos. This ratio cancels out the dark matter distribution itself leaving only a purely geometric distance measurement that can constrain dark energy through its effect on the expansion history.

Chapter 2

Probing Dark Matter Properties with the CMB [1]

Non-baryonic matter is a crucial ingredient in our current understanding of the cosmological history of the Universe. A significant fraction of the energy density of the Universe is contended to consist of 'dark matter' that interacts only very weakly (if at all) with ordinary matter. Dark matter is needed to explain numerous observations including gravitational lensing by clusters and galaxies, galaxy rotation curves, acoustic peaks in the power spectrum of the cosmic microwave background (CMB), and the growth of large-scale structure. However, all of the widely accepted evidence for dark matter is sensitive only to its gravitational effects, and the determination of its particle nature is an important open problem. Current efforts to address this can broadly be divided into (i) indirect detection experiments that aim to detect

[1] This chapter is a near-verbatim reproduction of [94], which has appeared in print in *Physical Review D*, and is titled "Current dark matter annihilation constraints from CMB and low-redshift data".

the products of dark matter annihilation or decay, (ii) direct detection experiments that attempt to detect dark matter particles via their recoil off heavy nuclei, and (iii) collider experiments where dark matter particles are hoped to be identified in the products of high-energy collisions.

One particular indirect detection method is to observe the effect of dark matter annihilation early in the history of the Universe ($1400 > z > 100$) on the CMB temperature and polarization anisotropies [48–52, 95–100]. If dark-matter particles self-annihilate at a sufficient rate, the expected signal would be directly sensitive to the thermally averaged cross section $\langle \sigma v \rangle$ of the dark matter particles in this epoch, the mass M_χ of the annihilating particle, and the particular annihilation channel. An advantage of this indirect detection method over more local probes is that it is free of astrophysical uncertainties such as the local dark matter distribution and the astrophysical background of high-energy particles. In Section 2.1, we review the physics behind the modification of the CMB power spectra by annihilating dark matter. We also discuss the universal energy deposition curve and systematic corrections to it as in [97], and the leverage in multipole-space of the dark matter constraints. Updated constraints including all available data are presented in Section 2.2. In Section 2.3, we discuss these results in light of recent data from other indirect and direct dark matter searches.

2.1 Effect of Dark Matter Annihilation on the CMB

The recombination history of the Universe could potentially be modified by dark matter particles annihilating into Standard Model particles, which in turn inject energy into the (pre-recombination) photon-baryon plasma and (post-recombination) gas and background radiation. Previous authors [48–52] have considered the effects of this energy injection, which broadly consist of (i) increased ionization of the gas, (ii) atomic excitation of the gas, and (iii) plasma/gas heating. These processes in turn lead to an increase in the residual ionization fraction (x_e) and baryon temperature (T_b) after recombination. For rates of energy injection low enough that there is minimal shift in the positions of the first few peaks of the CMB temperature power spectrum, the primary effect of the energy injection is to broaden the surface of last scattering. This leads to an attenuation of the temperature and polarization power spectra that is most pronounced at small scales. In addition, the positions of the temperature-polarization cross-spectrum (TE) and polarization auto-spectrum (EE) peaks shift, and the power of polarization fluctuations at large scales ($l < 500$) increases as the thickness of the last scattering surface grows. (See Figure 4 in [48] for a depiction of this effect.)

The rate of energy deposition per volume is given by,

$$\frac{dE}{dV\,dt} = \rho_c^2 c^2 \Omega_{\mathrm{DM}}^2 (1+z)^6 p_{\mathrm{ann}}(z) \tag{2.1}$$

$$p_{\mathrm{ann}}(z) = f(z) \frac{\langle \sigma v \rangle}{M_\chi} \tag{2.2}$$

where ρ_c is the critical density of the Universe today, Ω_{DM} is the density of cold dark matter today, $\langle\sigma v\rangle$ is the thermally averaged cross section of self-annihilating dark matter, M_χ is the dark matter mass, and $f(z)$ is an $\mathcal{O}(1)$ redshift-dependent function that describes the fraction of energy that is absorbed by the CMB plasma. In this parametrization, $f(z)$ captures the redshift-dependence of the energy deposition not included in the $(1+z)^3$ evolution of the dark matter density. The exact functional form of $f(z)$ depends on the specific annihilation channel of dark matter – however, as discussed in [52] and in Section 2.1.1, the first principal component formed from the $f(z)$ energy deposition curves of 41 representative dark matter models accounts for more than 99.9% of the variance in the CMB power spectra that is not degenerate with other standard cosmological parameters. The injected energy modifies the evolution of the ionization fraction, x_e, according to

$$\frac{dx_e}{dz} = \frac{1}{(1+z)H(z)}[R_s(z) - I_s(z) - I_X(z)] \tag{2.3}$$

where $R_s(z)$ and $I_s(z)$ are the standard recombination and ionization rates, respectively, in the absence of dark matter annihilation, $I_X(z)$ is the modification to ionization due to dark matter annihilation, and $H(z)$ is the Hubble constant at redshift z. Standard recombination, as discussed in [101], is described by

$$[R_s(z) - I_s(z)] = C \times [x_e^2 n_H \alpha_B - \beta_B(1-x_e)e^{-h_P\nu_{2s}/k_B T_b}] \tag{2.4}$$

where the C-factor is given by

$$C = \frac{[1 + K\Lambda_{2s1s} n_H (1 - x_e)]}{[1 + K\Lambda_{2s1s} n_H (1 - x_e) + K\beta_B n_H (1 - x_e)]} \tag{2.5}$$

Here, n_H is the hydrogen number density, T_b is the baryon gas temperature, α_B and β_B are the effective recombination and photoionization rates respectively for $n \geq 2$, ν_{2s} is the change in frequency from the $2s$ level to the ground state, Λ_{2s1s} is the decay rate of the metastable $2s$ level to $1s$, $K = \lambda_\alpha^3/(8\pi H(z))$, and λ_α is the wavelength of the Lyman-α transition from $n = 2$ to $n = 1$. This C-factor is approximately the probability that a hydrogen atom in the excited $n = 2$ state will decay by two-photon emission to the $n = 1$ state before being photodissociated [101].

Several authors have considered adding generic terms to the recombination equations, denoted by

$$I_X(z) = I_{Xi}(z) + I_{X\alpha}(z), \tag{2.6}$$

that account for additional ionization from the ground state and from the $n = 2$ state after energy injection [49, 102, 103]. Dark matter annihilation increases the ionization fraction through (i) direct ionization of hydrogen atoms from the ground state ($I_{Xi}(z)$), and (ii) ionization from the $n = 2$ state after hydrogen has been excited by Lyman-α photons produced by dark matter annihilation ($I_{X\alpha}(z)$).Following [51], the rate of additional ionization from the ground state is given by

$$I_{Xi} = \chi_i \frac{[dE/dV\,dt]}{n_H(z) E_i} \tag{2.7}$$

where E_i is the average ionization energy per baryon (13.6 eV), and χ_i is the fraction of absorbed energy that goes directly into ionization.

The term describing ionization from the $n = 2$ state is given by

$$I_{X\alpha} = (1 - C)\chi_\alpha \frac{[dE/dV\,dt]}{n_H(z)E_\alpha} \tag{2.8}$$

where χ_α is the fraction of absorbed energy that goes into excitation, E_α is the difference in binding energy between the $n = 1$ and $n = 2$ levels (10.2 eV), and $(1-C)$ is the probability of not decaying to the $n = 1$ state before being photoionized from the $n = 2$ state.

In addition, the baryon temperature evolution is modified by the last term in

$$\begin{aligned}(1+z)\frac{dT_b}{dz} = \frac{8\sigma_T a_R T_{\rm CMB}^4}{3m_e c H(z)} \frac{x_e}{1+f_{\rm He}+x_e}(T_b - T_{\rm CMB}) \\ + 2T_b - \frac{2}{3k_B H(z)}\frac{K_h}{1+f_{\rm He}+x_e}\end{aligned} \tag{2.9}$$

where $f_{\rm He}$ is the Helium fraction and

$$K_h = \chi_h \frac{[dE/dV\,dt]}{n_H(z)}. \tag{2.10}$$

Here, χ_h is the absorbed energy converted to heat. The energy fractions (χ_i, χ_α, and χ_h) are discussed further in Section 2.1.1.

2.1.1 Universal Energy Deposition Curve with Systematic Corrections

Many earlier studies of the impact of DM annihilation on recombination (e.g. [48, 49, 51, 52, 98, 100, 104–106]) have used an approximate form for the energy fractions χ_i, χ_α, and χ_h, derived from Monte Carlo studies by Shull and van Steenberg in 1985 [107], and following the approximate fit suggested in [108]:

$$\begin{aligned}\chi_i &= \chi_e = \frac{(1 - x_{\rm H})}{3} \\ \chi_h &= \frac{1 + 2x_{\rm H} + f_{\rm He}(1 + 2x_{\rm He})}{3(1 + f_{\rm He})}.\end{aligned} \tag{2.11}$$

Here χ_i is the hydrogen ionization fraction, χ_e is the hydrogen excitation fraction, and χ_h is the heating fraction. The Lyman-α contribution, χ_α, is some fraction of χ_e. Some past studies have taken $\chi_\alpha = 0$ to obtain conservative constraints, while others, including this work, set $\chi_\alpha = \chi_e$. The helium fraction $f_{\rm He}$ is given by $f_{\rm He} = Y_p/(4(1 - Y_p))$, where Y_p is the helium mass fraction. The ratio of ionized hydrogen to total hydrogen is given by $x_{\rm H}$, and the ratio of ionized helium to total helium is given by $x_{\rm He}$. In this work, we do not include ionization of helium due to dark matter annihilations since it has a negligible impact on the CMB power spectra [97, 106].

In reality, the dependence of the energy fractions on the background ionization fraction $x_{\rm H}$ is more complex than the simple linear dependence in Eq. 2.11. The energy fractions also possess a non-trivial dependence on the energy of the electron when it is "deposited" to the plasma (i.e. when its energy drops to the point where all subsequent cooling processes have timescales much faster than a Hubble time). In previous work (e.g. [50]), “deposited” photons with energies above 13.6 eV were treated exactly as deposited electrons, under the presumption that such photons would quickly ionize the gas, producing a free electron. While this is true, it is important to also account for the energy absorbed in the ionization itself. The free electron produced by photoionization will then deposit its energy subject to the appropriate energy fractions.

In this work we take these effects into account following the method described in detail in [97]; our results use the same set of assumptions as that paper's “best estimate” constraints. Electrons, positrons, and photons injected by DM annihilation are tracked down to a deposition scale of 3 keV, taking the expansion of the universe into account, using an improved version of the code first described in [50]. The spectra of photons and electrons below this energy are stored – many of the energy-loss processes are discrete rather than continuous, and thus these spectra are not simply spikes at the deposition scale – and then integrated over energy-dependent energy loss fractions computed by Monte Carlo methods, following [109–112]. This part of the code does not take redshifting into account, but at energies below 3 keV all cooling times are much faster than a Hubble time (with the notable exception of photons below 10.2 eV after the redshift of last scattering), so the expansion can be neglected. Energy losses to direct ionization, excitation, and heating by electrons and photons above the 3 keV threshold are calculated in the “high-energy” code (appropriate to energies above 3 keV) and added to the corresponding fractions. “Continuum” (below 10.2 eV) and Lyman-alpha photons produced by inverse Compton scattering

(ICS) of electrons above 3 keV are likewise calculated in the high-energy code; for electrons below 3 keV, ICS quickly becomes subdominant to atomic energy loss processes. Ionizations on helium are taken into account following [97].

The primary difference between the results of this method and earlier approximations is that the correct treatment of ICS by non-relativistic electrons predicts greater energy transfer into continuum photons, which cannot subsequently induce ionizations or Lyman-alpha excitations; the effect can be regarded as a high-energy distortion to the CMB energy spectrum. Consequently, the fraction of power going into ionization, excitation, and heating of the gas is somewhat depressed. There is an exception at high redshifts, where accounting for the additional ionization from *photon*-gas interactions (which was not done in e.g. [50], which treated low-energy electrons and photons as identical) can outweigh the reduced ionization from electron-gas interactions, since the latter is very small in any treatment (those electrons lose their energy dominantly to Coulomb heating, using either the approximate fractions or the more accurate ones).

We have computed the fraction of deposited energy going into ionization, χ_i, which largely controls the constraints (the Lyman-alpha fraction, χ_α, has a small, albeit not negligible, effect [97]), as a function of redshift, for each of the 41 annihilation channels described in [50]. The calculations of the energy fractions in [97] separately compute the ionization on helium; here we simply sum the total power into ionization on hydrogen and helium to obtain the χ_i fraction, since as mentioned previously, the effects of separating the helium fraction are small. For convenience, given the widespread use of the approximate fractions of Eq. 2.11 in the literature and in existing code, for each annihilation channel we can define a new "effective $f(z)$ curve", $f_{\text{sys}}(z)$, which yields the correct power-into-ionization when multiplied by the *approximate* value of χ_i. That is,

$$\chi_i^{\text{approx}}(z) f_{\text{sys}}(z) = \chi_i^{\text{updated}}(z) f_{\text{old}}(z), \tag{2.12}$$

where χ_i^{approx} and χ_i^{updated} are respectively the approximate (Eq. 2.11) and updated (following [97]) energy fractions, and $f_{\text{old}}(z)$ agrees with the results of [50]. (Note that in some cases this definition can lead to a very large value of $f_{\text{sys}}(z)$, much greater than 1, where $\chi_i^{\text{approx}}(z) \ll \chi_i^{\text{updated}}(z)$.) This curve should not generally be applied to compute the heating and Lyman-α components, in cases where they are important; it is designed to correctly normalize the power into ionization. However, since we expect the effect of additional ionizations to dominate over the modification due to excitations or heating, we use the same $f_{\text{sys}}(z)$ curve for the ionization, excitation, and heating terms. We checked that using the $f_{\text{sys}}(z)$ curve to multiply the ionization term and the old $f(z)$ curve for the excitation and heating terms makes no appreciable difference to the constraints obtained below.

Having derived new individual $f_{\text{sys}}(z)$ curves for a range of Standard Model final states, we can perform a principal component analysis using these curves as basis vectors, as described in detail in [52]. The first principal component describes the direction in this space (of linear combinations of the $f_{\text{sys}}(z)$ curves), which captures the greatest amount of the variance in the CMB power spectra – in this case, over 99.9%. Physically, the effects of the different annihilation channels on the CMB anisotropy spectra are very similar.

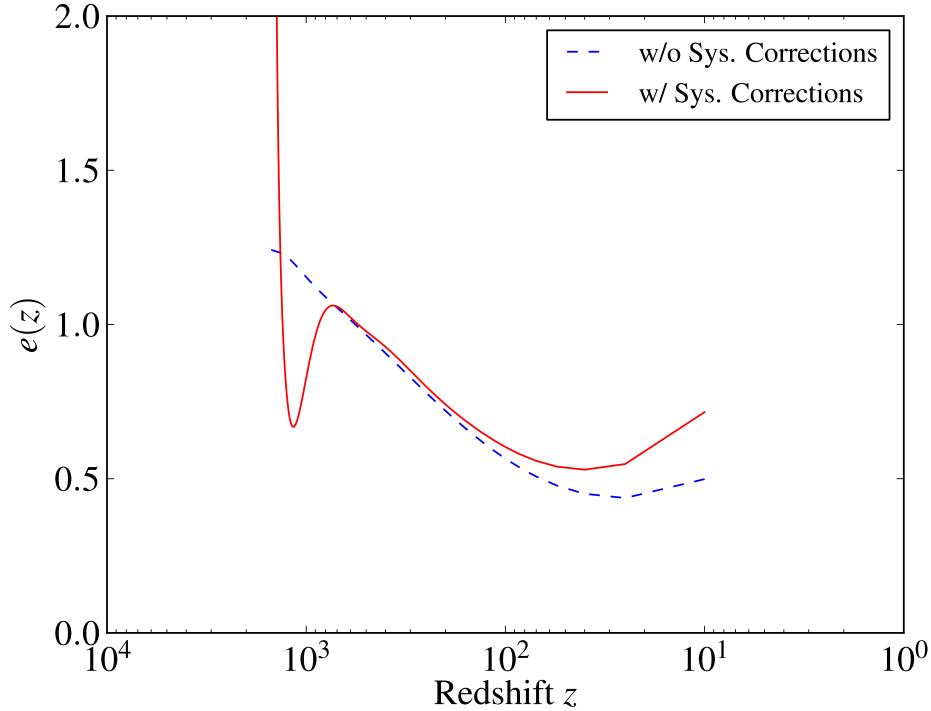

Figure 2.1: Universal energy deposition curve, $e(z)$, using approximations for the fraction of energy converted to heat, ionization, and excitation (dashed blue curve), and accounting for more accurate calculations of the energy fractions from [97] (solid red curve).

We show in Figure 2.1 the resulting first principal component as a function of redshift, which we refer to as the "universal" $e(z)$ curve. The overall normalization of the curve is arbitrary since it is precisely its amplitude that we wish to constrain, and hence a rescaling of $e(z)$ would be reflected in a proportional rescaling of the derived constraint on its coefficient. In order to fix the normalization, we adopt the convention used in [52], i.e., we fix the normalization such that if $p_{\rm ann}(z) = \epsilon\ e(z)$, the Fisher matrix constraint on ϵ is the same as that obtained for constant annihilation, $p_{\mathrm{ann}} = \epsilon$ (with approximate energy fractions), for some choice of experimental parameters. The advantage of this choice is that constraints on the coefficient of $e(z)$ can be directly compared to previously derived constraints using constant p_{ann}. In this work, the Fisher matrix computation and principal component analysis were performed for a Planck-like experiment in the range $\ell < 6000$; we have verified that performing the analysis instead for a cosmic variance limited (CVL) experiment in this ℓ range changes the shape and normalization of the $e(z)$ curve only at the sub-percent level. The principal components do not change appreciably when additional cosmological parameters that could be degenerate with the annihilation parameter are added. This is discussed in Appendix A5 of [52].

Note that this choice of normalization means that the $e(z)$ curve does not reflect the general reduction in amplitude of the $f_{\mathrm{sys}}(z)$ curves relative to the older $f(z)$ curves, arising from the fact that $\chi_i^{\mathrm{updated}}(z)$ is generally lower than $\chi_i^{\mathrm{approx}}(z)$. To the degree that the Fisher matrix approach is valid, we expect the constraint on the coefficient of the updated $e(z)$ curve to be identical to the corresponding bound for the older $e(z)$ curve presented in [52], since both should be equivalent to the constraint using constant p_{ann} and approximate energy fractions. However, constraints on specific *models* will change.

To translate from constraints on the coefficient of the $e(z)$ curve to constraints on a specific model, one must extract the coefficient of the first principal component, when the $f_{\mathrm{sys}}(z)$ curve for that model is expanded in the basis of principal components. This is referred to in [52] and [113] as taking a "dot product", but there is a subtlety here in that the dot product must be taken in the space defined by the 41 $f_{\text{sys}}(z)$ curves, not in the space of functions of z. In the Fisher matrix approach, this corresponds to taking the dot product between the (discretized) $f_{\text{sys}}(z)$ curve for that particular model and the vector $(e)^T F$, where e is the (discretized) universal $e(z)$ curve, and F is the marginalized Fisher matrix describing the effect on the CMB of energy depositions localized in redshift (see [52] for the precise construction). The dot product is normalized by dividing by the result where $f_{\text{sys}}(z)$ is replaced with $e(z)$, to obtain an "effective f" value $f_{\text{eff,new}}$:

$$f_{\text{eff,new}} = \frac{e(z) \cdot F \cdot f_{\text{sys}}(z)}{e(z) \cdot F \cdot e(z)}. \tag{2.13}$$

Below we present constraints on the dimensionful parameter ϵ, which we label as p_{ann} in Table 2.2 for ease of comparison with the constant p_{ann} case and general familiarity with that variable. In order to obtain a constraint on $\langle \sigma v \rangle / M_\chi$ for a specific DM model, the bound on p_{ann} should be divided by $f_{\text{eff,new}}$ for that model since

$$p_{\text{ann}} = f_{\text{eff,new}} \frac{\langle \sigma v \rangle}{M_\chi}. \tag{2.14}$$

(By definition, if $f_{\text{sys}}(z) = e(z)$, then $f_{\text{eff,new}} = 1$; the derived constraint on p_{ann} is exactly the constraint on $\langle \sigma v \rangle / M_\chi$ for such a model.) We have verified that this prescription accurately reproduces the constraints presented for individual leptonic annihilation channels in [97]. The fact that the $f_{\text{sys}}(z)$ curves are generally lower than the original $f(z)$ curves is reflected in lower $f_{\text{eff,new}}$ values, and hence weaker constraints on $\langle \sigma v \rangle / M_\chi$.

In Table 2.3, we provide both the $f_{\rm eff,new}$ values computed using our new $f_{\rm sys}(z)$ curves, and the $f_{\rm eff}$ values computed using the old $f(z)$ curves from [50], but using the correct Fisher-matrix weighting described in the previous paragraph (these values were computed in an online supplement to [52], but the dot product was not properly weighted by the Fisher matrix, leading to few-percent deviations).

2.1.2 Leverage in ℓ-space of Dark Matter Limits

The primary effects of dark matter annihilation on the CMB power spectra are an attenuation of power in both temperature and polarization especially at high-l, an enhancement of low-l polarization power, and low-l polarization peak shifts. Since a number of cosmological parameters result in an attenuation of power at high-l (e.g. n_s), one would expect most of the constraining leverage on dark matter limits to come from the low-l TE and EE spectra, which break parameter degeneracies. To demonstrate the importance of low-l polarization on improving constraints, we use Fisher forecasts to project the constraints obtainable by cumulatively adding the contribution to the Fisher matrix from each multipole below $l = 500$ to the contribution from the range $500 < l < 5000$. We use experimental parameters typical of Planck [114], a current generation polarization experiment like ACTpol, and a cosmic variance limited experiment (see Table 2.1). Including polarization information in the $100 < l < 500$ range improves the constraint by a factor of ~ 3 for ACTpol and ~ 5 for Planck (see Figure 2.2).

In contrast, the constraint obtained from adding high-l ($l > 2500$) temperature and polarization spectra to the full Planck data (temperature and polarization,

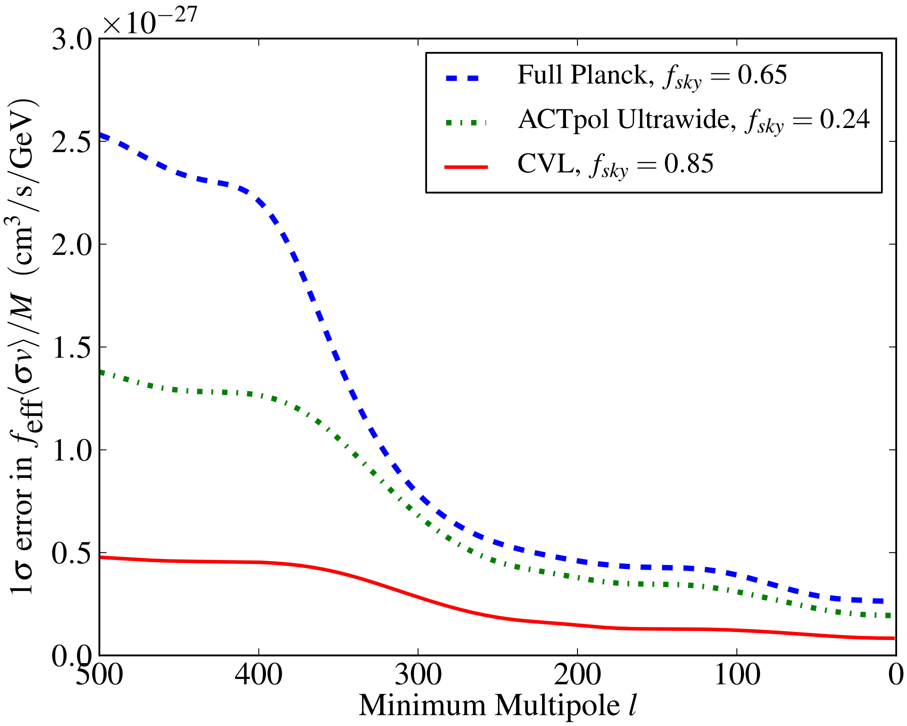

Figure 2.2: Fisher projected constraint obtained by including the range $500 < l < 5000$ and extending it cumulatively for each multipole below $l = 500$. Experimental parameters are from Planck, an ACTpol-like experiment, and a cosmic variance limited experiment (see Table 2.1). Most of the leverage comes from $250 < l < 400$.

$2 < l < 2500$) plateaus around $l = 4000$ for a future high-l experiment (see Table 2.1), with no more than a 6% improvement over full-Planck. There is only an 8% improvement over Planck for a cosmic variance limited experiment, including all l's up to 5000 (see Figure 2.3).

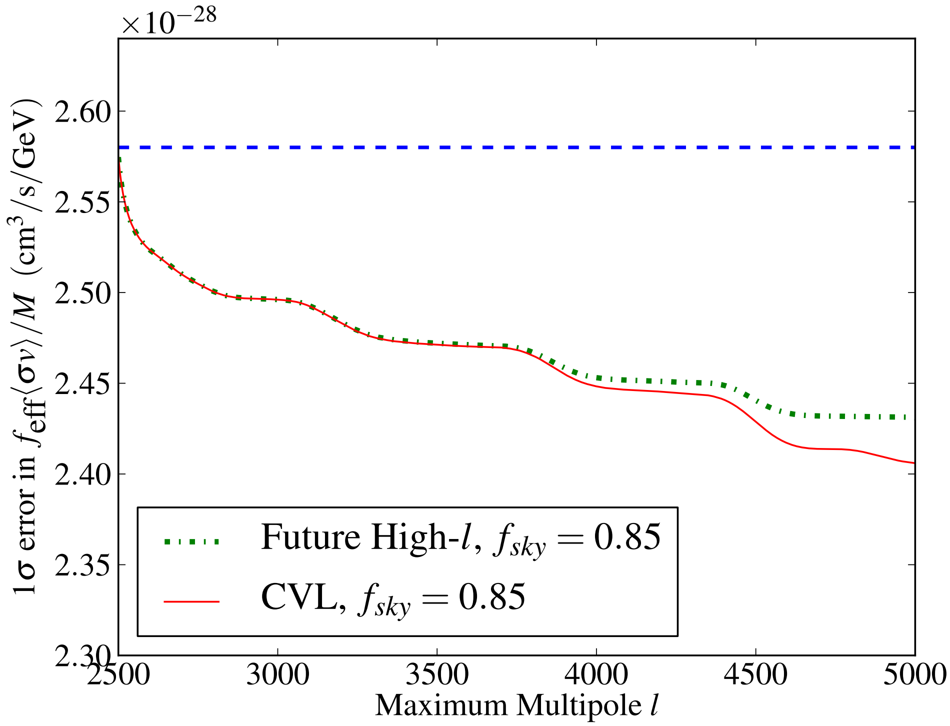

Figure 2.3: Fisher projected constraints including the complete Planck data from $2 < l < 2500$ (temperature and polarization) and extending it cumulatively for each multipole above $l = 2500$ up to $l = 5000$. Experimental parameters are from a future high-l experiment, and a cosmic variance limited experiment. The dashed line shows the Fisher projection for the full Planck temperature and polarization release (up to $l = 2500$). The improvements over Planck are 6% and 8% respectively, including all l's up to 5000.

Table 2.1: Experimental parameters used in forecasts

Experiment	Beam FWHM (arcmin)	$10^6 \Delta T/T$ (I)	$10^6 \Delta T/T$ (Q,U)	$f_{\rm sky}$
Planck	7.1	2.2	4.2	0.65
ACTpol Ultrawide[2]	1.4	4.5	6.3	0.24
CMB Stage 4	3.0	0.1	0.1	0.50
Future High-l	1.4	0.1	0.1	0.85

Note: Noise values are indicated per beam.

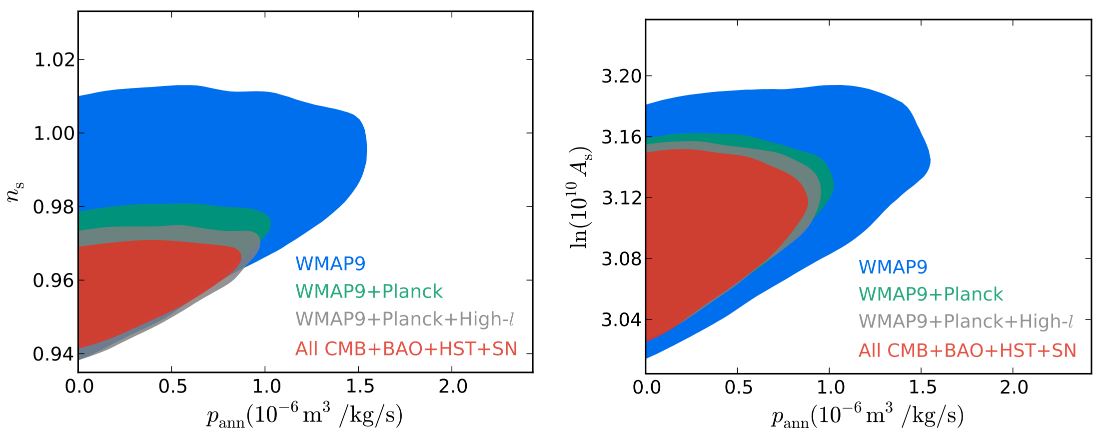

Figure 2.4: 95% confidence limit contours for n_s versus $p_{\rm ann}$ and $\ln(10^{10}A_s)$ versus $p_{\rm ann}$, marginalized over the other parameters, for selected combinations of datasets.

2.2 Current Constraints

To obtain 95% upper limits on $p_{\rm ann} = f_{\rm eff}\langle\sigma v\rangle/M_\chi$, we modified the recombination code RECFAST to include additional terms for the evolution of the hydrogen ionization fraction and matter temperature, given in Eqs. 2.7 to 2.10. We performed a likelihood analysis on various datasets using the Markov Chain Monte Carlo code COSMOMC [115]. We sampled the space spanned by $p_{\rm ann}$ and the six cosmological parameters: $\Omega_b h^2$, $\Omega_c h^2$, $100\theta_*$, τ, n_s, and $\ln 10^{10} A_s$.

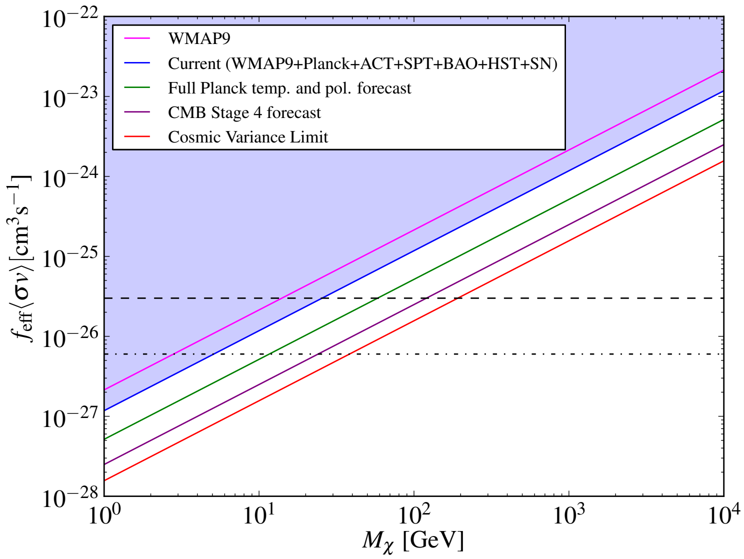

Figure 2.5: From top to bottom — constraints on $p_{\rm ann}$ from WMAP9 alone (pink) and from current data including WMAP9, Planck TT power spectrum and 4-point lensing signal, ACT, SPT, BAO, HST, and SN data (blue). Also shown are Fisher forecasts for the complete Planck temperature and polarization power spectra (green), for a proposed CMB Stage IV experiment ($50 < l < 4000$ combined with $l < 50$ from Planck, shown in purple), and for a cosmic variance limited experiment (up to $l = 4000$) (red). The dashed line shows the thermal cross section of $3 \times 10^{-26}{\rm cm}^3{\rm s}^{-1}$ for $f_{\rm eff} = 1$. The dot-dashed line shows the thermal cross section multiplied by a typical energy deposition fraction of $f_{\rm eff} = 0.2$ (see Table 2.3).

Table 2.2: Upper limits at 95% CL for $p_{\rm ann}$ combining various datasets. The first column provides constraints when $p_{\rm ann}$ is assumed to be constant with redshift. The second and third columns assume redshift-dependent energy deposition based on the 'universal' curve discussed in Section 2.1.1. The second column uses the original "universal" $e(z)$ curve derived in [52]; the third column uses an updated curve that incorporates systematic corrections discussed in [97].

Data Set	Const. Ann.	Non-Const. Ann.	Updated Non-Const. ($\mathrm{m^3 s^{-1} kg^{-1}}$)
WMAP9	$p_{\rm ann} < 1.20 \times 10^{-6}$	$p_{\rm ann} < 1.26 \times 10^{-6}$	$p_{\rm ann} < 1.21 \times 10^{-6}$
WMAP9 + Planck	$p_{\rm ann} < 0.87 \times 10^{-6}$	$p_{\rm ann} < 0.85 \times 10^{-6}$	$p_{\rm ann} < 0.80 \times 10^{-6}$
WMAP9 + Planck + Planck Lensing	$p_{\rm ann} < 0.85 \times 10^{-6}$	$p_{\rm ann} < 0.86 \times 10^{-6}$	$p_{\rm ann} < 0.79 \times 10^{-6}$
WMAP9 + Planck + Planck Lensing + ACT + SPT	$p_{\rm ann} < 0.75 \times 10^{-6}$	$p_{\rm ann} < 0.75 \times 10^{-6}$	$p_{\rm ann} < 0.73 \times 10^{-6}$
All CMB + BAO	$p_{\rm ann} < 0.70 \times 10^{-6}$	$p_{\rm ann} < 0.66 \times 10^{-6}$	$p_{\rm ann} < 0.67 \times 10^{-6}$
All CMB + BAO + HST	$p_{\rm ann} < 0.71 \times 10^{-6}$	$p_{\rm ann} < 0.74 \times 10^{-6}$	$p_{\rm ann} < 0.66 \times 10^{-6}$
All CMB + BAO + HST + Supernova	$p_{\rm ann} < 0.70 \times 10^{-6}$	$p_{\rm ann} < 0.71 \times 10^{-6}$	$p_{\rm ann} < 0.66 \times 10^{-6}$

Previous analyses using Planck data [116] utilized only a small part of the WMAP9 polarization power spectrum [117]. Incorporating a larger range of the TE power spectrum can improve the constraint by up to a factor of ~ 2.4, depending upon how much of the WMAP9 polarization spectrum is included. Using Fisher forecasts, we find that the strongest constraint is obtained by including the WMAP9 temperature auto-spectrum (TT) + TE cross spectrum from $l = 2$ to $l = 431$, and including the Planck TT spectrum for higher multipoles ($432 < l < 2500$). We also include 'high-l' data – a combination of ACT 2008-2010 [118] and SPT 2011-2012 [119] observations, using their power spectra in the range $2500 < l < 4500$, which is included in the publicly available Planck likelihood [120]. Several low-redshift (non-CMB) datasets are also combined. These include baryon acoustic oscillation data (BAO) from BOSS DR9 [121], Hubble Space Telescope measurements of over 600 Cepheid variables (HST) [122], and supernovae type Ia data from the Union 2.1 compilation (SN) [123].

When combining CMB datasets, we do not account for the covariance between disjoint l-ranges from different experiments as we expect this to be negligible [116]. In using the Planck likelihood code, we removed the TT power spectrum contribution from $l < 431$ by setting the relevant diagonal elements of the covariance matrix to effectively infinity (10^{10}) and the off-diagonal elements to zero.[3]

The dark matter annihilation constraints thus obtained are listed in Table 2.2. We checked for convergence of the chains using a Gelman-Rubin test statistic, en-

[3] We note that there is a 2.49% calibration difference between the Planck and WMAP9 power spectra [116]. Since the origin of this offset is unclear, in this work we take each dataset as given and do not adjust either.

suring that the corresponding $R - 1$ fell below 0.01. We obtained three sets of constraints, one with constant p_{ann}, one with $p_{\mathrm{ann}}(z)$ proportional to the original universal $e(z)$ curve (shown as the blue curve in Figure 2.1) to account for a generic redshift dependence of the energy deposition, and one with $p_{\mathrm{ann}}(z)$ proportional to an updated universal $e(z)$ curve that includes systematic corrections as detailed in Section 2.1.1. The constraints using the updated universal curve with systematic corrections are also shown in Figure 2.5. In general, there is a small improvement in the constraints using the updated $e(z)$ curve incorporating systematic corrections. As discussed above, this is not expected a priori from the Fisher matrix analysis using the CMB data only; it likely reflects some combination of the breakdown of the approximations in the Fisher matrix approach, differences between the data and the idealized ΛCDM baseline used for the Fisher analysis, the effect of including non-CMB datasets, and the few-percent uncertainty in the constraints due simply to scatter between CosmoMC runs.

The greatest improvement to the WMAP9-only constraint comes from adding the Planck TT spectrum ($\sim 50\%$) as it particularly constrains the spectral index n_s which is strongly degenerate with the annihilation parameter p_{ann} (see Figure 2.4). The high-l CMB and BAO datasets improve our constraints by 8% and 9%, respectively. Adding to this the HST and Supernova data do not considerably improve these limits.

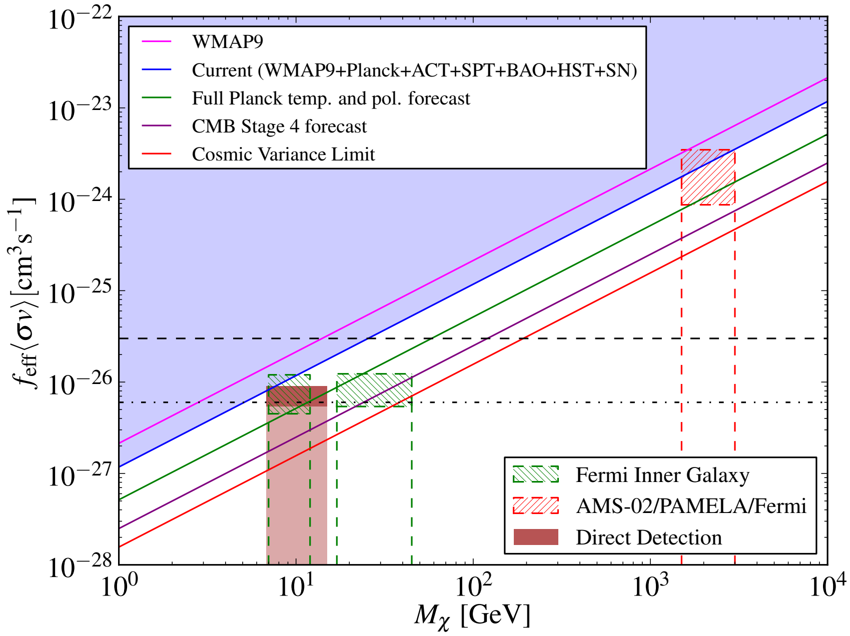

Figure 2.6: Current constraints are compared with dark matter model fits to data from other indirect and direct dark matter searches. The data from indirect searches include that from AMS-02, PAMELA, and Fermi, and the data from direct searches include that from CDMS, CoGeNT, CRESST, and DAMA. The lighter shaded direct detection region allows for p-wave annihilations, and the dashed vertical lines for the indirect detection regions allow for p-wave annihilations for non-thermally produced dark matter.

2.3 Discussion

The constraint obtained from using the updated universal deposition curve and including all available datasets is a factor of ~ 2 stronger than that from WMAP9 data alone [116]. The strongest constraint, including all available data, of $p_{\rm ann} <$

$0.66 \times 10^{-6}\mathrm{m}^3\mathrm{s}^{-1}\mathrm{kg}^{-1}$ at 95% CL, excludes annihilating dark matter of masses $M_\chi < 26$ GeV, assuming a thermal cross section of $3 \times 10^{-26}\mathrm{cm}^3\mathrm{s}^{-1}$ and perfect absorption of injected energy ($f_{\mathrm{eff}} = 1$). Using a more realistic absorption efficiency of $f_{\mathrm{eff}} = 0.2$, we exclude annihilating thermal dark matter of masses $M_\chi < 5$ GeV at the 2σ level.[4]

These constraints can be compared to dark matter models explaining a number of recent anomalous results from other indirect and direct dark matter searches. Recent measurements by the AMS-02 collaboration [44] confirm a rise in the cosmic ray positron fraction at energies above 10 GeV, which was found earlier by the PAMELA [43] and Fermi collaborations [45]. Such a rise is not easy to reconcile with known astrophysical processes, although contributions from Milky Way pulsars within ~ 1 kpc of the Earth could provide a possible explanation [124–128]. Dark matter annihilating within the galactic halo also remains a possible explanation of the positron excess [129–132]. Dark matter models considered in [130] to explain the AMS-02/PAMELA positron excess cannot have significant annihilation into Standard Model gauge bosons or quarks in order to be consistent with the antiproton-to-proton ratio measured by PAMELA, which is found to agree with expectations from known astrophysical sources [133]. In addition, the combination of the Fermi electron plus positron fraction [134, 135] and the AMS-02/PAMELA positron excess suggest that a viable dark matter candidate would need to have a mass greater than ~ 1 TeV. As found by [130], dark matter particles in the $\sim 1.5 - 3$ TeV range with a cross section of $\langle \sigma v \rangle \sim (6 - 23) \times 10^{-24}\mathrm{cm}^3/\mathrm{s}$, that annihilate into light intermediate

[4]This constraint on p_{ann} is a factor of two weaker than that found by [98], possibly due to the priors chosen in that work.

states that in turn decay into muons and charged pions, can fit the Fermi, PAMELA, and AMS-02 data. Direct annihilations into leptons do not provide good fits [130]. Such high cross sections can be reconciled with the current dark matter abundance in the Universe in three ways: (i) Dark matter can have a thermal cross section at freeze-out, and the cross section can have a $1/v$ dependence, called Sommerfeld enhancement [136, 137]. If the cross section is Sommerfeld enhanced to be $\sim 10^{-24}$ today in the Galactic halo, then it would be orders of magnitude larger at recombination (since $v_{\rm recom} < v_{\rm halo}$). Such a possibility is strongly excluded by the CMB constraints (as noted in [50]) for a wide range of masses including those that fit the AMS-02 data. (ii) Dark matter has a thermal cross section at freeze-out, and Sommerfeld enhancement saturates at a cross section of $\sim 10^{-24}\mathrm{cm}^3/\mathrm{s}$. So dark matter has this cross section just before (and during) recombination, and also in the halo of the Milky Way. (iii) Dark matter particles are non-thermal, in which case the cross section has always been ($\sim 10^{-24}\mathrm{cm}^3/\mathrm{s}$). The last two possibilities are shown in Figure 2.6, and are probed but not excluded by our current constraints. Here we use the updated $f_{\rm eff}$ values from Table 2.3 corresponding to the best-fit annihilation channels found by [130].

One additional possibility is that dark matter has a p-wave annihilation cross section, i.e a cross-section with a $\sim v^2$ dependence on velocity, as opposed to an s-wave cross section with no dependence on velocity. Dark matter that has a p-wave cross section and fits the AMS-02/PAMELA data would have to be non-thermal, since the cross section during freezeout would be orders of magnitude larger and would vastly over-deplete the relic density. Since $v_{\rm recom} \ll v_{\rm halo}$, the cross section around recombination can be orders of magnitude smaller in this case. We indicate this by dashed vertical lines in Figure 2.6.

Recent direct detection experiments such as CDMS, CoGeNT, CRESST, and DAMA, have also reported anomalous signals that could potentially be interpreted as arising from dark matter [39–42]. For example, the CDMS collaboration recently reported three events above background where they expected only 0.7 events, by measuring nuclear recoils using Silicon semiconductor detectors operating at 40 mK [40]. If the CDMS anomalous events are explained by dark matter, then they favor a best-fit dark matter mass of 8.6 GeV and a dark matter-nucleon cross section of $1.9 \times 10^{-41}\text{cm}^2$ (with 68% CL ranges of 6.5-15 GeV and $2 \times 10^{-42} - 2 \times 10^{-40}\text{cm}^2$) (see Figure 4 in [40]). The dark matter candidates that potentially explain the anomalous signals from the other direct detection experiments have best-fit regions that do not completely overlap in the two-dimensional mass/nucleon cross section space, but have mass ranges that are comparable [40]. If we assume a thermal s-wave annihilation cross section during the recombination era and an f_{eff} from Table 2.3 corresponding to annihilation into $b\bar{b}$, the current constraints presented above start to probe, but do not exclude, such a dark matter candidate. However, future Planck results and those from a proposed CMB Stage IV experiment [138, 139] will more definitively probe the relevant regime, as shown in Figure 2.6. If dark matter has p-wave annihilations instead, then generic thermal dark matter can have annihilation cross sections at recombination orders of magnitude lower than the thermal cross section. This is indicated by a lighter shaded direct detection region in Figure 2.6.

Observations of the Galactic Center and inner Galaxy by the Fermi Gamma-ray

Telescope reveal an extended Gamma-ray excess above known backgrounds, peaking at around 2-3 GeV. A population of unresolved millisecond pulsars has been proposed as a possible explanation, but as found by [140], in order for pulsars to reproduce the excess in the inner Galaxy their luminosities and abundances would need to be quite different from any observed pulsar population. However, these measurements are well fit by dark matter particles with mass in the ranges 7-12 GeV (if annihilating mostly to leptons) and 25-45 GeV (if annihilating mostly to hadrons), and are consistent with a cross section of $\sim 10^{-26}\mathrm{cm}^3/\mathrm{s}$ [141–144]. For the higher mass range, we assume annihilations into quarks and gauge bosons and a thermal cross section. For the lower mass range, we assume annihilations into muons and taus and a thermal cross section. Figure 2.6 shows that we can probe but not exclude this interpretation. The complete Planck data will better examine this possibility, as will data from the proposed CMB Stage IV experiment.

The constraints on dark matter annihilation cross section and mass from the CMB are complementary and competitive with other indirect detection probes, and offer a relatively clean way to measure dark matter properties in the early Universe. Current CMB experiments are starting to probe very interesting regions of dark matter parameter space, and future CMB polarization measurements have the potential to significantly expand the constrained regions or detect a dark matter signal.

Table 2.3: Effective energy deposition fractions for 41 dark matter models. The third column is an updated version of Table I in [50], and the fourth column includes systematic corrections discussed in Section 2.1.1.

Channel	DM Mass (GeV)	$f_{\rm eff}$	$f_{\rm eff,new}$
Electrons	1	0.85	0.45
$\chi\chi \to e^+e^-$	10	0.77	0.67
	100	0.60	0.46
	700	0.58	0.45
	1000	0.58	0.45
Muons	1	0.30	0.21
$\chi\chi \to \mu^+\mu^-$	10	0.29	0.23
	100	0.23	0.18
	250	0.21	0.16
	1000	0.20	0.16
	1500	0.20	0.16
Taus	200	0.19	0.15
$\chi\chi \to \tau^+\tau^-$	1000	0.19	0.15
XDM electrons	1	0.85	0.52
$\chi\chi \to \phi\phi$	10	0.81	0.67
followed by	100	0.64	0.49
$\phi \to e^+e^-$	150	0.61	0.47
	1000	0.58	0.45
XDM muons	10	0.30	0.21
$\chi\chi \to \phi\phi$	100	0.24	0.19
followed by	400	0.21	0.17
$\phi \to \mu^+\mu^-$	1000	0.20	0.16
	2500	0.20	0.16
XDM taus	200	0.19	0.15
$\chi\chi \to \phi\phi, \phi \to \tau^+\tau^-$	1000	0.18	0.14
XDM pions	100	0.20	0.16
$\chi\chi \to \phi\phi$	200	0.18	0.14
followed by	1000	0.16	0.13
$\phi \to \pi^+\pi^-$	1500	0.16	0.13
	2500	0.16	0.13
W bosons	200	0.26	0.19
$\chi\chi \to W^+W^-$	300	0.25	0.19
	1000	0.24	0.19
Z bosons	200	0.24	0.18
$\chi\chi \to ZZ$	1000	0.23	0.18
Higgs bosons	200	0.30	0.22
$\chi\chi \to h\bar{h}$	1000	0.28	0.22
b quarks	200	0.31	0.23
$\chi\chi \to b\bar{b}$	1000	0.28	0.22
Light quarks	200	0.29	0.22
$\chi\chi \to u\bar{u}, d\bar{d}$ (50% each)	1000	0.28	0.21

Chapter 3

Mapping Dark Matter with Optical Weak Lensing[1]

Unbiased estimators are recipes for producing an estimate of a quantity which, averaged over many realizations of the data from the same underlying model, will average towards the true value of the quantity we seek to measure (assuming the averaging is unweighted, or symmetrically weighted).

A typical example of where unbiased estimators might be useful is the estimation of cosmic shear. One can write the complete likelihood for the observed galaxy image given the parameters of the galaxy model. Such a model might include parameters describing the intrinsic ellipticity of the galaxy, its size, etc. and also the quantities that one wants to measure, such as shear. In general, the resulting likelihood will be very non-Gaussian, i.e. it cannot be usefully described by the position of maximum

[1]This chapter is a near-verbatim reproduction of [145], which has appeared in print in *Journal of Cosmology and Astroparticle Physics*, and is titled "Building unbiased estimators from non-Gaussian likelihoods with application to shear estimation".

likelihood and the second derivative matrix around that point in parameter space. In order to carry out an analysis in an unbiased manner, one would need to propagate the full likelihood shape in the subsequent analysis of the data. This is prohibitive in the limit of millions of galaxies whose shear one hopes to measure in forthcoming surveys. One could attempt to maximize the likelihood for each individual galaxy, but this typically leads to wrong answers – since galaxies are round on average, a given galaxy might be best explained as a result of massive shearing of an intrinsically round galaxy. But we know that a model with a shear of say 0.3 does not make much sense for a typical field galaxy. In [85] (BA14 hereafter), the authors have argued for the expansion of the marginalized likelihood around zero shear, i.e. compressing the likelihood to the value of the first and second derivatives of the log-likelihood expanded around zero shear. The fact that the likelihood for each individual galaxy is highly non-Gaussian does not matter. Since the shear is small, when many log-likelihoods are added (i.e. likelihoods combined), the resulting likelihood has to collapse to a Gaussian by the central limit theorem. For such a collapsed likelihood, one can use a Newton-Raphson step (using the first and second derivatives of the combined likelihood) to calculate an estimate of the underlying shear. In BA14, the authors show that this method works on a toy example (also employed later in this paper), and [146] demonstrates that it also performs as expected in more realistic settings (e.g. working with real pixelated galaxy images, but still using simulations).

However, one caveat to the method discussed above is that, in its simplest incarnation presented in BA14, it only works when the shears of all galaxies are assumed to be the same - something that is clearly not true in reality. The method requires the likelihood to be combined for a sufficiently large number of galaxies so that central limit theorem ensures we can get a sufficiently Gaussian shear estimate for the ensemble. Therefore, in order to calculate a correlation function or a power spectrum, one can either perform shear averaging in cells where the shear can be roughly assumed constant, or, alternatively, attempt to appropriately weight the estimates using cells in Fourier space to recover individual Fourier modes of the shear field (see Section 2.2 in [85]).

In this paper, we develop a related scheme. In contrast to the BA14 method, where one does not recover an estimate of the shear of a single galaxy, the method in this paper does return an unbiased estimate of the shear for each galaxy. For each individual galaxy, we make no guarantee as to the probabilistic distribution for the error $\boldsymbol{\epsilon} = \tilde{\boldsymbol{g}} - \boldsymbol{g}$ (where $\tilde{\boldsymbol{g}}$ is the shear estimate and $\boldsymbol{g}$ is the true shear), except that $\langle \boldsymbol{\epsilon} \rangle = 0$, where the average is over all possible realizations of the data. Again, while the error properties for a single galaxy are unknown, they must converge to a normal distribution when many galaxies are considered by the central limit theorem. An important advantage in returning the shear of each galaxy, is that we are now not limited to the case of constant shear and can calculate any correlation function using these estimates, since it is trivial to show, for example, that $\langle \tilde{\boldsymbol{g}}_1 \tilde{\boldsymbol{g}}_2 \rangle = \boldsymbol{g}_1 \boldsymbol{g}_2$, where indices 1 and 2 correspond to two galaxies, $\tilde{\boldsymbol{g}}$ corresponds to the estimated shear, and $\boldsymbol{g}$ corresponds to the true shear.

In section 3.1, we develop the formalism used in this work, which is completely general and independent of any particular inference problem. It will turn out that in general, an estimator can be constructed that is unbiased to a certain order in the difference between the true and assumed fiducial values for the theory parameters. In Section 3.2, we re-derive the optimal quadratic estimator in our formalism, and in Section 3.3, we apply our formalism to the toy problem of BA14.

3.1 Formalism

Consider a general likelihood function $L(\boldsymbol{D};\boldsymbol{\theta})$, which is a function of a vector of N theory parameters $\boldsymbol{\theta}$ and a vector of M observable data values $\boldsymbol{D}$.[2] We will denote the log likelihood as $\mathcal{L} = \log L$. The likelihood is normalized as

$$\int L d^M \boldsymbol{D} = \int e^{\mathcal{L}} d^M \boldsymbol{D} = 1. \tag{3.1}$$

The above is true for *any* set of theory parameters $\boldsymbol{\theta}$. We will write the average of any quantity over the likelihood at theory parameter $\boldsymbol{\theta}$ as

$$\langle X(\boldsymbol{D};\boldsymbol{\theta}')\rangle_\theta = \int X(\boldsymbol{D};\boldsymbol{\theta}') e^{\mathcal{L}(\boldsymbol{D};\boldsymbol{\theta})} d^M \boldsymbol{D} \tag{3.2}$$

Note that the function X can in general be a function of both data and the theory parameters, but the resultant average $\langle X(\boldsymbol{D};\boldsymbol{\theta}')\rangle_{\boldsymbol{\theta}}$ is a function of $\boldsymbol{\theta}$ and $\boldsymbol{\theta}'$, but not $\boldsymbol{D}$. Let us denote the derivative with respect to the theory parameters with a comma, i.e. $\mathcal{L}_{,i} = \frac{\partial \mathcal{L}}{\partial \theta_i}$. The first derivative $\mathcal{L}_{,i}$ is a vector of size N, the second derivative $\mathcal{L}_{,ij}$ is a symmetric matrix of size $N \times N$, etc.

Taking n derivatives of Equation (3.1) with respect to theory parameters, we find

[2] We follow standard notation where vectors and matrices which are not explicitly indexed are denoted with bold-face italic font and bold-face roman fonts respectivelly.

that

$$\langle {}^{n}\mathbf{U}(\boldsymbol{\theta})\rangle_{\boldsymbol{\theta}} = 0 \tag{3.3}$$

where we have introduced the shorthand notation

$$
\begin{aligned}
{}^{1}U_i &= \frac{L_{,i}}{L} = \mathcal{L}_{,i} && (3.4)\\
{}^{2}U_{ij} &= \frac{L_{,ij}}{L} = \mathcal{L}_{,ij} + \mathcal{L}_{,i}\mathcal{L}_{,j} && (3.5)\\
{}^{3}U_{ijk} &= \frac{L_{,ijk}}{L} = \mathcal{L}_{,ijk} + \mathcal{L}_{,ij}\mathcal{L}_{,k} + \mathrm{cyc} + \mathcal{L}_{,i}\mathcal{L}_{,j}\mathcal{L}_{,k} && (3.6)\\
{}^{n}\mathbf{U} &= \frac{1}{L}\frac{\partial^n L}{\partial \boldsymbol{\theta}^n} = \frac{\partial}{\partial \boldsymbol{\theta}}{}^{n-1}\mathbf{U} + {}^{n-1}\mathbf{U}{}^{1}\mathbf{U} && (3.7)
\end{aligned}
$$

Note that Equation 3.3 only holds when both the $\boldsymbol{\theta}$ inside the brackets and outside the brackets are the same. In general, however, in Equation 3.2, the $\boldsymbol{\theta}'$ appearing in X need not be at the same position in theory space as the $\boldsymbol{\theta}$ appearing in $L(\boldsymbol{D};\boldsymbol{\theta})$.

The first of the above equations, namely $\langle \mathcal{L}_{,i}\rangle = 0$ has a very clear physical interpretation. It is telling us, that if one chooses a theoretical model specified by $\boldsymbol{\theta}^{(T)}$, generates a set of observed data points $\boldsymbol{D}$ given that model, calculates the first derivative of the log-likelihood at the true model value $\mathcal{L}_{,i}(\boldsymbol{D};\boldsymbol{\theta}^{(T)})$, and then averages this quantity over all possible realizations of the data, then the result will be zero. In fact, this must intuitively be so: if one has access to many realizations of the data from the same theory available, multiplying likelihoods (or equivalently adding log-likelihoods) will result in a Gaussian likelihood that will become increasingly tightly centered on the true value. In the limit of the infinite number of data realizations, it becomes a delta function at the true value.

Of course, this is not very helpful, since if we knew the true value, we would not need to measure it. So, let us assume that the true value is at some nearby position $\boldsymbol{\theta}^{(T)} = \boldsymbol{\theta} + \Delta\boldsymbol{\theta}$. If we expand the likelihood around $\boldsymbol{\theta}$ (note that we are not expanding around the true model, but around a chosen fiducial model), we find

$$e^{\mathcal{L}(\boldsymbol{\theta}^{(T)})} = e^{\mathcal{L}(\boldsymbol{\theta})}\left(1 + \sum_{n=1}^{\infty}\frac{1}{n!}{}^{n}\mathbf{U}(\boldsymbol{\theta})\Delta\boldsymbol{\theta}^{n}\right). \tag{3.8}$$

Note that the n-th term in the Taylor expansion is a product of ${}^{n}U$, which has n indices, with $\Delta\boldsymbol{\theta}^n = \Delta\theta_i\Delta\theta_j\ldots\Delta\theta_l$, which also has n indices.

Substituting the right side of Equation 3.8 into Equation 3.2 gives

$$\langle {}^{m}\mathbf{U}(\boldsymbol{\theta})\rangle_{\boldsymbol{\theta}^{(T)}} = \sum_{n=1}^{\infty}\frac{1}{n!}{}^{mn}\mathbf{W}\Delta\boldsymbol{\theta}^{n}, \tag{3.9}$$

where

$${}^{mn}\mathbf{W} = \langle {}^{m}\mathbf{U}{}^{n}\mathbf{U}\rangle_{\boldsymbol{\theta}} \tag{3.10}$$

Note that the ${}^{mn}\mathbf{W}$ object has $m+n$ indices and is only a function of $\boldsymbol{\theta}$, not $\boldsymbol{D}$. We see that quantities ${}^{n}\mathbf{U}$ are special. They average to zero, if we are sitting on a true model ($\left\langle {}^{n}\mathbf{U}(\boldsymbol{\theta}^{(T)})\right\rangle_{\boldsymbol{\theta}^{(T)}} = 0$ as in Equation 3.3 since $\Delta\boldsymbol{\theta} = 0$ when $\boldsymbol{\theta} = \boldsymbol{\theta}^T$). However, as the true model slips away, those averages analytically respond to the difference between the true and the fiducial model (as described by Equation 3.9).

The motivation for all this may be opaque at this point. The important thing to recognize is that both ${}^{m}\mathbf{U}(D;\boldsymbol{\theta})$ and ${}^{mn}\mathbf{W}(\boldsymbol{\theta})$ are things that we can compute, given data and a choice of fiducial parameters $\boldsymbol{\theta}$, so estimators of $\boldsymbol{\theta}^T$, or equivalently $\Delta\boldsymbol{\theta} = \boldsymbol{\theta}^T - \boldsymbol{\theta}$, can be constructed out of them.

3.1.1 First-order estimator

Before proceeding, we note that

$$^{11}W_{ij} = \langle \mathcal{L}_{,i}\mathcal{L}_{,j} \rangle = -\langle \mathcal{L}_{,ij} \rangle = F_{ij} \tag{3.11}$$

is the Fisher matrix (where we have used Equation 3.3 for $n = 2$).

Our first-order estimator comes from inspecting Equation 3.9 for the case when $\Delta\boldsymbol{\theta}$ is sufficiently small that the series can be truncated at the first order. We can write down the ansatz

$$\boldsymbol{E}_1 = (^{11}\mathbf{W})^{-1}\, {}^{1}\mathbf{U} = F^{-1}_{ij}\mathcal{L}_{,j}. \tag{3.12}$$

Plugging this solution back into Equation 3.9 and remembering that $^{mn}\mathbf{W}$ is not a function of $\boldsymbol{D}$ gives

$$\begin{aligned} \langle \boldsymbol{E}_1 \rangle_{\boldsymbol{\theta}^{(T)}} &= (^{11}\mathbf{W})^{-1} \left\langle {}^{1}\mathbf{U} \right\rangle_{\boldsymbol{\theta}^{(T)}} & (3.13)\\ &= \Delta\boldsymbol{\theta}_1 + \frac{1}{2}\left(\mathbf{F}^{-1}\right)\, {}^{12}\mathbf{W}\Delta\boldsymbol{\theta}^2 + \ldots & (3.14) \end{aligned}$$

This estimator is thus unbiased to quadratic order in $\Delta\boldsymbol{\theta}$. Note that since $\boldsymbol{\theta}$ is known (i.e. it is the assumed fiducial model), we can simply add it to $\boldsymbol{E}_1$ to convert an estimator of $\Delta\boldsymbol{\theta}$ to an estimator of $\boldsymbol{\theta}^{(T)}$. The variance of the estimator is given by

$$\mathrm{Var}(\boldsymbol{E}_1) = \mathbf{F}^{-1} + \mathbf{F}^{-1}\mathbf{F}^{-1}\Delta\boldsymbol{\theta}\left\langle {}^{1}\mathbf{U}^{1}\mathbf{U}^{1}\mathbf{U} \right\rangle + \ldots, \tag{3.15}$$

where the contraction of indices goes as $[\mathbf{F}^{-1}\mathbf{F}^{-1}\Delta\boldsymbol{\theta}\,\langle {}^{1}\mathbf{U}^{1}\mathbf{U}^{1}\mathbf{U}\rangle]_{ij} = F^{-1}_{ik}F^{-1}_{jl}\Delta\boldsymbol{\theta}_m\,\langle {}^{1}U^{1}_{k}U^{1}_{l}U_m\rangle$.

Thus, given the Cramer-Rao bound, we have shown that this estimator is unbiased to quadratic order in $\boldsymbol{\Delta\theta}$ and optimal to first order in $\boldsymbol{\Delta\theta}$.

3.1.2 Higher-order estimators

To construct higher-order estimators, we need to use higher order $\mathbf{U}$s. A quantity of the form

$$\boldsymbol{E}_o = \sum_{m=1}^{o} ({}^m\mathbf{A})({}^m\mathbf{U}), \tag{3.16}$$

where ${}^m\mathbf{A}$ is a $m+1$ index object (indices of the parameter derivatives, i.e., see Eq. 3.4, etc.), will have the mean given by

$$\langle \boldsymbol{E}_o \rangle_{\boldsymbol{\theta}^{(T)}} = \sum_{n=1}^{\infty} \frac{1}{n!} \left(\sum_{m=1}^{o} ({}^m\mathbf{A})({}^{mn}\mathbf{W}) \right) \boldsymbol{\Delta\theta}^n \tag{3.17}$$

For a given order o, the weights $\mathbf{A}$ can be arranged so that the pre-factor to $\Delta\boldsymbol{\theta}$ is unity and the prefactor to $\delta\boldsymbol{\theta}^2$ and higher are zero up to order o. For a concrete example see Section 3.3 and Appendix 3.B. One should note that higher order estimators, in general, have higher variance with respect to the first-order estimator, however, they are less biased.

Finally, we note that while this construction uniquely specifies one possible estimator unbiased to a given order, it is clearly not unique, since one could imagine constructing estimators that are non-linear in $\mathbf{U}$ quantities and which might, in general, perform better or worse than this one. We leave investigation of these questions to future work.

3.1.3 A note on iterations

Since the first-order estimator is accurate to $\Delta\boldsymbol{\theta}$, one might be tempted to simply iterate: start with a first-order estimator, move by $\Delta\boldsymbol{\theta}$, do another iteration there, etc. Note, that such a process will in general take you to the maximum likelihood point, since the first-order estimator resembles a Newton-Raphson step.

It is known that maximum likelihood is not, in general, an unbiased estimator (although it often happens to be, e.g. for mean and variance of a Gaussian likelihood). We provide a concrete example in Appendix 3.A. So, why does an iterative process not produce an unbiased estimate? The subtlety lies in the fact that the above derivation assumes that the fiducial $\boldsymbol{\theta}$ was chosen without knowing about the data. Any iterative process necessarily breaks this assumption. Thus, to estimate the mean of an estimator after several iterations, one would need to average not only over possible realizations of the data, but also over all possible "paths" in the theory space that a certain iterative process might take. So, in general, one should use a higher-order estimator to improve on the accuracy of the first-order estimator, instead of iterating. Of course, we expect that the bias due to iteration will be small when the signal-to-noise is high, so that this will not matter in practice in those cases.

3.2 Optimal quadratic estimator

For completeness, we begin by applying the above formalism to a common inference problem. To construct an optimal quadratic estimator [147–149], we start with the data vector $\boldsymbol{D}_i$, with zero mean ($\langle \boldsymbol{D} \rangle = 0$), whose covariance can be modeled as

$$\mathbf{C} = \left\langle \boldsymbol{D}\boldsymbol{D}^T \right\rangle = \mathbf{N} + \theta_i \mathbf{S}_i. \tag{3.18}$$

Here θ_i are some parameters describing the two-point function of the data, i.e. power spectrum or correlation function bins, $\mathbf{S}_i$ is the response of the covariance to a change in the value of θ_i, and $\mathbf{N}$ is assumed to be a known "noise" matrix.

Ignoring constant terms, the log-likelihood can be written as

$$\mathcal{L} = -\frac{1}{2} \log \det \mathbf{C} - \frac{1}{2} \boldsymbol{D}^T \mathbf{C}^{-1} \boldsymbol{D}. \tag{3.19}$$

In our notation, we have

$${}^1U_i = -\frac{1}{2} \mathrm{Tr}\left(\mathbf{C}^{-1}\mathbf{S}_i\right) + \frac{1}{2} \mathrm{Tr}\left(\boldsymbol{D}^T \mathbf{C}^{-1} \mathbf{S}_i \mathbf{C}^{-1} \boldsymbol{D}\right). \tag{3.20}$$

A brief calculation gives

$$\left\langle {}^1U_i \right\rangle_{\boldsymbol{\theta}^{(T)}} = \frac{1}{2} \mathrm{Tr}\left(\mathbf{C}^{-1}\mathbf{S}_i \mathbf{C}^{-1} \mathbf{S}_j\right) \Delta\theta_j \tag{3.21}$$

where we have used $\mathbf{C}(\boldsymbol{\theta}^T) = \left\langle \boldsymbol{D}\boldsymbol{D}^T \right\rangle_{\boldsymbol{\theta}^{(T)}} = \mathbf{N} + \boldsymbol{\theta}_i^T \mathbf{S}_i = \mathbf{C}(\boldsymbol{\theta}) + \Delta\theta_i \mathbf{S}_i$, and hence

$$\left\langle \mathrm{Tr}\left(\boldsymbol{D}^T \mathbf{C}(\boldsymbol{\theta})^{-1} \mathbf{S}_i \mathbf{C}(\boldsymbol{\theta})^{-1} \boldsymbol{D}\right) \right\rangle_{\boldsymbol{\theta}^{(T)}} = \tag{3.22}$$

$$\mathrm{Tr}\left(\mathbf{C}(\boldsymbol{\theta})^{-1} \mathbf{S}_i \mathbf{C}(\boldsymbol{\theta})^{-1} (\mathbf{C}(\boldsymbol{\theta}) + \Delta\theta_j \mathbf{S}_j)\right). \tag{3.23}$$

It follows that

$$
\begin{aligned}
{}^{11}\mathbf{W} &= F_{ij} = \frac{1}{2}\mathrm{Tr}\left(\mathbf{C}^{-1}\mathbf{S}_i\mathbf{C}^{-1}\mathbf{S}_j\right) && (3.24)\\
{}^{n1}\mathbf{W} &= 0 \ \text{ for } \ n > 1. && (3.25)
\end{aligned}
$$

Plugging these into Equation (3.12), we recover the standard optimal quadratic estimator

$$
\boldsymbol{E}_1 = \frac{1}{2}\left[\mathbf{F}^{-1}\right]_{ij}\left[\boldsymbol{D}^T\mathbf{C}^{-1}\mathbf{S}_j\mathbf{C}^{-1}\boldsymbol{D} - b_j\right], \tag{3.26}
$$

where $b_i = \mathrm{Tr}\left(\mathbf{C}^{-1}\mathbf{S}_i\right)$. We have therefore recovered the standard optimal quadratic estimator and at the same time shown that it is unbiased at all orders. The fact that ${}^{n1}\mathbf{W} = 0$ for $n > 1$ implies that this estimator is unbiased at all orders. Additionally, it can be shown that this estimator is unbiased regardless of the assumption of a Gaussian likelihood by calculating the expectation value of the above equation. However, this is not directly connected to the framework here. (Again, we note that the expectation value proving that the standard quadratic estimator is unbiased assumes that the covariance matrix that appears in it does not depend on the data, but this assumption is invalidated by iteration.)

These beautiful properties are, of course, crucially dependent on the theory covariance matrix being linear in theory parameters in Equation (3.18). Fortunately, this is the case in the standard for measurement of the power spectrum and its linear cousins such as correlation function. If this is not the case, one can always Taylor expand around fiducial model and the derivation is then the same with $\mathbf{N}$ replaced with $\mathbf{N} + \mathbf{C}_{\text{fid.}}$, but the estimator is then only valid within the accuracy of this approximation.

While this result is not new, it is important to put this into context. Traditionally, quadratic estimators are often cast as a Newton-Raphson step towards higher likelihood (see e.g. [150]), but here one must remember that, if the goal is simply function maximization, the true second derivative may not give the best performance. Numerical work has shown that performing a Newton-Raphson step with the true second derivative instead of the Fisher matrix can be an order of magnitude slower in convergence to the maximum (e.g., when starting power spectrum parameters are far below the true value). This is because the true second derivative and the Fisher matrix are increasingly different as we move away from the true position in parameter space. Since the Fisher matrix estimate is unbiased, one might expect that anything that deviates from the Fisher estimate must be suboptimal with slower convergence (strictly speaking, being unbiased does not guarantee faster convergence if the scatter around the mean is larger but in practice we do not expect this to happen). We note however, that even though an estimate is unbiased when starting with a model that is a very poor match to the true model, the uncertainties based on a Fisher matrix will nevertheless be grossly misestimated.

3.3 Shear estimation

To apply the formalism above to the problem of shear estimation, we take as a starting point work in [85]. We describe the likelihood for shear, $L(\boldsymbol{g})$, through its

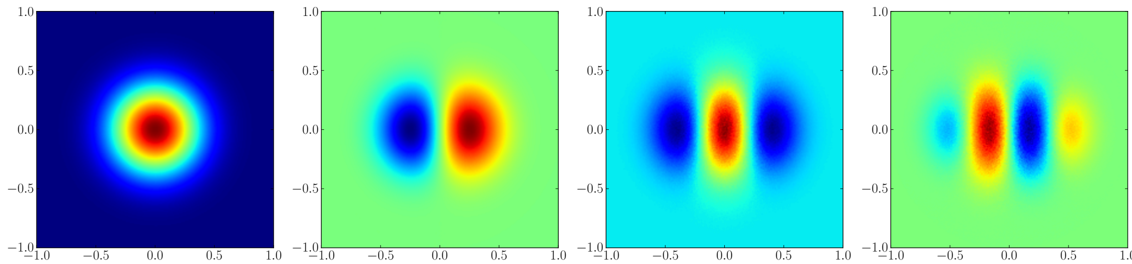

Figure 3.1: The i-th derivative of the likelihood with respect to g_1 for the posterior distribution at zero shear, where i=0,1,2,3 for the toy model described in the text. The x and y axis are the measured ellipticities for e_1 and e_2 respectively, and the color bar saturates positively at red and negatively at blue.

derivatives at zero shear as:

$$P = L(\boldsymbol{D}|\boldsymbol{g}=0) \tag{3.27}$$

$$\mathbf{Q} = \nabla_{\boldsymbol{g}} L(\boldsymbol{D}|\boldsymbol{g})|_{\boldsymbol{g}=0} \tag{3.28}$$

$$\mathbf{R} = \nabla_{\boldsymbol{g}}\nabla_{\boldsymbol{g}} L(\boldsymbol{D}|\boldsymbol{g})|_{\boldsymbol{g}=0} \tag{3.29}$$

$$\mathbf{S} = \nabla_{\boldsymbol{g}}\nabla_{\boldsymbol{g}}\nabla_{\boldsymbol{g}} L(\boldsymbol{D}|\boldsymbol{g})|_{\boldsymbol{g}=0} \tag{3.30}$$

BA14 expand to second order, but we generalize to third. Note that theory parameters here are the two components of shear, and we will use $\boldsymbol{g}$ and $\boldsymbol{\theta}$ interchangeably

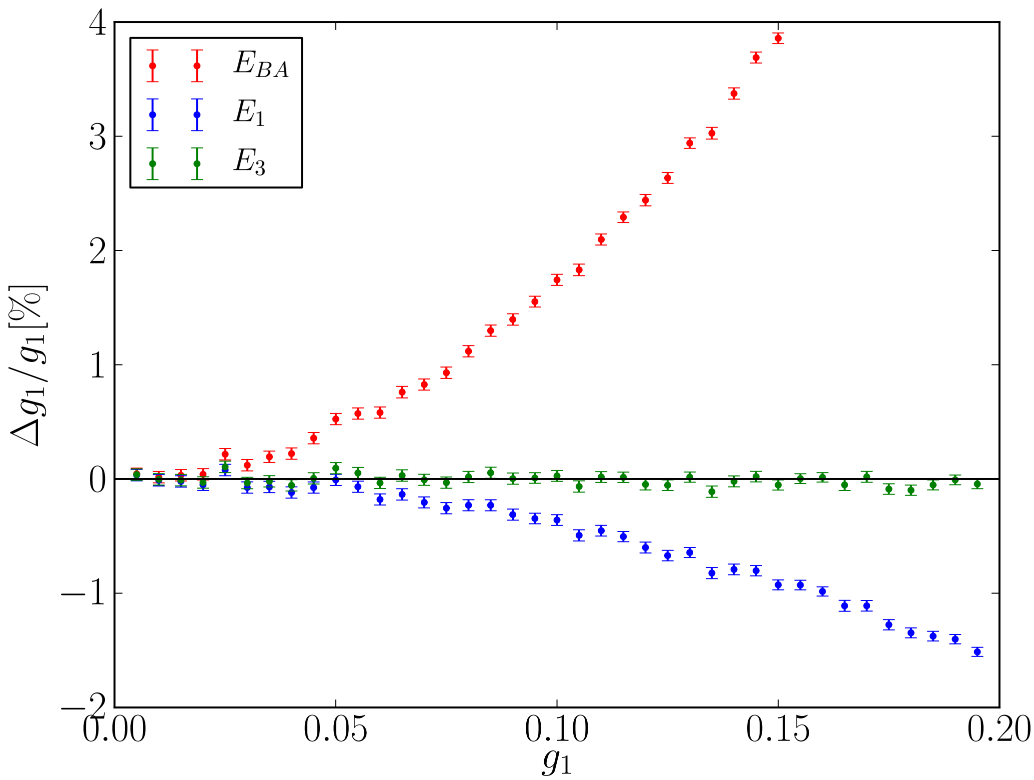

Figure 3.2: The relative biases in the recovered g_1 as a function of the input g_1, with input g_2 held at zero. For the E_1 and E_3 estimators, the error was calculated from the variance in estimates, while for the E_{AB} estimator, it was assumed to be given by the inverse of the second derivative of the posterior.

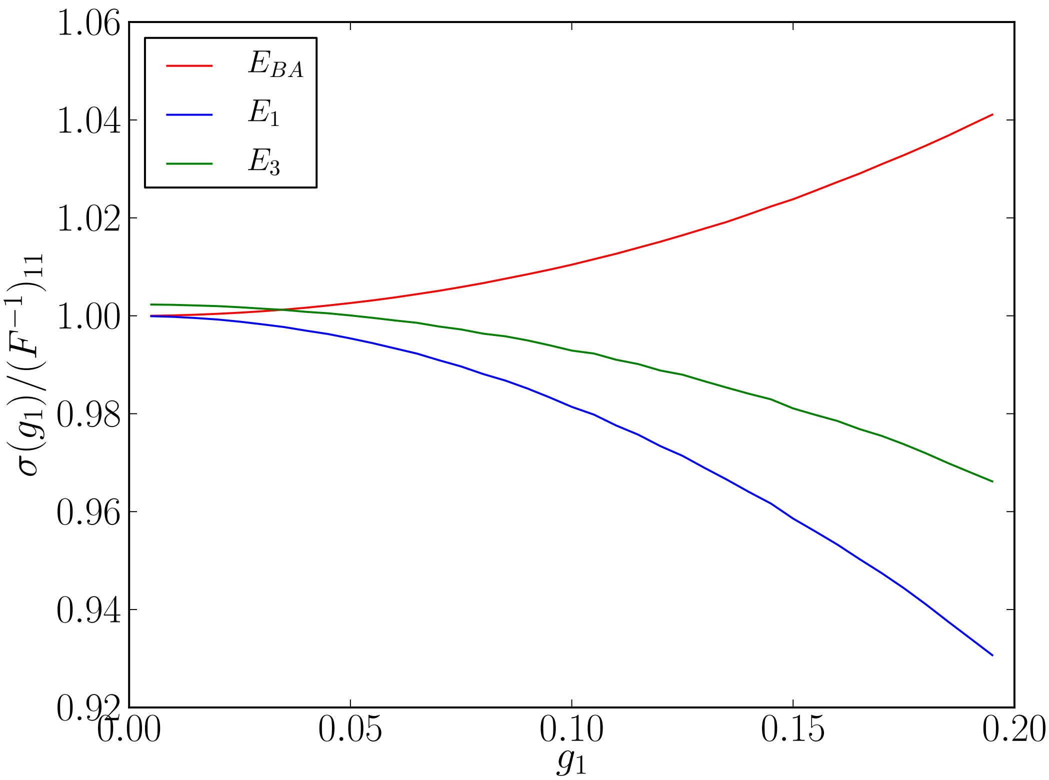

Figure 3.3: The error of estimators relative to the Fisher matrix prediction at zero shear. For the E_1 and E_3 estimators, the error was calculated from the variance in estimates, while for the E_{AB} estimator, it was assumed to be given by the inverse of the second derivative of the posterior.

below. Derivatives of log likelihood (at zero shear) are thus given by

$$\begin{aligned}
\mathcal{L}_{,i} &= \frac{Q_i}{P} && (3.31)\\
\mathcal{L}_{,ij} &= \frac{R_{ij}}{P} - \frac{Q_i Q_j}{P^2} && (3.32)\\
\mathcal{L}_{,ijk} &= \frac{S_{ijk}}{P} - \left(\frac{R_{ij}Q_k}{P^2} + \mathrm{cyc}\right) + 2\frac{Q_i Q_j Q_k}{P^3}, && (3.33)
\end{aligned}$$

and the U quantities are given simply by

$$\begin{aligned}
{}^1U_i &= \frac{Q_i}{P} && (3.34)\\
{}^2U_{ij} &= \frac{R_{ij}}{P} && (3.35)\\
{}^3U_{ijk} &= \frac{S_{ijk}}{P}. && (3.36)
\end{aligned}$$

BA14 advocate calculating the above quantities for each galaxy. If all galaxies have the same shear, the total probability can be calculated by summing derivatives of the log likelihood. For a sufficient number of galaxies, the likelihood collapses to a Gaussian and the shear can be estimated as

$$\boldsymbol{E}_{BA} = -\left(\sum \mathcal{L}_{,ij}\right)^{-1}\left(\sum \mathcal{L}_{,j}\right) \tag{3.37}$$

For a sufficiently large number of galaxies N_g, the sum of second derivatives will approach

$$\sum_{1}^{N_g} \mathcal{L}_{,i} \quad \rightarrow \quad N_g \left\langle \mathcal{L}_{,i} \right\rangle_{\boldsymbol{\theta}^{(T)}} \tag{3.38}$$

$$\sum_{1}^{N_g} \mathcal{L}_{,ij} \quad \rightarrow \quad N_g \left\langle \mathcal{L}_{,ij} \right\rangle_{\boldsymbol{\theta}^{(T)}} \tag{3.39}$$

Summing the first and second derivatives of the log likelihood is akin to averaging over the true distribution. Therefore, in the limit of an infinite number of galaxies, the estimator will give

$$\left\langle \boldsymbol{E}_{BA} \right\rangle_{\boldsymbol{\theta}^{(T)}} = -\left(\left\langle \mathcal{L}_{,ij}(\boldsymbol{\theta}) \right\rangle_{\boldsymbol{\theta}^{(T)}} \right)^{-1} \left\langle \mathcal{L}_{,j} \right\rangle_{\boldsymbol{\theta}^{(T)}} \tag{3.40}$$

Note that this is subtly different from our estimator, which uses the Fisher matrix, $F_{ij} = -\left\langle \mathcal{L}_{,ij}(\boldsymbol{\theta}) \right\rangle_{\boldsymbol{\theta}}$, which is the mean of the second derivative of the log likelihood *assuming zero shear*:

$$\left\langle \boldsymbol{E}_{1} \right\rangle_{\boldsymbol{\theta}^{(T)}} = -\left(\left\langle \mathcal{L}_{,ij}(\boldsymbol{\theta}) \right\rangle_{\boldsymbol{\theta}} \right)^{-1} \left\langle \mathcal{L}_{,j} \right\rangle_{\boldsymbol{\theta}^{(T)}} \tag{3.41}$$

3.3.1 Toy model

To test the above ideas, we use the same toy model that was used in BA14. We draw a source ellipticity from an isotropic unlensed distribution with probability distribution given by

$$P(|\boldsymbol{e}^i|) \propto (1 - |\boldsymbol{e}^i|^2)^2 \exp\left(-\frac{|\boldsymbol{e}^i|^2}{2\sigma_p^2} \right) \tag{3.42}$$

for the magnitude of the ellipticity and a random orientation. The effect of shear is most easily expressed if we cast the intrinsic ellipticity and shear as complex vectors $\boldsymbol{e}^i = e_1^i + ie_2^i$ and $\boldsymbol{g} = g_1 + ig_2$. Then the sheared ellipticity vector is given by

$$\boldsymbol{e}^s = \frac{\boldsymbol{e}^i - \boldsymbol{g}}{1 - \boldsymbol{g}^* \boldsymbol{e}^i}. \tag{3.43}$$

Finally, we add random Gaussian noise to obtain the observed ellipticity $\boldsymbol{e}^o$:

$$\boldsymbol{e}^o = \boldsymbol{e}^s + \boldsymbol{\epsilon}, \tag{3.44}$$

where each component of $\boldsymbol{\epsilon}$ is drawn from a truncated Gaussian with variance σ_n ensuring that $|\boldsymbol{e}^o| < 1$ (in practice random realizations of noise are added to $\boldsymbol{e}^s$ until $|\boldsymbol{e}^o| < 1$ is satisfied). In this work we limit ourselves to the example of $\sigma_p = 0.3$ and $\sigma_n = 0.05$.

3.3.2 Third-order estimator

It is clear that at least in the case of this particular problem, symmetry ensures that the second order correction to the estimator vanishes if one expands around zero shear. There are several ways to see this. First, given that shear is a spin-2 quantity, the lowest order scalar one can make is $|\boldsymbol{g}|^2$ and therefore, one expects the lowest-order correction to an estimate of $\boldsymbol{g}$ to scale as $\boldsymbol{g}|\boldsymbol{g}^2|$, which is third order in $\boldsymbol{g}$. Second, if one only estimates g_1, it is natural to expect that the correction to g_1 must be the same and of opposite sign to the correction to $-g_1$ – estimation of shear must be symmetric with respect to mirroring over the origin. Therefore, it cannot receive a g_1^2 correction, and the lowest order correction to the estimator must scale as g_1^3. Note that in Equation 3.14, this means that ${}^{12}\mathbf{W} = 0$.

Therefore, we construct a third-order estimator from quantities ${}^{1}\mathbf{U}$ and ${}^{3}\mathbf{U}$. Again, because of the symmetry of the problem, we construct it assuming the problem is one dimensional, i.e., we are attempting to recover the g_1 component. In that case all $\mathbf{W}$ quantities are scalar.

Starting with the system of equations:

$$\left\langle {}^{1}\mathbf{U} \right\rangle = {}^{11}\mathbf{W}\Delta\boldsymbol{\theta} + \frac{{}^{13}\mathbf{W}}{6}\Delta\boldsymbol{\theta}^3 + \ldots, \tag{3.45}$$

$$\left\langle {}^{3}\mathbf{U} \right\rangle = {}^{31}\mathbf{W}\Delta\boldsymbol{\theta} + \frac{{}^{33}\mathbf{W}}{6}\Delta\boldsymbol{\theta}^3 + \ldots, \tag{3.46}$$

it is not difficult to show that, ignoring higher order terms,

$$\frac{{}^{33}\mathbf{W} \left\langle {}^{1}\mathbf{U} \right\rangle -^{31} \mathbf{W} \left\langle {}^{3}\mathbf{U} \right\rangle}{{}^{11}\mathbf{W}{}^{33}\mathbf{W} -^{13} \mathbf{W}{}^{31}\mathbf{W}} = \Delta\boldsymbol{\theta} \tag{3.47}$$

Hence, we can write an ansatz:

$$\boldsymbol{E}_3 = \frac{{}^{33}\mathbf{W}{}^{1}\mathbf{U} -^{31} \mathbf{W}{}^{3}\mathbf{U}}{{}^{11}\mathbf{W}{}^{33}\mathbf{W} -^{13} \mathbf{W}{}^{31}\mathbf{W}} \tag{3.48}$$

Since $\mathbf{W}$ quantities do not depend on data, $\langle \boldsymbol{E}_3 \rangle = \Delta\boldsymbol{\theta}$ and hence this is our third order estimator. For more realistic cases, the rotational symmetry might be broken due to systematic and instrumental effects and for completeness we show how to build a complete 3$^{\mathrm{rd}}$ order estimator in Appendix 3.B.

3.3.3 Results for toy model

For this toy example, we can calculate the likelihood and its derivatives simply by brute force Monte Carlo - we can draw a large enough number of samples from the parent distribution such that the gridded values of sampled $\boldsymbol{e}$ become a good approximation for the probability distribution. The derivatives are then calculated by finite difference methods from gridded likelihoods. Note that this short-cut is unlikely to work in a more realistic setting due to the higher dimensionality of the problem.

In Figure 3.1, we plot the i-th derivative of the likelihood with respect to g_1, that is quantities P, Q_1, R_{11}, S_{111}, showing how the posterior distribution of ellipticities responds to shear at each order.

In Figure 3.2, we show results for the three estimators discussed in this text. As expected, the $\boldsymbol{E}_{BA}$ and $\boldsymbol{E}_1$ estimators show a quadratic increase in bias as a function of shear, which is mostly removed by the $\boldsymbol{E}_3$ estimator. In this particular case, our $\boldsymbol{E}_1$ estimator seems to be performing somewhat better than the original $\boldsymbol{E}_{BA}$ estimator, although it is not clear whether this will translate to similar gains in more realistic scenarios. However, the $\boldsymbol{E}_3$ estimator is designed to be more accurate and performs with a 0.1% relative precision all the way to shears of 0.2, at which point we are well out of the validity of the small shear approximation, and flexion effects [151] become important, which are not captured in this toy model.

In Figure 3.3, we show the error (square root of variance) for the three estimators discussed here, normalized to the Fisher matrix prediction at zero shear. As we can see, both $\boldsymbol{E}_{BA}$ and $\boldsymbol{E}_1$ converge to the Fisher matrix prediction at zero shear, but

$\boldsymbol{E}_3$ is marginally noisier. The effect is small, sub 1%, but clearly detectable. For higher shear, the $\boldsymbol{E}_1$ and $\boldsymbol{E}_3$ estimators begin to become slightly less noisy than the zero-shear Fisher prediction. Note that this does not violate the Cramer-Rao bound, since the bound only holds if the true shear is zero.

Finally, we demonstrate explicitly that our estimator can measure correlations. To that end, we draw pairs of galaxies with shear $\boldsymbol{g}_a$ and $\boldsymbol{g}_b$, which we randomly choose to follow

$$\left\langle \boldsymbol{g}_a \boldsymbol{g}_a^T \right\rangle = \left\langle \boldsymbol{g}_b \boldsymbol{g}_b^T \right\rangle = \begin{pmatrix} 0.05^2 & 0 \\ 0 & 0.05^2 \end{pmatrix} \tag{3.49}$$

and

$$\left\langle \boldsymbol{g}_a \boldsymbol{g}_b^T \right\rangle = \begin{pmatrix} 0.00125 & 0.00075 \\ 0.00075 & 0.00125 \end{pmatrix} . \tag{3.50}$$

These pairs of galaxies are modeled using Equations 3.42, 3.43, and 3.44 with $\sigma_p = 0.3$, $\sigma_n = 0.05$ to obtain observed values and then with the E_3 estimator to obtain an estimate. These estimates where then used to obtain the correlations: $\left\langle \tilde{\boldsymbol{g}}_a \tilde{\boldsymbol{g}}_b^T \right\rangle_{11} = 0.00125319 \pm 2.8 \times 10^{-6}$ and $\left\langle \tilde{\boldsymbol{g}}_a \tilde{\boldsymbol{g}}_b^T \right\rangle_{12} = 0.007552 \pm 2.8 \times 10^{-6}$, consistent with the input values and sub-percent level accurate. Of course, this exercise *had* to work, so it is really just a sanity check.

3.4 Conclusions

In this paper, we have derived a general framework for generating unbiased estimators. The framework is general and can be used wherever we are measuring a quantity which is perturbatively close to the assumed model. We have shown that the inverse of Fisher matrix multiplied by the first derivative vector is a general formula for a first order unbiased estimator. In special cases such as an optimal quadratic estimator, the estimator is unbiased at all orders. We have applied our framework to the problem of estimating weak lensing shear and constructed a first and third-order estimator.

In the realm of the toy problem of BA14, our third-order estimator is unbiased for all relevant shear magnitudes with a negligible increase in the estimator variance compared to the Fisher prediction at zero shear. In typical weak-lensing analyses, shears are small enough that the first-order estimator may be sufficient. However, there are two cases where third order correction might matter. First, when measuring the cosmic shear power spectrum, an error term proportional to g^3 will "renormalize" to give a correction to the measured shear power spectrum proportional to $\left\langle |\boldsymbol{g}|^2 \right\rangle P_{gg}$, where P_{gg} is the true shear power spectrum. This is of the same order of magnitude as the overall LSST error [152]. Second, in regions of high-shear, such as those around clusters of galaxies, the third-order estimator will be useful, simply because shear are large-enough that the third order correction matters. The formalism presented here can trivially be extended to the flexion measurement, and it should correctly account for the correlation between shear and flexion. We refrain from making more quantitative statements since it is not clear how realistic the toy model is.

More importantly, we have constructed an estimator which performs as well as the BA14 estimator, but also returns shear estimates for individual galaxies, which makes it usable in direct measurements of the n-point function of the shear field.

We also note that to some extent the main problem with shear measurements is not the underlying framework, which is the focus of this paper, but the bias arising from inadequate modeling of the properties of unlensed galaxies, and it might turn out that these problems are best solved using very phenomenological approaches as those discussed in e.g. [153, 154].

Putting this estimator into practice might be more complicated. In particular, in its current incarnation, it gives the same weight to all galaxies, while we know that this will not hold in reality. The correct way to solve this problem is to separate galaxies into sub-classes in a way that does not correlate (or negligibly correlates) with the underlying shear. A separate estimator can be constructed for each class, and the Fisher matrix is the appropriate weight. We leave testing of this framework in more realistic settings for the future work.

Appendix

3.A Example of bias of ML estimator

Here we give a concrete example of a likelihood for which the maximum likelihood estimator is biased. In general, this happens with asymmetric likelihoods. Consider:

$$L = x\lambda^2 e^{-\lambda x}, \tag{3.51}$$

where $x > 0$ is the "data" and $\lambda > 0$ is the theory parameter. Given exactly one measurement x, the maximum likelihood estimator (i.e. the estimator where one would end up upon iterations of Newton-Raphson steps) is

$$E_{ML} = \frac{2}{x}, \tag{3.52}$$

whose expectation value is 2λ, i.e, wrong by a factor of two. Expanding around $\lambda = l$, our first order estimator is given by

$$E_1 = \frac{l(4 - lx)}{2} \tag{3.53}$$

which is unbiased up to quadratic order in $\lambda - l$. Interestingly,

$$E = \frac{1}{x} \tag{3.54}$$

is unbiased at all orders and is neither ML nor our perturbative estimator.

3.B General 3$^{\mathrm{rd}}$ order estimator

For completeness we demonstrate how to build a full third order estimator. This procedure can be trivially generalized to any order. We write the Equation (3.9) to up to third order in an "unrolled" matrix form

$$\langle \mathbf{U} \rangle = \mathbf{W}\boldsymbol{g}, \tag{3.55}$$

where we have, assuming that there are two theory parameters that we want to recover (g_1 and g_2),

$$\mathbf{U} = \begin{bmatrix} \langle {}^1U_1 \rangle \\ \langle {}^1U_2 \rangle \\ \langle {}^2U_{11} \rangle \\ \langle {}^2U_{12} \rangle \\ \langle {}^2U_{22} \rangle \\ \langle {}^3U_{111} \rangle \\ \langle {}^3U_{112} \rangle \\ \langle {}^3U_{122} \rangle \\ \langle {}^3U_{222} \rangle \end{bmatrix} \tag{3.56}$$

and

$$\mathbf{W} = \begin{bmatrix} {}^{11}W_{1|1} & {}^{11}W_{1|2} & {}^{12}W_{1|11} & {}^{12}W_{1|12} & {}^{12}W_{1|22} & {}^{13}W_{1|111} & {}^{13}W_{1|112} & {}^{13}W_{1|122} & {}^{13}W_{1|222} \\ {}^{11}W_{2|1} & {}^{11}W_{2|2} & {}^{12}W_{2|11} & {}^{12}W_{2|12} & {}^{12}W_{2|22} & {}^{13}W_{2|111} & {}^{13}W_{2|112} & {}^{13}W_{2|122} & {}^{13}W_{2|222} \\ {}^{21}W_{11|1} & {}^{21}W_{11|2} & {}^{22}W_{11|11} & {}^{22}W_{11|12} & {}^{22}W_{11|22} & {}^{23}W_{11|111} & {}^{23}W_{11|112} & {}^{23}W_{11|122} & {}^{23}W_{11|222} \\ {}^{21}W_{12|1} & {}^{21}W_{12|2} & {}^{22}W_{12|11} & {}^{22}W_{12|12} & {}^{22}W_{12|22} & {}^{23}W_{12|111} & {}^{23}W_{12|112} & {}^{23}W_{12|122} & {}^{23}W_{12|222} \\ {}^{21}W_{22|1} & {}^{21}W_{22|2} & {}^{22}W_{22|11} & {}^{22}W_{22|12} & {}^{22}W_{22|22} & {}^{23}W_{22|111} & {}^{23}W_{22|112} & {}^{23}W_{22|122} & {}^{23}W_{22|222} \\ {}^{31}W_{111|1} & {}^{31}W_{111|2} & {}^{32}W_{111|11} & {}^{32}W_{111|12} & {}^{32}W_{111|22} & {}^{33}W_{111|111} & {}^{33}W_{111|112} & {}^{33}W_{111|122} & {}^{33}W_{111|222} \\ {}^{31}W_{112|1} & {}^{31}W_{112|2} & {}^{32}W_{112|11} & {}^{32}W_{112|12} & {}^{32}W_{112|22} & {}^{33}W_{112|111} & {}^{33}W_{112|112} & {}^{33}W_{112|122} & {}^{33}W_{112|222} \\ {}^{31}W_{122|1} & {}^{31}W_{122|2} & {}^{32}W_{122|11} & {}^{32}W_{122|12} & {}^{32}W_{122|22} & {}^{33}W_{122|111} & {}^{33}W_{122|112} & {}^{33}W_{122|122} & {}^{33}W_{122|222} \\ {}^{31}W_{222|1} & {}^{31}W_{222|2} & {}^{32}W_{222|11} & {}^{32}W_{222|12} & {}^{32}W_{222|22} & {}^{33}W_{222|111} & {}^{33}W_{222|112} & {}^{33}W_{222|122} & {}^{33}W_{222|222} \end{bmatrix} \tag{3.57}$$

and

$$\boldsymbol{g} = \begin{bmatrix} g_1 \\ g_2 \\ g_1 g_1 \\ 2 \times g_1 g_2 \\ g_2 g_2 \\ g_1 g_1 g_1 \\ 3 \times g_1 g_1 g_2 \\ 3 \times g_1 g_2 g_2 \\ g_2 g_2 g_2 \end{bmatrix}. \tag{3.58}$$

In the expression for $\mathbf{W}$, we have used a pipe symbol to separate indices corresponding to the left and right sides of the equation. Solving this matrix equation for the vector $\boldsymbol{g}$. We have

$$\boldsymbol{g} = \mathbf{W}^{-1} \langle \mathbf{U} \rangle \tag{3.59}$$

We can now write an ansatz for the estimator:

$$\boldsymbol{E} = \mathbf{W}^{-1} \mathbf{U} \tag{3.60}$$

Since $\mathbf{W}$ does not depend on data, it trivially follows that

$$\langle \boldsymbol{E} \rangle = \mathbf{W}^{-1} \langle \mathbf{U} \rangle = \boldsymbol{g} \tag{3.61}$$

Hence, the first two components of $\boldsymbol{E}$, namely E_1 and E_2 are unbiased estimators for the first two components of $\boldsymbol{g}$, that is g_1 and g_2. In other words, the linear algebra has given us the particular *linear* combination of $\mathbf{U}$ quantities which average to g_1 and g_2 without any contribution from terms quadratic and cubic in $\boldsymbol{g}$.

Chapter 4

Mapping Dark Matter with CMB Lensing[1]

Measuring the gravitational lensing of the cosmic microwave background (CMB) by intervening structure is a potentially powerful way to map out the mass distribution in the Universe. Advantages of CMB lensing over lensing measured at other wavelengths include that the CMB is a source that fills the whole sky, is at a known redshift, and has well understood statistical properties. To date, the lensing of the CMB caused by the large-scale projected dark matter distribution has been observed by a number of CMB experiments with ever increasing statistical significance [155–159]. This lensing signal has been detected in both CMB temperature and polarization maps and in cross-correlation with other tracers of large-scale structure [155, 156, 159–172]. These CMB lensing measurements have become precise

[1]This chapter is a near-verbatim reproduction of [65], which has appeared in print in *Physical Review Letters*, and is titled "Evidence of Lensing of the Cosmic Microwave Background by Dark Matter Halos".

enough that they now provide interesting constraints on a number of cosmological parameters such as curvature and the amplitude of matter fluctuations [173]. These constraints can be expected to significantly improve with the advent of near-term and next-generation CMB datasets [174–176].

Previous studies have focused on the lensing of the CMB by large-scale structure corresponding to scales between tens and several hundred comoving Mpc. As the data improve it is possible to shift focus to smaller scales, particularly those which have undergone appreciable nonlinear growth. On small enough scales, the CMB is lensed by individual dark matter halos. We refer to this small-scale signal as "CMB halo lensing," and note that this lensing can be due to individual galaxy clusters, galaxy groups, and massive galaxies. Before now, CMB experiments did not have the sensitivity or resolution to detect this signal which was hypothesized to exist over a decade ago [177–189].

In this work, we present evidence of the CMB halo lensing signal using the first season of data from ACTPol. This detection is made by stacking ACTPol reconstructed convergence maps at the positions of CMASS galaxies that have been optically selected from the Sloan Digital Sky Survey-III Baryon Oscillation Spectroscopic Survey Tenth Data Release (SDSS-III/BOSS DR10) ([190–192]). This signal is detected at a significance of 3.2σ when we combine the nighttime data from three ACTPol first-season survey regions. We see an excess of 1.3σ or greater in each indiviudual survey region, although all fields are needed to give a statistical detection.

4.1 CMB Data

ACT is located in Parque Astronómico Atacama in northern Chile at an altitude of 5190 m. The 6-meter primary mirror has a resolution of 1.4 arcminutes at a wavelength of 2 millimeters. Its first polarization-sensitive camera, ACTPol, is described in detail in [193] and [194]. ACTPol observed from Sept. 11 to Dec. 14, 2013 at 146 GHz. Four "deep field" patches were surveyed near the celestial equator at right ascensions of 150°, 175°, 355°, and 35°, which we call D1 (73 deg^2), D2 (70 deg^2), D5 (70 deg^2), and D6 (63 deg^2). The scan strategy allows for each patch to be observed in a range of different parallactic angles while scanning horizontally, which aids in separating instrumental effects from celestial polarization. White noise map sensitivity levels for the patches are 16.2, 17, 13.2, and 11.2 μK-arcmin respectively in temperature, with polarization noise levels higher by roughly $\sqrt{2}$. All patches were observed during nighttime hours for some fraction of the time. The nighttime data fraction is $50\%, 25\%, 76\%$, and 94% for D1, D2, D5, and D6 respectively. We use only nighttime data from D1, D5, and D6 in this analysis. Further details about the observations and mapmaking can be found in [194].

We template-subtract point sources from these maps by filtering the D1, D5, and D6 patches with a filter matched to the ACTPol beam profile. Point sources with a signal at least five times larger than the background uncertainty in the filtered maps are identified, and their fluxes are measured. A template of beam-convolved point sources is then constructed for each patch and subsequently subtracted from the corresponding patch. As a result, point sources with fluxes above 8 mJy are removed from D1, and sources with fluxes above 5 mJy are removed from D5 and

D6.

Overall calibration of the ACTPol patches is achieved by comparing to the Planck 143 GHz temperature map [195] and following the method described in [196]. The patches are then multiplied by a factor of 1.012 to correspond to the WMAP calibration as in [194].

4.2 Optical Data

SDSS I and II obtained imaging data of 11,000 deg^2 using the 2.5-meter SDSS Telescope [197, 198]. This survey has five photometric bands. SDSS-III BOSS extended this imaging survey by 3,000 deg^2 [190]. Based on the resulting photometric catalog of galaxies, CMASS ("constant mass") galaxies were selected extending the luminous red galaxy (LRG) selection of [199] to bluer and fainter galaxies. These galaxies form a roughly volume-limited sample with $z > 0.4$ and satisfy the criterion that their number density be high enough to probe large-scale structure at redshifts of about 0.5 [200]. The BOSS spectroscopic survey targeted these galaxies obtaining spectroscopic redshifts, and these galaxies have been used in a number of cosmological analyses [200, 201].

Using the tenth SDSS public data release (DR10), we selected CMASS galaxies from the BOSS catalog.[2] This selection resulted in 6144, 5211, and 5420 CMASS galaxies that lie within D1, D5, and D6 respectively. These galaxies span a redshift

[2] `https://data.sdss3.org/datamodel/files/SPECTRO_REDUX/specObj.html`. We used the keywords `BOSS_TARGET1 && 2, SPECPRIMARY == 1, ZWARNING_NOQSO == 0`, and `(CHUNK != "boss1") && (CHUNK != "boss2")`. The keywords are described here: `https://www.sdss3.org/dr10/algorithms/boss_galaxy_ts.php`

range of about $z = 0.4$ to $z = 0.7$, with a mean redshift of $z = 0.54$. The galaxies were cross referenced with galaxies in the SDSS-III photometric catalog,[3] using a shared galaxy identification number, to obtain more accurate celestial position information.

A subset of CMASS galaxies have optical weak-lensing mass estimates of their average halo masses using the publicly-available CFHTLenS galaxy catalog [202,203]. This subset has an additional redshift cut of $z \in [0.47, 0.59]$ and a stellar mass cut of $10^{11.1}\ h_{70}^{-2} M_{\odot} < M_{\star} < 10^{12.0}\ h_{70}^{-2} M_{\odot}$ relative to the full CMASS sample.[4] The average halo mass estimate for this CMASS galaxy subsample is $M_{200\bar{\rho}_0} = (2.3 \pm 0.1) \times 10^{13}\ h^{-1} M_{\odot}$ [202], where $M_{200\bar{\rho}_0}$ is defined as the mass within R_{200}, a radius within which the average density is 200 times the mean density of matter today. If we had adopted the additional redshift and stellar mass cuts of this subsample of CMASS galaxies, then the number of galaxies falling in the ACTPol patches would have been reduced by roughly a factor of two; so we instead stack on the full CMASS galaxy sample within our survey regions for this work.

Since we cut out a $70' \times 70'$ 'stamp' centered on each CMASS galaxy from the ACTPol temperature maps, we exclude all galaxies whose stamp does not fall entirely within the corresponding ACTPol patch. We find from simulations that this stamp size is roughly the minimum required to obtain unbiased lensing reconstructions using the pipeline described here. We also note that performing reconstructions on small stamps allows us to obtain the necessary precision for the mean field subtraction described in the next section. To avoid noisy parts of the ACTPol patches, we also

[3] `http://data.sdss3.org/datamodel/files/BOSS_PHOTOOBJ/RERUN/RUN/CAMCOL/photoObj.html`

[4] The full CMASS sample has a stellar mass range of roughly $10^{10.6}\ h_{70}^{-2} M_{\odot} < M_{\star} < 10^{12.2}\ h_{70}^{-2} M_{\odot}$.

remove galaxies for which the mean value of its corresponding inverse variance weight stamp is lower than 0.7, 0.3, and 0.3 times the mean of the weight map of the full patch for D1, D5, and D6 respectively. These factors were chosen so that all of the stamps in our stacks had an average detector hit count above the same minimum value. These cuts leave 4400, 3665, and 4032 galaxies to stack on in D1, D5, and D6 respectively.

4.3 Pipeline

The analysis pipeline used in this work is as follows. We set the mean of each galaxy-centered $70' \times 70'$ stamp to zero to prevent leakage of power on scales larger than the stamp size due to windowing effects. Each stamp is then multiplied by an apodization window, a function that smoothly varies the edges of the image to zero in order to facilitate Fourier transforms. The window consists of the corresponding inverse variance weight stamp that has been smoothed and tapered with a cosine window of width 14 arcminutes. Each of the stamps is then beam-deconvolved and filtered with the quadratic filter given in [186].

The filter is constructed by noting that lensing of the CMB temperature field shifts the unlensed temperature field, $\tilde{T}(\hat{\mathbf{n}})$, to the lensed temperature field, $T(\hat{\mathbf{n}})$, so that

$$T(\hat{\mathbf{n}}) = \tilde{T}(\hat{\mathbf{n}} + \nabla\phi) \tag{4.1}$$

where ϕ is the deflection potential and $\nabla\phi$ is the deflection angle. The lensing convergence, κ, is given by

$$\nabla^2 \phi = -2\kappa. \tag{4.2}$$

On the arcminute scales of individual dark matter halos, the unlensed CMB can be approximated as a gradient, and lensing induced by the halo alters the CMB field along this gradient direction. Thus, we search for this signal by looking for deflections correlated with the background CMB gradient. In order to do this, we reconstruct the lensing convergence field, κ, by constructing two filtered versions of the data: one that is filtered to isolate the background gradient and one that is filtered to isolate small-scale CMB fluctuations. Then we take the divergence of the product of these two maps as described in [186] and summarized below.

The first filtered map is constructed by taking the weighted gradient of the lensed CMB map

$$\mathbf{G}_{\boldsymbol{l}}^{TT} = i\,\boldsymbol{l}\,W_l^{TT}\,T_{\boldsymbol{l}}, \tag{4.3}$$

where the weight filter is

$$W_l^{TT} = \tilde{C}_l^{TT}(C_l^{TT} + N_l^{TT})^{-1} \tag{4.4}$$

for $l \leq l_{\mathrm{G}}$, and $W_l^{TT} = 0$ for $l > l_{\mathrm{G}}$, where TT refers to the temperature auto-spectrum. Note that $\tilde{C}_l$ and C_l are the unlensed and lensed CMB power spectra respectively from a fiducial theoretical model based on *Planck* best-fit parameters, and N_l is the noise power. Here l_{G} is a cutoff scale and is set to $l_{\mathrm{G}} = 2000$. We choose this cutoff since, as shown in [186], the unlensed CMB gradient does not have contributions above $l = 2000$, and we want to remove smaller-scale fluctuations. This cutoff in the gradient filter is the main difference between the filter used in this work and the filter used for large-scale structure lensing [204]. When the convergence, κ, is large (of order 1), as it is for clusters, only the filter with the gradient cutoff returns an unbiased estimate of the convergence [186]. For smaller convergence values, as measured for galaxy groups in this work, both filters return similar results.

The second filtered map is an inverse-variance weighted map given by

$$L_{\boldsymbol{l}}^{T} = W_{l}^{T}\, T_{\boldsymbol{l}}, \tag{4.5}$$

where

$$W_{l}^{T} = (C_{l}^{TT} + N_{l}^{TT})^{-1}. \tag{4.6}$$

Taking the divergence of the product of these filtered maps, as prescribed in [186], gives,

$$\frac{\kappa_{\boldsymbol{l}}^{TT}}{A_{l}^{TT}} = -\int \mathrm{d}^2\hat{\mathbf{n}}\, e^{-i\hat{\mathbf{n}}\cdot\boldsymbol{l}} \left\{\nabla \cdot \left[\mathbf{G}^{TT}(\hat{\mathbf{n}})\, L^{T}(\hat{\mathbf{n}})\right]\right\}. \tag{4.7}$$

Here the real-space lensing convergence field constructed from temperature data is

$$\kappa^{TT}(\hat{\mathbf{n}}) = \int \frac{\mathrm{d}^2 l}{(2\pi)^2}\, e^{i\boldsymbol{l}\cdot\hat{\mathbf{n}}}\, \kappa_{\boldsymbol{l}}^{TT}. \tag{4.8}$$

The normalization factor is given by

$$\frac{1}{A_{l}^{TT}} = \frac{2}{l^2} \int \frac{\mathrm{d}^2 l_1}{(2\pi)^2}\, [\boldsymbol{l}\cdot\boldsymbol{l}_1]\, W_{l_1}^{TT}\, W_{l_2}^{T}\, f^{TT}(\boldsymbol{l}_1, \boldsymbol{l}_2), \tag{4.9}$$

with

$$f^{TT}(\boldsymbol{l}_1, \boldsymbol{l}_2) = [\boldsymbol{l} \cdot \boldsymbol{l}_1]\tilde{C}^{TT}_{l_1} + [\boldsymbol{l} \cdot \boldsymbol{l}_2]\tilde{C}^{TT}_{l_2} \tag{4.10}$$

and $\boldsymbol{l} = \boldsymbol{l}_1 + \boldsymbol{l}_2$.

The mean of each reconstructed convergence stamp is set to zero to remove fluctuations on scales larger than the size of the stamp. Each reconstructed convergence stamp is then low-pass filtered by setting modes with $l > 5782$ to zero. This corresponds to ignoring modes smaller than the 1.4' beam scale.

The reconstructed lensing convergence stamps from a given ACTPol patch are then stacked (i.e., averaged). A 'mean field' stamp needs to be subtracted from this stack since the apodization window does not leave the mean of the reconstructed stack identically zero in the absence of any signal [205, 206]. We construct a mean field stamp from the average reconstruction of 15 realizations of random positions in the corresponding ACTPol patch. Each random-position-realization has the same number of stamps as are in the galaxy stack. Thus, by construction, the mean-field-subtracted galaxy stacks show any excess signal above that from random locations.

In order to construct the covariance matrix for each patch, we construct 50 independent realizations of simulated ACTPol data for each patch. These simulations have noise and beam properties matched to the data and include only lensing by large-scale structure. We repeat the procedure performed on the data on each of the 50 independent simulations. The covariance matrix for each patch is then obtained by calculating the covariance of radial profiles across these 50 mean-field-subtracted, mean stamps. In this way, the covariance matrices capture the correlations between radial bins. This procedure also takes into account any additional covariance coming from overlapping stamps. In addition, it also folds in the uncertainty in the subtracted mean field.[5]

The pipeline described above is implemented for each ACTPol patch separately as well as for all the patches combined. The latter is done by stacking the three mean-field-subtracted galaxy stacks for each ACTPol data patch. The combined-patch covariance matrix is obtained by combining the 50 mean simulated convergence stamps for each patch, and calculating the variance across all 150 mean stamps.

This pipeline is tested on a suite of simulations where $70' \times 70'$ CMB stamps are lensed with Navarro-Frenk-White (NFW) cluster profiles [207] with varying levels of instrument noise, beam resolution, and pixelization. The pipeline returns unbiased reconstructions (to $\approx 0.1\sigma$) and S/N estimates in agreement with previous analyses [186]. In particular, the expected detection significance stacking a sample of roughly 12,000 galaxies in lensed CMB stamps with ACTPol beam and noise properties is 4.2σ. For this estimate, the masses, concentrations, and redshifts of the lensing galaxies are assumed to be the mean values of the CMASS subsample with optical weak lensing follow up described above [202].

4.4 Results

We show the result of the combined-patch stack of reconstructed convergence stamps centered on CMASS galaxies in Figure 4.1. The left panel shows the mea-

[5]Note that we use simulations to characterize the covariance matrix since stacking on random positions in the data does not capture the variance due to overlapping stamps and meanfield subtraction. A typical mean-field amplitude is 0.03, and the uncertainty is $\approx 20\%$ of the errorbars shown in Figure 4.1.

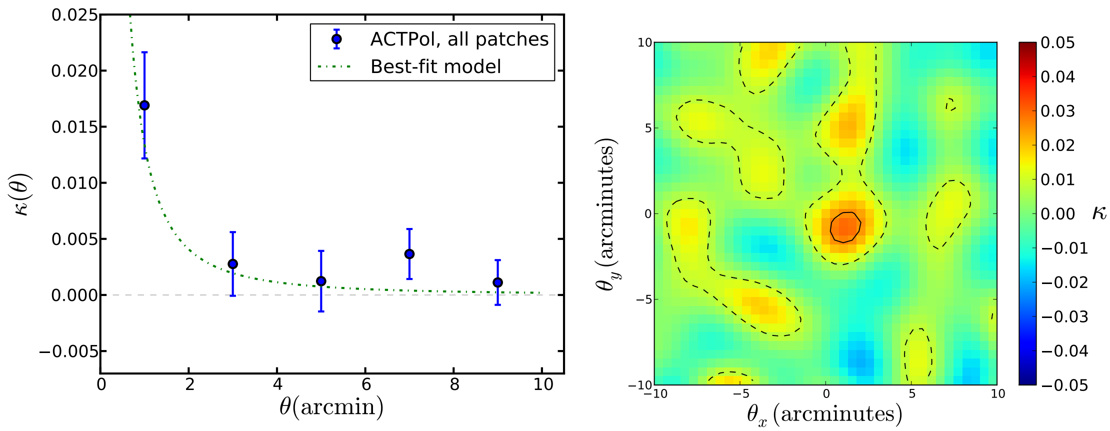

Figure 4.1: *Left*: The azimuthally averaged signal from stacked reconstructed convergence stamps centered on CMASS galaxy positions for all three ACTPol deep fields combined. The green dashed curve shows the best-fit NFW profile. *Right*: The reconstructed convergence stack in the two-dimensional plane, where the horizontal and vertical scales are in arcminutes. We also show 1σ (dashed) and 3σ (solid) contours; the signal is the dark red spot in the middle. The peak is offset by about $1'$ from the center; offsets of $> 1'$ are seen roughly 20% of the time in simulations of centered input halos given ACTPol noise levels. The detection significance above null is 3.8σ within 10 arcminutes, and the best-fit curve from [202] is preferred over null with a significance of 3.2σ within 10 arcminutes.

sured azimuthally averaged lensing convergence profile, and the right panel shows the reconstructed lensing stack in the two-dimensional plane. We note that the signal peak in the two-dimensional plot is offset by about $1'$. This is also seen in simulations of centered input halos given ACTPol noise levels, where offsets of $> 1'$ are seen roughly 20% of the time. We also note that this offset is well within the virial radius

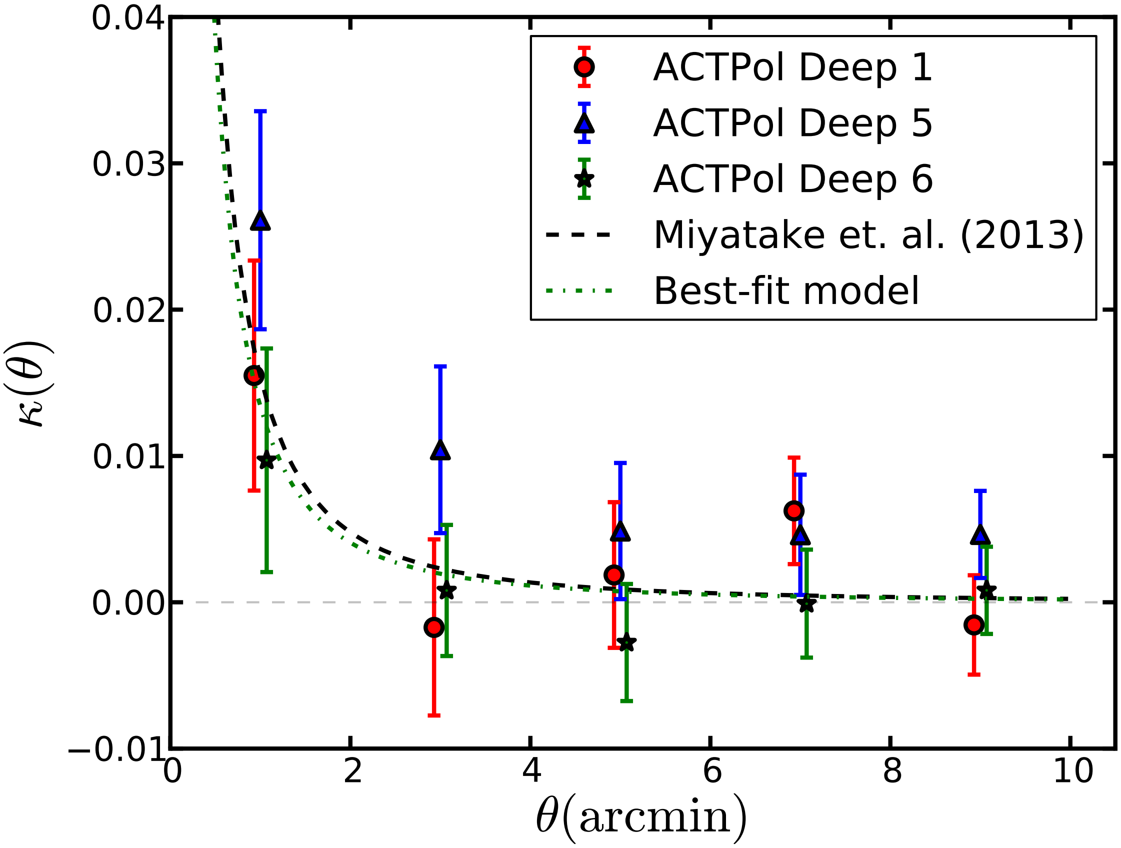

Figure 4.2: Shown are reconstructed convergence profiles centered on CMASS galaxy positions for each ACTPol deep field separately. The significance with respect to null within 4 arcminutes is 2.0σ, 3.6σ, and 1.3σ for ACTPol Deep 1, 5, and 6 respectively. The green dashed curve is the best-fit NFW profile from all the Deep fields combined, and the black dashed curve is the best-fit NFW profile from a subset of the CMASS galaxies measured via optical weak lensing [202].

of CMASS halos. The profile has been binned, with inverse-variance weighting, in annuli that are four-pixels (2 arcminutes) wide so that correlations between neighboring bins in general do not exceed 50%. The exceptions are that for the stacks on galaxy positions, the 3rd and 4th bins are correlated by 65% and the 4th and 5th bins are correlated by 70%. This is due to overlapping stamps, as the galaxy locations are more correlated than random positions.

The significance of this detection above the null hypothesis, including measured points within 10 arcminutes of the profile center, is 3.8σ. This is calculated using the combined-patch covariance matrix, $\mathbf{C}$, where

$$\left(\frac{S}{N}\right)^2 = \chi^2_{\rm null} = \sum_{\theta_1,\theta_2 \leq 10'} \kappa(\theta_1)\mathbf{C}^{-1}\kappa(\theta_2). \tag{4.11}$$

Restricting this to 4 arcminutes from the profile center, where most of the S/N is from, gives a detection significance above null of 3.6σ.

We fit the data points within 10 arcminutes from the center with an NFW profile, which is the projected and redshift-averaged mass density as in, e.g., [208]. We vary the mass and concentration and obtain a best-fit profile with a mass of $M_{200\bar{\rho}_0} = (2.0 \pm 0.7) \times 10^{13}\ h^{-1}M_\odot$ and a concentration of $c_{200\bar{\rho}} = (5.4 \pm 0.8)$. This result is obtained by imposing a prior on the c-M relation from [209] assuming Gaussian errors on the normalization of this relation of 20% as found in [202]. We note that the best-fit mass and mass error are unchanged with and without the prior; however, since there is significant degeneracy in the concentration, given our noise levels, the prior influences the best-fit $c_{200\bar{\rho}_0}$ and corresponding error. This best-fit curve gives a reduced chi-square of $\chi^2/\nu = 1.5$ for $\nu = 3$ degrees of freedom, and is consistent with the best-fit curve from [202]. The data also favors the best-fit curve from [202] over the null line ($\kappa = 0$) at a significance of 3.2σ within 10 arcminutes, where we calculate this significance using $\sqrt{\chi^2_{\rm null} - \chi^2_{\rm best-fit}}$. Restricting to within 4 arcminutes, the model is favored over null with a significance of 2.9σ.

The profile of the reconstructed lensing stack for each ACTPol patch is shown in Figure 4.2. An excess above null is seen in all three patches with a significance of 2.0σ, 3.6σ, and 1.3σ within 4 arcminutes for D1, D5, and D6 respectively. The black-dashed curve in Figure 4.2 is an NFW profile with the best-fit mass and concentration found from optical weak lensing of a subset of the CMASS galaxy sample [202]. This best-fit mass and concentration for the subset is $M_{200\bar{\rho}_0} = 2.3 \times 10^{13}\ h^{-1} M_{\odot}$ and $c_{200\bar{\rho}_0} = 5.0$, where the concentration is from the best-fit concentration-mass relation found in [202], calculated at the mean redshift of the subset ($z = 0.55$).[6]

4.5 Systematic Checks

Two different null tests are performed to verify the robustness of the signal. The first is to stack on random positions in the data. As mentioned above, all of the stacked images have a subtracted mean field stamp that is determined from averaging 15 realizations of randomly selected stamps from the data. Therefore, by construction the measured signal is the excess above that from random locations. However, we show a single random-position realization which contains the same number of stamps as are in the galaxy stack. We subtract the mean field stamp from this single realization and plot the resulting profile in the top panel of Figure 4.1 (brown circles). The data points are consistent with the null hypothesis with a probability-to-exceed (PTE) of 0.92.

[6] In [202], a best-fit of $c_{200\bar{\rho}_0} = 5.0$ is found for CMASS galaxies when their model allows for off-centering of CMASS galaxies in dark matter halos. Without this degree of freedom, a best-fit of $c_{200\bar{\rho}_0} = 3.2$ is found.

The second null test is a curl test where we repeat the analysis of stacking reconstructions centered on CMASS galaxies and subtract a mean field stamp as before. However, this time the divergence in Eq 4.7 is replaced with a curl, and the first instance of the dot product $\boldsymbol{l} \cdot \boldsymbol{l}_1$ in Eq 4.9 (not in f^{TT}) is replaced with a cross product [158, 210, 211], where both the curl and cross product are projected perpendicular to the image plane. The reconstruction is then expected to contain only noise since lensing is not expected to generate a curl signal in temperature maps. The curl reconstruction data points scatter about zero, with a PTE of 0.08, as shown in Figure 4.1 (red stars).

As can be seen in Figure 4.2, the mean signal is highest in D5. A histogram analysis of the stamps in both D5 and in the quadrant of D5 with the highest mean signal shows no apparent outliers. We note that excluding this quadrant from our analysis still results in a S/N $> 3\sigma$ within 10 arcminutes.

We also consider several possible contaminants that could bias a detection of CMB halo lensing. Ionized gas in clusters hosting the stacked galaxies could produce a decrement in the CMB temperature at 146 GHz due to the thermal Sunyaev-Zeldovich (tSZ) effect [212, 213]. In order to determine the effect of such a contaminant on the lensing reconstruction, we added a Gaussian decrement with a peak value of $-35\mu K$ and 1σ width of 1 arcminute[7] to CMB temperature maps lensed by NFW profiles as discussed above. We adopted this as a conservative level of tSZ for CMASS halos (see for example [214]). This contamination resulted in the reconstruction being biased low by about 0.3σ within 3 arcminutes at ACTPol noise

[7]The virial radius of a $10^{13} M_{\odot}$ halo at $z = 0.6$ is roughly $1.5'$.

levels, with negligible bias beyond 3 arcminutes. An identical check was performed for $35\mu K$ increments (corresponding to point source emission) with a similar suppression of the signal. In addition, no appreciable tSZ decrement or point source increment is found when stacking the stamps taken directly from CMB temperature maps and centered on the CMASS galaxies, after these stamps have been filtered to isolate modes between $1000 < l < 8000$. These checks indicate that the detected positive signals in Figures 4.1 and 4.2 do not arise from tSZ or point source emission. The kinetic SZ effect due to the bulk motion of the cluster will produce a similar symmetric increment or decrement. Furthermore, asymmetric contaminants, like those due to the kinetic SZ effect from internal gas motions, do not coherently align with the CMB gradient and only add noise by construction of the estimator.

The stacked lensing convergence measured in Figures 4.1 and 4.2 could also have contributions that are not due to CMB lensing by the halo that each galaxy resides in (the 1-halo term), but instead are due to correlated halos in the vicinity of the galaxies (the 2-halo term, [215, 216]). Since most of our detected signal is within a 2 arcminute region, where the 1-halo term dominates over the 2-halo term (see for example Figure 7 in [202]), one would not expect the 2-halo term to contribute significantly to the detection significance in this work.

4.6 Discussion

We have presented the stacked reconstructed lensing convergence of CMASS galaxies within the first season ACTPol deep fields and shown evidence of CMB lensing from these halos at a significance of 3.8σ above null. The lensing convergence is directly related to the projected density profile of these halos and hence our results demonstrate that it is possible to constrain the mass profile of massive objects using CMB lensing alone.

We find a best-fit mass and concentration from the stacked convergence stamps of $M_{200\bar{\rho}_0} = (2.0 \pm 0.7) \times 10^{13}\ h^{-1} M_\odot$ and $c_{200\bar{\rho}} = (5.4 \pm 0.8)$ fitting to an NFW profile. These mass and concentration values are in broad agreement with the optical weak lensing estimates in [202] based on a subset of the CMASS galaxy sample. Our data also favors the best-fit profile from [202] over a null line at a significance of 3.2σ within 10 arcminutes.

With this work we demonstrate that CMB observations are now achieving the sensitivity and resolution to provide mass estimates of dark matter halos belonging to galaxy groups and clusters. With the advent of next-generation CMB surveys, we expect this technique to be further exploited, thus opening a new window on the dark Universe.

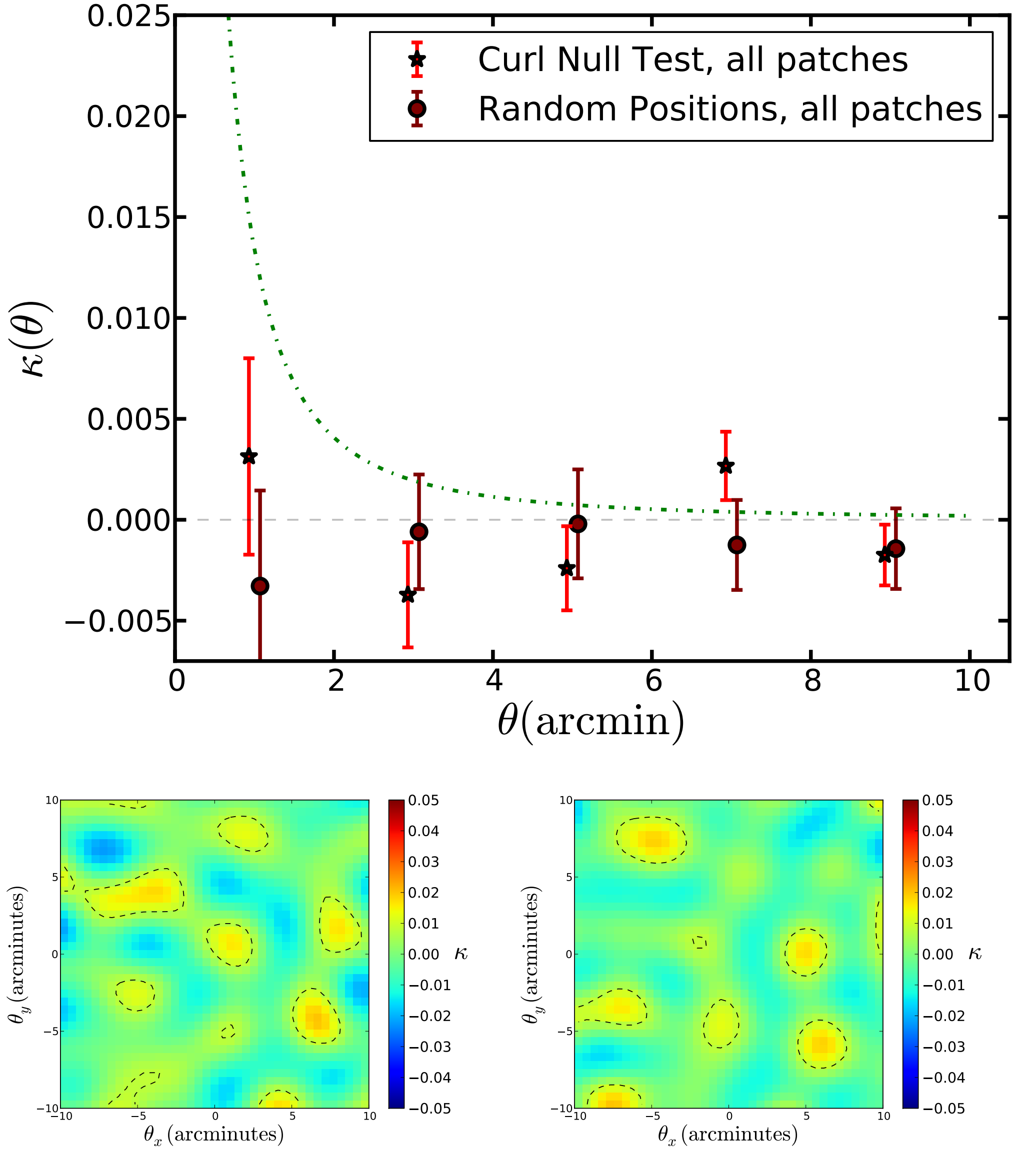

Figure 4.1: *Top panel*: Shown are the curl null test performed on the stack of reconstructed convergence stamps centered on CMASS galaxy positions, and a random-position null test where reconstructed convergence stamps are centered on random positions in the data. *Bottom panels*: Shown are the curl and random-position null tests, respectively, in the two-dimensional plane. We also show 1-sigma contours; the lack of a red spot in the middle confirms the null test.

Chapter 5

Expansion Probes of Dark Energy[1]

Cross-correlating optical weak lensing and cosmic microwave background (CMB) lensing is emerging as a powerful tool for measuring cosmological parameters and quantifying systematic uncertainties. In particular, cross-correlations between optical and CMB lensing are sensitive to structure growth, and thus dark energy properties and modifications to General Relativity on large scales [218–221]. These cross-correlations can also isolate systematic effects such as, for example, multiplicative and photo-z biases in optical weak lensing measurements [89, 90]. Recently cross-correlations using CMB lensing data from ACT, SPT, and *Planck* and optical lensing data from the CFHTLenS and DES surveys have been presented with detections of modest significance [65,89,222–227]. However, the precision of these measurements is expected to increase rapidly with newer data from, e.g., ACTPol, SPTpol, CMB-S4, HSC, DES, KiDS, and LSST.

[1]This chapter is a near-verbatim reproduction of [217], which has been submitted to *Physical Review Letters* ("Measurement of a Cosmographic Distance Ratio with Galaxy and CMB Lensing", Miyatake, Madhavacheril, Sehgal, Slosar, Spergel, Sherwin, van Engelen)

In this chapter, we present the first measurement of a particularly useful cross-correlation between optical and CMB lensing: the cosmographic distance ratio. This measurement is obtained by measuring the gravitational lensing shear around a particular set of dark matter halos, first using background galaxies as the lensed source plane and then using the CMB as the lensed source plane. Taking the ratio of these shear measurements results in a purely geometric distance measurement that is insensitive to the details of the mass distribution around the lensing halos, their galaxy bias, or potential miscentering [91, 228–231]. The ratio is given by

$$r = \frac{\gamma_t^o}{\gamma_t^c} \sim \frac{d_A(z^c) d_A(z^L, z^g)}{d_A(z^g) d_A(z^L, z^c)} \tag{5.1}$$

where γ_t^o and γ_t^c are the optical and CMB tangential shear, d_A is the angular diameter distance, and z^c, z^g, and z^L are the redshifts to the CMB, the background galaxy source plane, and the lensing structure respectively [92, 93]. This ratio has been measured previously when both source planes have been background galaxies with $z < 2.5$ [232–236]. However, the advantage of using the CMB as the second source plane is that it provides the longest lever arm for distance ratios, which can result in an order of magnitude higher sensitivity to dark energy parameters [92, 93]. In this chapter, we present the first measurement of such a ratio using data from *Planck*, CFHTLenS, and the BOSS CMASS galaxy sample. The CFHTLenS measurement is made for 8,899 CMASS galaxies spanning an area of 105 square degrees, and the *Planck* measurement is made for 654,279 CMASS galaxies spanning an area of 8,502 square degrees.

5.1 Data & Method

5.1.1 The Lenses: BOSS CMASS Galaxies

For the foreground lens sample, we use the CMASS selection of galaxies from the DR11 release of the BOSS spectroscopic survey. These mostly red galaxies constitute an approximately volume-limited selection of luminous galaxies from SDSS-III that span a redshift range of $0.4 < z < 0.7$. They are very often (90%) at the center of their host halos [237] with masses of around $M_{200} = 2 \times 10^{13} M_{\odot}$, measured both from optical [238] and CMB lensing [65]. As such, they are excellent tracers of massive halos that lens background sources. The entire sample covers roughly 20% of the sky.

In both the optical and CMB analyses, each CMASS lens galaxy is weighted as follows,

$$w_l = (w_{\rm noz} + w_{\rm cp} - 1) w_{\rm see} w_{\rm star} \tag{5.2}$$

so as to account for redshift failures ($w_{\rm noz}$), fiber collisions ($w_{\rm cp}$), effects of seeing ($w_{\rm see}$) and stars ($w_{\rm star}$) [239]. To reduce systematics associated with the width in redshift of the sample, we divide the sample into three redshift slices (see Table 5.1) and perform the analysis separately in each redshift slice, combining the results only when calculating the final distance ratio at an effective redshift (see Results Section). For completeness, we also perform the analysis on the full sample in one wide redshift bin (see Figure 5.3), but do not obtain cosmological constraints from this.

Table 5.1: Number of CMASS Galaxies Used

Redshift Range	Galaxy Density (per arcmin^2)	Optical Analysis	CMB Analysis
$0.43 < z < 0.51$	0.007	2,895	211,441
$0.51 < z < 0.57$	0.007	2,896	213,497
$0.57 < z < 0.7$	0.008	3,108	229,341
$0.43 < z < 0.7$	0.021	8,899	654,279

5.1.2 Source Plane 1: CFHTLenS Galaxies

We use the public CFHTLenS catalog [240, 241] for calculating the optical tangential shear. The total area of the CFHTLenS survey is 154 deg^2 in four distinct fields. The overlapping area with the SDSS DR11 data is 105 deg^2 which contains 8,899 CMASS galaxies.

The catalog has galaxy shapes, which were measured by a Bayesian model-fitting method called *lens*fit [242], and photometric-redshifts (photo-zs) which were estimated with the BPZ code [243, 244] by using point-spread-function (PSF) matched photometry [245]. The effective number density of CFHTLenS source galaxies is 14 arcmin^{-2}.

The tangential shear in the i-th radial bin is measured by stacking galaxy shapes of lens-source pairs;

$$\langle \gamma_t^o(R_i) \rangle = \frac{\sum_{R_i} w_{ls} e_t^{ls}}{\sum_{R_i} w_{ls}}, \tag{5.3}$$

where e_t is the tangential component of galaxy shapes, w_{ls} is a weight which is the product of the CMASS galaxy weight w_l given by Eq. (5.2) and the inverse-variance weight for galaxy shapes w_s provided by the CFHTLenS catalog that is estimated from the intrinsic galaxy shape and measurement error due to photon noise. Here the source galaxies are selected so that the best-fit photo-z is greater than the lens redshift.

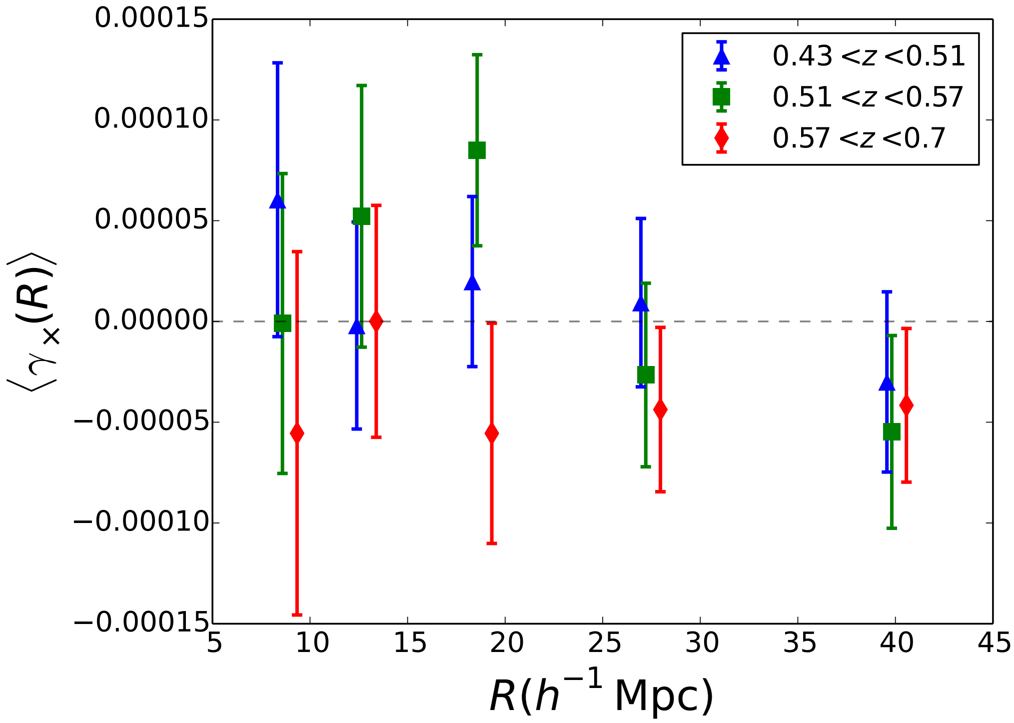

Figure 5.1: Null test of optical lensing signal. The $R \sim 40\,h^{-1}$Mpc bins are consistently smaller than zero for all the redshift slices, and thus we do not use them. The p-value based on the χ^2 per degree of freedom of the 12 $R \lesssim 30\,h^{-1}$Mpc bins over the redshift slices is 0.82, which is within a 95%CL region. Thus we use these 12 data points for the distance ratio analysis.

The covariance matrix of the tangential shear is estimated by measuring the tangential shear around 150 realistic mock catalogs of the CMASS sample generated from N-body simulations [246,247]. Using these CMASS mocks, we naturally include sample variance, which can be important given the small area of the CFHTLenS suvey. We use 150 realizations of mocks to reduce the uncertainty of the covariance. At the scales used for this distance ratio analysis, the uncertainty due to lens shot noise and sample variance dominates the statistical uncertainty; it is about 1.5 times larger than the statistical uncertainty due to intrinsic galaxy shapes and becomes as large as a factor of four in the largest radial bin. The noise due to sample variance also induces correlations between neighboring bins, which are typically ~ 0.5 for the $R \gtrsim 10\, h^{-1}$Mpc bins. Note that we could have canceled this sample variance exactly, by using exactly the same subset of galaxies to measure lensing of the CMB. However, given the large noise in the *Planck* convergence map, our overall statistical uncertainty would have increased.

If the PSF correction is imperfect, it can contaminate the tangential shear. To estimate this effect, we calculate the tangential shear around random points. We use 50 realizations of random points to reduce statistical uncertainties [248]. The random signal is non-zero for $R \gtrsim 20 h^{-1}$Mpc. We then make a PSF correction by subtracting this random signal from the lensing signal. If the correction works, the 45-degree-rotated shear should be consistent with zero. Figure 5.1 shows the 45-degree-rotated shear after the correction for each radial bin in each redshift slice. We use signal at $R \lesssim 30\, h^{-1}$Mpc for the distance ratio analysis. The $R \sim 40\, h^{-1}$Mpc radial bins are consistently smaller than zero for all the redshift slices, and thus we do not use them. The p-value based on the χ^2 per degree of freedom of the 12 $R \lesssim 30\,h^{-1}$Mpc radial bins over the redshift slices is 0.82, which is within a 95%CL region. Thus we use these 12 data points for the distance ratio analysis shown in Figure 5.1. We show the final optical tangential shear for the full redshift range in Fig. 5.3.

5.1.3 Source Plane 2: Planck CMB Map

To extract a corresponding shear profile of CMASS halos using the CMB as the background light source, we prepare a `HEALPIX` map [249] of the CMASS galaxy overdensity (with $\texttt{nside} = 1024$) for each redshift slice and cross-correlate it with the *Planck* reconstructed lensing convergence κ map [250]. Thus we obtain an estimate of $C_l^{\kappa\delta_g}$ in Fourier-space, which we then convert to a real-space shear estimate, $\langle\gamma_t^c(R)\rangle$, as discussed below.

To create the galaxy overdensity map of CMASS galaxies, for each `HEALPIX` pixel $\mathbf{x}$, we assign a number given by

$$\delta_g(\mathbf{x}) = \frac{\sum_{i\in\mathbf{x}} w_i}{\frac{1}{N}\sum_i w_i} - 1 \tag{5.4}$$

where $\sum_{i\in\mathbf{x}} w_i$ sums over the weights of each CMASS galaxy i that falls in that pixel $\mathbf{x}$, and where $\frac{1}{N}\sum_i w_i$ sums over the weights of all CMASS galaxies in all unmasked pixels and then divides by the total number of unmasked pixels N. Here the weight $w_i = w_l w_s(z)$, where w_l is the BOSS systematic weight given in Eq. (5.2) and $w_s(z)$ is an effective CFHTLens weight. We include the CFHTLens weights here, which have been interpolated as a function of lens redshift, because in the optical analysis they change the median redshift of the lens galaxies within a redshift slice.

When comparing with the CMB signal, it is important that the median redshift of the lens sample is the same since galaxy properties could evolve as a function of redshift. Although the effect of such an evolution is mitigated by our use of thin redshift slices, we still weight the lens galaxies in the CMB analysis consistently with the optical analysis.

The mask used in this analysis is a combination of a mask derived from the completeness of the BOSS galaxies, where we exclude regions where the completeness is below 70%, and the convergence mask provided with the *Planck* 2015 lensing data release. For the CMASS mask, we have checked that decreasing the minimum completeness to 10% has a negligible impact on the results since most of the survey area is close to 100% complete. For the *Planck* convergence mask, we note that it masks out galaxy clusters identified through the thermal Sunyaev-Zeldovich effect.

We obtain a C_l estimate of the cross-correlation by summing over spherical harmonic transform coefficients of the galaxy overdensity and CMB kappa maps, with the appropriate correction for fractional sky coverage ($f_{\rm sky} = 0.206$ for 8,501 deg^2),

$$\hat{C}_l^{\kappa\delta_g} = \frac{1}{(2l+1)f_{\rm sky}^{\kappa\delta}} \sum_{m=-l}^{l} \delta_{lm}\kappa_{lm}. \tag{5.5}$$

We then convert the cross-correlation estimate in Fourier-space to the real-space tangential shear of the CMB associated with CMASS galaxies, $\langle\gamma_t^c(R)\rangle$, via a Hankel transform (e.g Eq.2 in [254]),

$$\langle\gamma_t^c(R)\rangle = \frac{1}{2\pi}\int \ell d\ell J_2(\ell R/\chi) C_\ell^{\kappa\delta_g}. \tag{5.6}$$

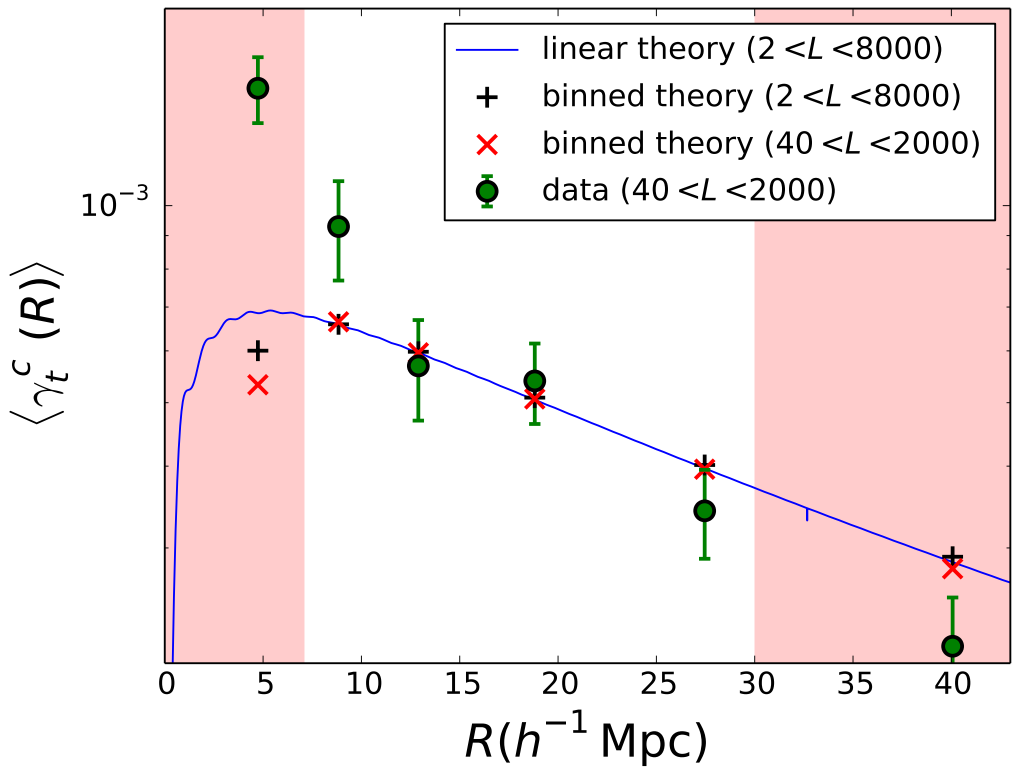

Figure 5.2: Theory expectation of CMB tangential shear using an input $C_l^{\kappa\delta_g}$ curve from $2 < L < 8000$ generated with a linear matter power spectrum from `CAMB Sources` [251–253] with a linear galaxy bias of 2. We also show the effect of restricting the $C_l^{\kappa\delta_g}$ to the range $40 < L < 2000$, which is the L range of the *Planck* κ-map. We do not use radial bins that have a mismatch between black crosses and red x's (shaded regions) as that would make the optical and CMB analyses inconsistent. The green points show the shear from the data, and where those points deviate from the theory at small scales is where there is sensitivity to the one-halo term from the CMASS galaxy halos themselves.

Note that this is exact only in the flat-sky limit, however we do not probe radial scales large enough that we should be sensitive to the effects of a curved sky. Using Simpson's rule on the discrete set of $C_l^{\kappa\delta_g}$'s, this integral is calculated at 5000 radial points and averaged in radial bins R corresponding to the optical analysis. Note that the errors are uncorrelated between l bins to a very good approximation in Fourier space, and are highly correlated between radial bins in real space. The latter is appropriately accounted for as described below.

To generate an expected theory curve we compute the shear transform in Eq. (5.6) using an input $C_l^{\kappa\delta_g}$ curve generated with a linear matter power spectrum from `CAMB Sources` [251–253] with a linear galaxy bias of 2. This is shown in Figure 5.2 both as the unbinned blue curve and as the black crosses binned identically to the data. We also show here the result of restricting the $C_l^{\kappa\delta_g}$ to the range $40 < L < 2000$, which is the L range of the *Planck* κ-map used in this analysis. (Modes with $L < 40$ can be affected by the treatment of the mask, and *Planck* does not report modes with $L > 2048$). Including $2000 < L < 8000$ corresponds better to the resolution of the CFHTLenS survey, and in Figure 5.2 we show a significant difference at $R \sim 5\ h^{-1}$Mpc between $L < 2000$ and $L < 8000$. Thus we do not include this bin in our distance ratio analysis. For a similar reason, we exclude the radial bin at $R \sim 40\ h^{-1}$Mpc. The green points in Figure 5.2 show the real-space shear from the data, and where those points deviate from the theory curve at small scales indicates where the measurement is sensitive to the one-halo term from the CMASS galaxy halos themselves (which is not included in the theory curve).

We use 600 realizations of the CMASS mocks to make the covariance matrix and repeat the procedure above, cross-correlating a galaxy overdensity map generated from each mock with the *Planck* data κ-map, and then transforming that into a shear estimate. We note that there is no correlated structure between the *Planck* data map and the CMASS mocks, so that the resulting covariance matrix does not include sample variance from this correlated structure. However, this effect is expected to be negligible since the noise in the CMB κ-map is expected to dominate. We check this by calculating Fisher-matrix theory errors with and without this $C_l^{\kappa\delta_g}$ term (see, e.g., Eq. 15 in [225]), and find agreement to within 1% between the two.

5.2 Results

Shear profiles, $\gamma_t(R)$, are related to the underlying projected mass density, $\Sigma(R) = \int d\chi\rho(R,\chi)$, through the relation

$$\gamma_t(R) = \frac{\Delta\Sigma(R)}{\Sigma_{\rm cr}} = \frac{\bar{\Sigma}(<R) - \Sigma(R)}{\Sigma_{\rm cr}} \tag{5.7}$$

where $\bar{\Sigma}(<R)$ is the average mass density within a circle of radius R, and $\Sigma_{\rm cr}$ is the critical surface mass density. We note that $\Delta\Sigma(R)$ depends only on the total matter distribution of the lens, and $\Sigma_{\rm cr}$ is a purely geometric quantity since it depends only on the distances to the lens and background sources. Since the criteria used to select the lensing galaxies is the same in the regions where the optical and CMB analyses are performed, we assume that the underlying $\Delta\Sigma(R)$ is identical in both cases. This

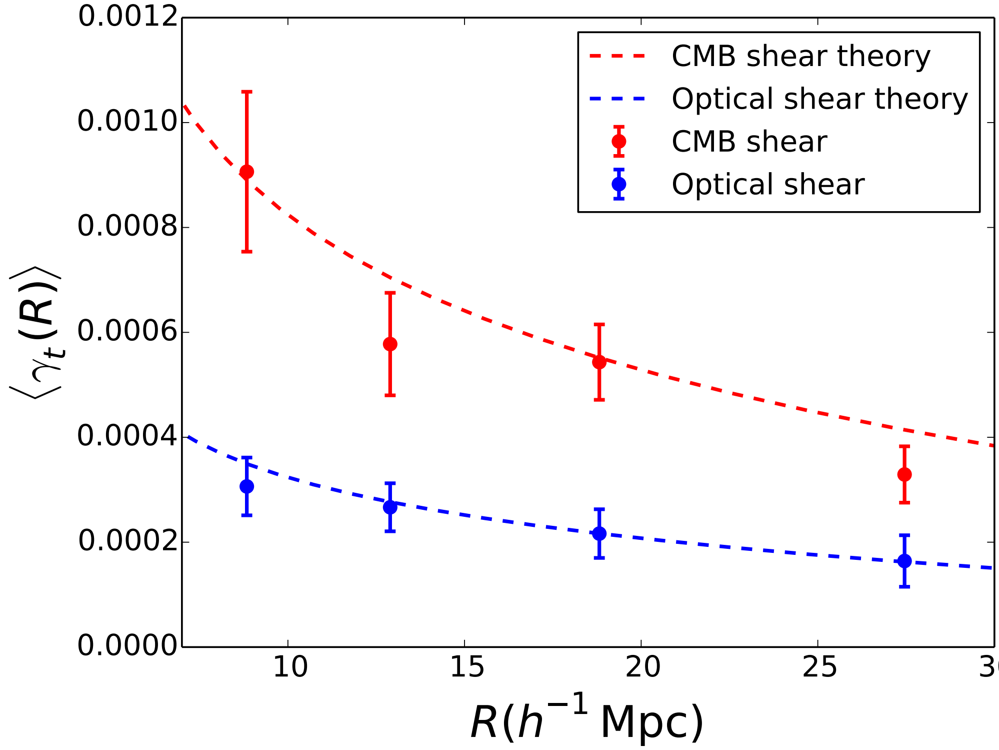

Figure 5.3: CMB and optical shear around CMASS halos in the redshift range $0.43 < z < 0.7$. The dashed blue curve shows a theory fit to the optical data, which includes both the 1-halo and 2-halo terms. This red curve is given by scaling up the blue curve to the CMB source redshift.

allows us to write the expected distance ratio as

$$r(\{c_p\}) = \frac{\gamma_t^o}{\gamma_t^c} = \frac{\Sigma_{\rm cr}^{\rm CMB}(\{c_p\})}{\Sigma_{\rm cr}^{\rm opt}(\{c_p\})} \tag{5.8}$$

where the dependence on the cosmological parameters, $\{c_p\}$, enters through the distance-redshift relations. Here the numerator is the critical surface density for

CMB lensing, which is calculated as

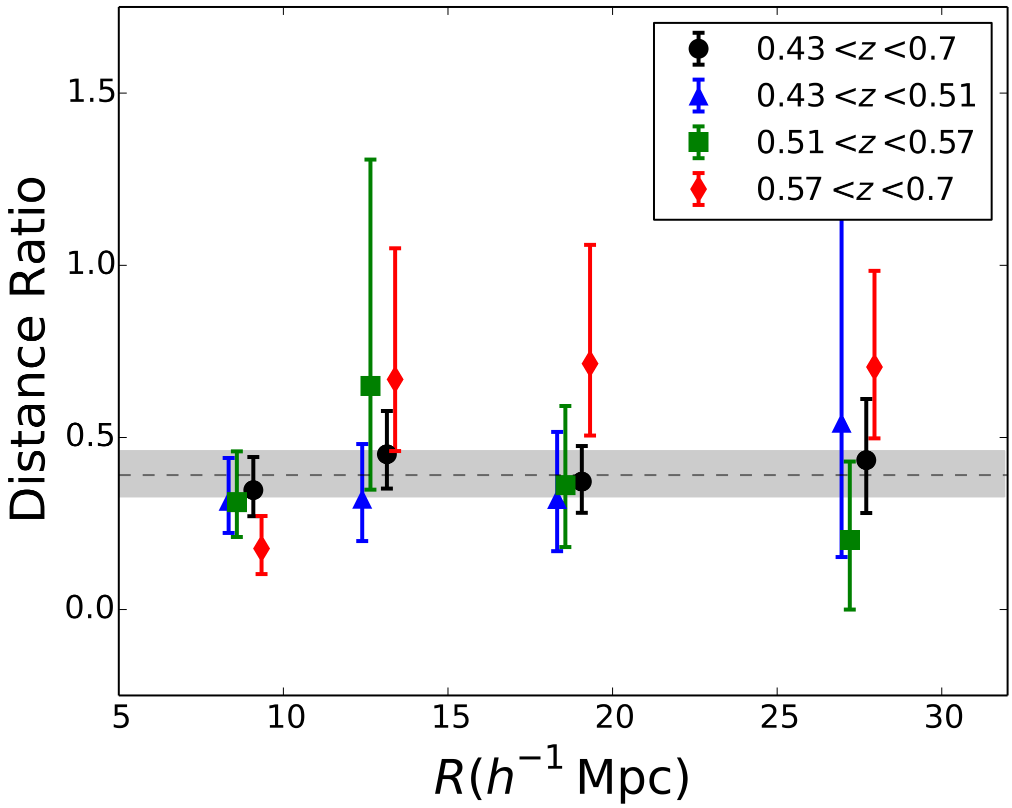

Figure 5.1: Measured distance ratio for each radial bin and redshift slice of CMASS galaxies. Here the error bars are derived by Monte Carloing the covariance matrices for optical and CMB measurements, taking the ratio for each realization, and showing the 68% CL region around the mean ratio. The dashed line and error band show $r = 0.390^{+0.070}_{-0.062}$, the best-fit value coadding all the radial bins and simultaneously fitting to the three redshift slices.

$$\Sigma_{\rm cr}^{\rm CMB} = \left[\frac{\sum_{ls} w_l P_{\rm stacked}(z_s|z_l) \Sigma_{\rm cr}^{-1}(z_l, z_{\rm CMB}; \{c_p\})}{\sum_{ls} w_l P_{\rm stacked}(z_s|z_l)} \right]^{-1} \tag{5.9}$$

where $z_{\rm CMB} = 1100$ is the redshift to the surface of last scattering, and the sum is over CMASS lenses. The critical surface density $\Sigma_{\rm cr}^{-1}$ is related to the angular diameter distances as,

$$\Sigma_{\rm cr}^{-1} = \frac{4\pi G}{c^2}\frac{d_A(z_l, z_s)d_A(z_l)(1+z_l)^2}{d_A(z_s)}. \tag{5.10}$$

Here $d_A(z_s), d_A(z_l)$, and $d_A(z_l, z_s)$ are the angular diameter distances to the source, lens, and between the source and lens respectively. The $(1+z_l)^2$ factor comes from our use of comoving transverse separation R in $\Delta\Sigma(R)$. To use the same weight as the optical measurement, we use the photo-z PDF stacked over optical source galaxies behind a given lens redshift;

$$P_{\rm stacked}(z|z_l) = \frac{\sum_s w_s P_s(z|z_l)}{\sum_s w_s}. \tag{5.11}$$

The denominator in Eq. (5.8) is given by the equivalent expression for optical lensing.

$$\Sigma_{\rm cr}^{\rm opt} = \left[\frac{\sum_{ls} w_l P_{\rm stacked}(z_s|z_l)\Sigma_{\rm cr}^{-1}(z_l, z_s; \{c_p\})}{\sum_{ls} w_l P_{\rm stacked}(z_s|z_l)}\right]^{-1}. \tag{5.12}$$

Note that the dilution effect due to foreground galaxies selected as source galaxies is effectively corrected for here.

Comparison with Different Cosmological Models: In Fig. 5.3 and 5.1, we show the measured tangential shear for the wide redshift slice and distance ratio for each radial bin and redshift slice of CMASS galaxies, respectively. Fig. 5.2 shows the coadded distance ratio for each redshift slice. We also include the distance ratio simultaneously fitted to the three redshift slices. In doing this, we assume the ratio linearly depends on redshift, i.e., $r(z) = r_0 + r'(z - z_\mathrm{p})$, where z_p is the "pivot" redshift determined so that the errors on r_0 and r' are uncorrelated. This yields $r = 0.390^{+0.070}_{-0.062}$ at a pivot redshift of $z_\mathrm{p} = 0.53$, a 17% measurement of distance ratio. In Fig. 5.2, we also show the ratio predicted for different cosmological models as a function of lens redshift using Eq. (5.8), assuming all the lenses are at a single redshift. Measurements of r' are very poor due to the limited redshift span and were included in this solely to determine the pivot redshift.

In Fig. 5.2, we also show the ratio predicted for different cosmological models as a function of lens redshift using Eq. (5.8), assuming all the lenses are at a single redshift. The solid/dashed curves show the ratio for the best-fit ΛCDM/wCDM models from the *Planck* TT + lowP spectra [255]. The ratio between ΛCDM and wCDM models changes within a smaller range compared to our statistical uncertainty, which means it is difficult to place tight constraints in spite of the 17% accuracy of our measurement.

Since we have thin redshift slices that have a finite width, as opposed to being delta functions in redshift, we explore how the finite width of our slices affects our measurement. We test this by recalculating the predicted ratio in each redshift slice with a delta-function distribution at the median redshift, and find that the predictions differ from those calculated with finite redshift distirbutions by 13% to 27% of the statistical uncertainty of our measurement, depending on the redshift slice. This can be regarded as the maximum systematic uncertainty due to our finite-width redshift slices, and indicates the impact is small compared to the statistical uncertainty of our measurement.

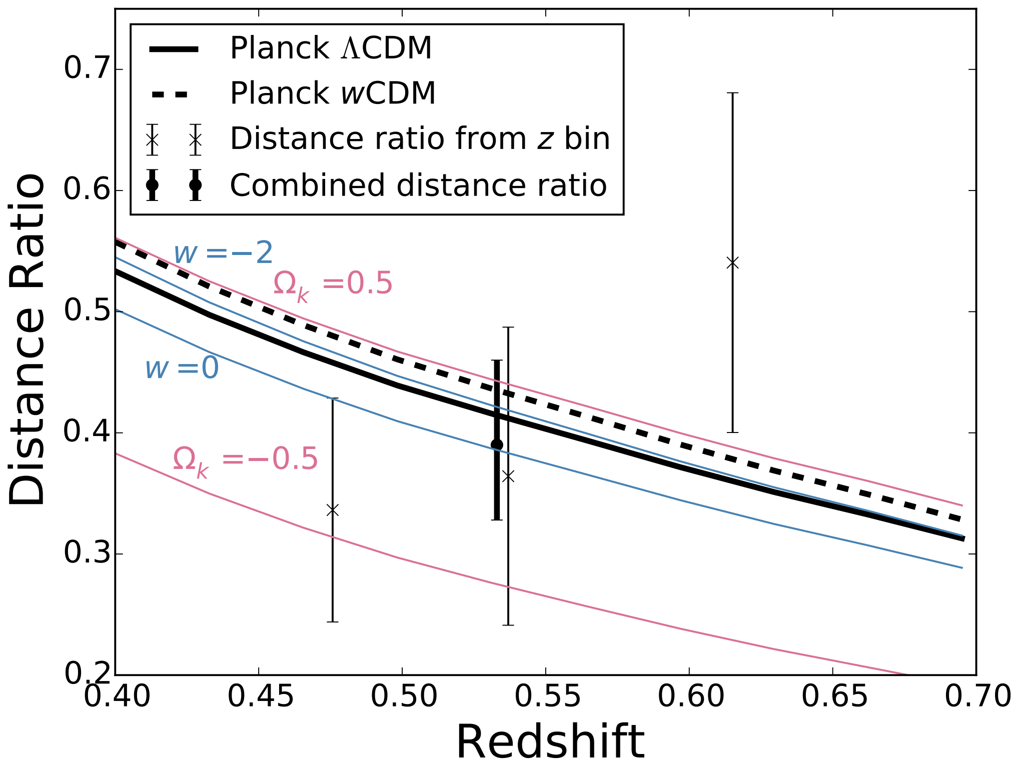

Figure 5.2: Comparison of the measured distance ratio with that predicted from different cosmological models. The thin cross points show the measured distance ratio fitted separately for each redshift slice. The thick dot point shows the distance ratio fitted to all the redshift slices simultaneously assuming linear dependence of the ratio on redshift (see text for details). The black solid and dashed curves show the ratio for the best-fit ΛCDM and wCDM models respectively from the *Planck* TT + lowP spectra [255]. The thin solid curves show deviations from the best-fit *Planck* ΛCDM model as indicated.

As potential systematic uncertainties of the optical shear analysis, we explore the effect of possible multiplicative shear bias m and photo-z bias b_z on the optical measurement. To constrain these biases, we minimize the following quantity,

$$\chi^2(m, b_z) = \sum_\alpha \sum_{ij} d_i \mathrm{Cov}_{ij}^{-1} d_j, \tag{5.13}$$

where $d_i = \gamma^o(R_i; m) - r(\{c_p\}, b_z)\gamma^c(R_i)$ for the ith radial bin, and the covariance is given by

$$\begin{aligned} \mathrm{Cov}_{ij} \;=\;& \mathrm{Cov}(\gamma^o(R_i), \gamma^o(R_j)) \\ & -2r\mathrm{Cov}(\gamma^o(R_i), \gamma^c(R_j)) \\ & +r^2\mathrm{Cov}(\gamma^c(R_i), \gamma^c(R_j)). \end{aligned} \tag{5.14}$$

We ignore the second term in Eq. (5.14) because the overlapping region for the two measurements is less than 2% of the region used in our CMB analysis. The index α in Eq. (5.13) runs over the three redshift bins of the CMASS sample shown in Table 5.1. Correlations between z-bins due to sample variance are not included because the contribution from clustering of CMASS galaxies was found to be subdominant to the contributions from CMB lensing reconstruction noise, Poisson noise of CMASS counts, and shape noise of CFHTLens galaxies.

Since these biases affect the overall amplitude of the lensing signal, they are totally degenerate. Thus we investigate these biases separately. First, we parametrize multiplicative bias as $\gamma^o_{\mathrm{obs}} = (1+m)\gamma^o_{\mathrm{true}}$, and fit the distance ratio with cosmological parameters fixed to the *Planck* best-fit ΛCDM cosmology. The obtained constraint is $m = 0.00^{+0.18}_{-0.16}$. Second, we parameterize the photo-z bias as a shift of photo-z PDF, i.e., $P(z) \to P(z + b_z)$. To avoid calculating the optical lensing signal with a new source galaxy selection every time b_z is updated, we calculate the lensing signal without any source galaxy selection, which means all the dilution correction is put into $\Sigma_{\rm cr}^{\rm opt}$. With the fixed cosmology, we obtain $b_z = 0.00^{+0.13}_{-0.12}$. These results indicate (under the assumption of standard ΛCDM cosmology) that there is no significant evidence of systematic uncertainties in our optical shear measurement.

The central values of these biases are close to zero because the theoretical expectation of the ratio is quite close to our measurement (within 1%) when using our finite-width redshift slices, as opposed to the expected value from a delta-function lens redshift as shown by the solid curve in Fig 5.2.

We also note that our analysis includes CMB lensing angular scales in the range $400 < L < 2000$, which region was excluded from the *Planck* lensing autospectrum analysis [250]. The reason for this exclusion was due to a failure of the curl null test around $L \sim 700$. While there may be a systematic affecting the autospectrum analysis, in general, one would expect many systematics to not be present in a cross-correlation analysis. However, as the cause of the autospectrum systematic is unknown, we flag this as a caveat to the above analysis.

5.3 Discussion

In this work we have for the first time computed the distance ratio using optical and CMB weak lensing, yielding a 17% measurement. We have used BOSS CMASS galaxies for the lensing galaxies, and CFHTLenS galaxy shapes and the *Planck* convergence map for optical and CMB background sources, respectively. The distance ratio extracts a purely geometrical factor by canceling out the matter distribution around halos, and thus we are free from systematic uncertainties arising from modeling galaxy bias and miscentering. Our distance ratio is consistent with the predicted ratio from the *Planck* best-fit ΛCDM cosmology.

Separation of the lenses into thin redshift slices, which is enabled by the spectroscopic information in the CMASS sample, (a) allows us to make independent measurements of the distance ratio at three different redshifts, providing consistency checks, (b) makes the measurement less sensitive to variations in the mass distribution as a function of redshift, and (c) naturally avoids loss of signal-to-noise due to weighting of CMASS galaxies by CFHTLenS weights when applying these weights in the CMB analysis, although the latter effect is almost negligible.

In our CMB shear anlaysis, the dominant contribution to the noise is from the noise in the *Planck* reconstructed lens map. In our optical shear analysis, sample variance and shot noise of the CMASS subsample dominates the statistical uncertainty. This is because the CFHTLenS survey consists of four small fields far apart from each other. This fact demonstrates the importance of correct covariance estimation for a survey with patchy configuration of fields.

Optical surveys such as HSC, DES, KiDS, LSST, WFIRST and Euclid are expected to provide orders of magnitude larger samples of background sources as well as large foreground samples with accurate photometric redshifts from red sequence calibration. In addition, datasets from surveys like DESI and PFS will provide large foreground samples with spectroscopic redshifts. Combining this with wide and deep high-resolution maps of CMB lensing from AdvancedACT, SPT3G, the Simons

Observatory, and eventually CMB Stage-4, the coming decade will allow for measurements of the distance ratio to within 1% making it a competitive and complementary probe of curvature and cosmic acceleration.

Chapter 6

Summary and Conclusions

Understanding the nature of dark matter and dark energy is a major goal in the study of cosmology. One aspect of this is using astronomical techniques to constrain the different possible particle physics models of dark matter. By utilizing measurements of the CMB, in Chapter 2 we set tight constraints on the mass and cross-section of dark matter particles through the effect of their annihilations on the physics of the early Universe. The way that matter clusters as the Universe expands is affected by the precise nature of dark energy, so it is crucial to map the distribution of matter (including the dominant dark matter) as a function of cosmic time. Gravitational lensing of light sources behind the matter distribution is the most promising way of mapping dark matter. In Chapter 3, we improve upon methods of estimating the lensing signal from shapes of galaxies by developing a prescription that avoids bias due to noise in galaxy images. Because the CMB is behind every possible matter distribution that can act as a lens, and because the distance to the CMB is very well measured, lensing of the CMB is a more promising way of measuring the masses of dark matter halos at high redshifts than lensing of galaxies. We present the first measurement of lensing of the CMB by dark matter halos in Chapter 4. This thesis concludes in Chapter 5 by tying optical and microwave measurements together. We demonstrate for the first time a way of constraining dark energy through its effect on the expansion history using ratios of CMB and galaxy lensing signals. Together, this work demonstrates the incredible potential that measurements in the microwave and optical have for constraining theories of dark matter and dark energy.

Several large cosmological surveys will deploy in the coming decade, allowing for vast improvements in the measurements made in this thesis. The Large Synoptic Survey Telescope (LSST) [79] and the proposed Cosmic Microwave Background Stage IV (CMB-S4) experiments, both deploying after 2020, will be game-changers whose immense statistical power will set stringent requirements on control of systematics. In the nearer term, Advanced ACTPol [256] has already seen first light, and will map half the CMB sky at the same or better sensitivity as ACTPol.

We saw in Chapter 2 that the potential for improving the constraint on dark matter annihilation comes primarily from improved large scale polarization power spectra, rather than from small scales. The constraint we set has been improved by more than a factor of three in the Planck 2015 release [257], primarily thanks to the addition of newly released large-scale polarization power spectra. Since polarization power spectra are not yet cosmic variance limited at large scales, there is some room for improvement, and we forecast that a Stage IV CMB experiment comes very close to exhausting the cosmic variance limit. If the reported anomalous signals from direct and indirect experiments are due to thermal WIMPs, then CMB-S4 can confirm or rule out these signals.

In Chapter 3, we demonstrated with a toy model how a generalized higher-order estimator can be used to avoid biases in measurements of the shear when the shear is not constant across the sky. We have left a demonstration of the feasibility of this method on realistic galaxy images to future work. Recently, the GREAT3 public challenge for shear estimation [258] received several submissions that pass the LSST requirement for control on systematics in the case of constant shear, but for the case of varying shear, the submissions did not meet the target. This highlights the importance of further work on robust estimation of varying shear.

The first detection of halo lensing of the CMB presented in Chapter 3 was subsequently followed by measurements from the South Pole Telescope (SPT) [66] and Planck experiments [67]. The 3.1σ SPT measurement utilized a maximum likelihood technique to estimate the mass scale of 512 tSZ-selected galaxy clusters. Shortly after, the Planck experiment measured halo lensing of the CMB, and used it as one of the way of calibrating the masses of galaxy clusters in a full cosmological analysis of their sample of tSZ selected clusters. Using a matched filter on CMB lensing maps reconstructed (from tSZ-cleaned maps) using a quadratic estimator technique similar to our analysis, they obtained a $\sim 5\sigma$ detection of the mass scale of 439 galaxy clusters. The mass scale that they obtain is in slight tension with that required for their estimation of the amplitude of matter fluctuations to be consistent with the expectation from the Planck primordial CMB power spectrum, and also in slight tension with optical weak lensing measurements used in their analysis. Very soon, experiments like Advanced ACT, SPT-3G [259], the Simons Observatory [1] and eventually CMB-S4 will have several thousand tSZ-selected galaxy clusters that can be used in a cosmological analysis, and these will be accompanied by high resolution deep maps that can be used to estimate the lensing signal to very high precision (see Figure 6.1 for projected mass sensitivities for a futuristic CMB survey). It is therefore of great importance that detailed studies of the systematics affecting these measurements is undertaken. For example, the effects of residual tSZ in component separated maps and mis-centering when stacking are of immediate concern. The kinetic Sunyaev-Zeldovich (kSZ) effect due to the motion of galaxy clusters cannot be removed by component separation due to its weak spectral dependence and could hence pose an unavoidable limiting systematic. The effect of tSZ and kSZ could however be mitigated to a significant degree by using polarization maps instead of temperature maps, since the S/N in the 'EB' lensing estimator becomes almost comparable to that in the 'TT' estimator at the low noise levels of upcoming CMB experiments.

As noted in Chapter 4, several planned CMB, optical and spectroscopic surveys plan to have large overlapping regions. For example, Advanced ACT and CMB-S4 will map microwave temperature and polarization over roughly 40% of the sky, which will overlap significantly with photometric imaging of galaxies from LSST and also with spectroscopic redshifts of galaxies from DESI [260]. A measurement like the cosmographic distance ratio will benefit hugely from this since AdvACT/StageIV can provide high-fidelity measurements of the CMB as a source that is lensed, LSST will provide dense catalogs of background galaxies as a second set of sources that

[1] `https://twitter.com/SimonsObs/status/730824405312376832`

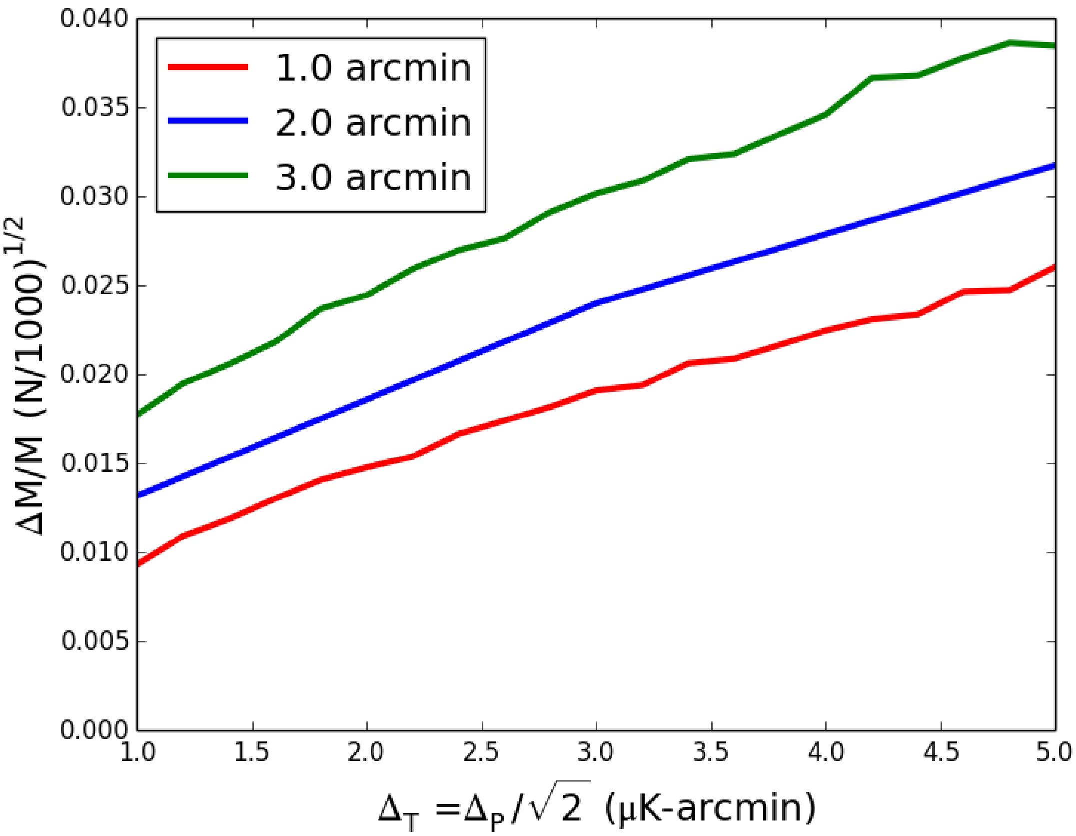

Figure 6.1: The mass sensitivity for galaxy clusters achievable by a future CMB survey like CMB-S4 as a function of noise in the CMB maps for various beam sizes.

are lensed, and DESI can provide the foreground massive galaxies that host the lensing halos. This can lead to a 1% distance ratio measurement that will provide a powerful check on the cosmological concordance model (see Fig 6.2 for projected improvements).

The next two decades will bring a deluge of data from across the electromagnetic spectrum[2]. In preparation for this, there is a marked shift towards a focus

[2]Recent detections of gravitational waves by LIGO [261] add a whole other window for investi-

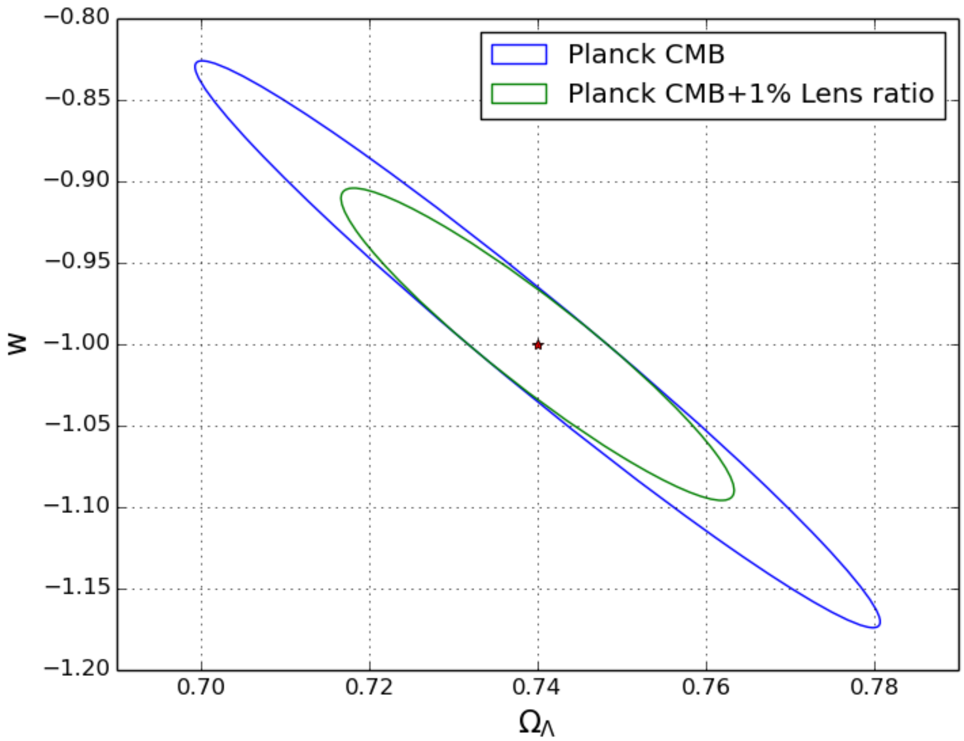

Figure 6.2: The improvement in 68% constraints on the dark energy density and equation of state when adding a 1% distance ratio measurement to the Planck primary CMB measurements. (From [93])

on exquisite control of systematics and cross-correlations between different probes. The increased precision on cosmological parameters and the availability of multiple probes for cross-checks will bring us closer to uncovering the nature of dark matter and dark energy.

---

gating the Universe.

Bibliography

[1] H. W. Babcock, "The rotation of the Andromeda Nebula," *Lick Observatory Bulletin*, vol. 19, pp. 41–51, 1939.

[2] V. C. Rubin and W. K. Ford, Jr., "Rotation of the Andromeda Nebula from a Spectroscopic Survey of Emission Regions," *Astrophysical Journal*, vol. 159, p. 379, Feb. 1970.

[3] V. C. Rubin, W. K. J. Ford, and N. . Thonnard, "Rotational properties of 21 SC galaxies with a large range of luminosities and radii, from NGC 4605 /R = 4kpc/ to UGC 2885 /R = 122 kpc/," *Astrophysical Journal*, vol. 238, pp. 471–487, June 1980.

[4] U. G. Briel, J. P. Henry, and H. Boehringer, "Observation of the Coma cluster of galaxies with ROSAT during the all-sky survey," Astron. Astrophys. , vol. 259, pp. L31–L34, June 1992.

[5] S. D. M. White, J. F. Navarro, A. E. Evrard, and C. S. Frenk, "The baryon content of galaxy clusters: a challenge to cosmological orthodoxy," *Nature*, vol. 366, pp. 429–433, Dec. 1993.

[6] E. E. Falco, C. S. Kochanek, and J. A. Muñoz, "Limits on Cosmological Models from Radio-selected Gravitational Lenses," *Astrophysical Journal*, vol. 494, pp. 47–59, Feb. 1998.

[7] G. Hinshaw, J. L. Weiland, R. S. Hill, N. Odegard, D. Larson, C. L. Bennett, J. Dunkley, B. Gold, M. R. Greason, N. Jarosik, E. Komatsu, M. R. Nolta, L. Page, D. N. Spergel, E. Wollack, M. Halpern, A. Kogut, M. Limon, S. S. Meyer, G. S. Tucker, and E. L. Wright, "Five-Year Wilkinson Microwave Anisotropy Probe Observations: Data Processing, Sky Maps, and Basic Results," *ApJS*, vol. 180, pp. 225–245, Feb. 2009.

[8] E. Komatsu, J. Dunkley, M. R. Nolta, C. L. Bennett, B. Gold, G. Hinshaw, N. Jarosik, D. Larson, M. Limon, L. Page, D. N. Spergel, M. Halpern, R. S. Hill, A. Kogut, S. S. Meyer, G. S. Tucker, J. L. Weiland, E. Wollack, and E. L. Wright, "Five-Year Wilkinson Microwave Anisotropy Probe Observations: Cosmological Interpretation," *ApJS*, vol. 180, pp. 330–376, Feb. 2009.

[9] A. G. Riess, A. V. Filippenko, P. Challis, A. Clocchiatti, A. Diercks, P. M. Garnavich, R. L. Gilliland, C. J. Hogan, S. Jha, R. P. Kirshner, B. Leibundgut, M. M. Phillips, D. Reiss, B. P. Schmidt, R. A. Schommer, R. C. Smith, J. Spyromilio, C. Stubbs, N. B. Suntzeff, and J. Tonry, "Observational Evidence from Supernovae for an Accelerating Universe and a Cosmological Constant," *AJ* , vol. 116, pp. 1009–1038, Sept. 1998.

[10] S. Perlmutter, G. Aldering, G. Goldhaber, R. A. Knop, P. Nugent, P. G. Castro, S. Deustua, S. Fabbro, A. Goobar, D. E. Groom, I. M. Hook, A. G. Kim,

M. Y. Kim, J. C. Lee, N. J. Nunes, R. Pain, C. R. Pennypacker, R. Quimby, C. Lidman, R. S. Ellis, M. Irwin, R. G. McMahon, P. Ruiz-Lapuente, N. Walton, B. Schaefer, B. J. Boyle, A. V. Filippenko, T. Matheson, A. S. Fruchter, N. Panagia, H. J. M. Newberg, W. J. Couch, and T. S. C. Project, "Measurements of Ω and Λ from 42 High-Redshift Supernovae," *Astrophysical Journal*, vol. 517, pp. 565–586, June 1999.

[11] P. J. Peebles and B. Ratra, "The cosmological constant and dark energy," *Reviews of Modern Physics*, vol. 75, pp. 559–606, Apr. 2003.

[12] J. P. Ostriker and P. J. Steinhardt, "The observational case for a low-density Universe with a non-zero cosmological constant," *Nature*, vol. 377, pp. 600–602, Oct. 1995.

[13] B. D. Sherwin, J. Dunkley, S. Das, J. W. Appel, J. R. Bond, C. S. Carvalho, M. J. Devlin, R. Dünner, T. Essinger-Hileman, J. W. Fowler, A. Hajian, M. Halpern, M. Hasselfield, A. D. Hincks, R. Hlozek, J. P. Hughes, K. D. Irwin, J. Klein, A. Kosowsky, T. A. Marriage, D. Marsden, K. Moodley, F. Menanteau, M. D. Niemack, M. R. Nolta, L. A. Page, L. Parker, E. D. Reese, B. L. Schmitt, N. Sehgal, J. Sievers, D. N. Spergel, S. T. Staggs, D. S. Swetz, E. R. Switzer, R. Thornton, K. Visnjic, and E. Wollack, "Evidence for Dark Energy from the Cosmic Microwave Background Alone Using the Atacama Cosmology Telescope Lensing Measurements," *Physical Review Letters*, vol. 107, p. 021302, July 2011.

[14] N. Aghanim, S. Majumdar, and J. Silk, "Secondary anisotropies of the CMB," *Reports on Progress in Physics*, vol. 71, p. 066902, June 2008.

[15] V. Springel, C. S. Frenk, and S. D. M. White, "The large-scale structure of the Universe," *Nature*, vol. 440, pp. 1137–1144, Apr. 2006.

[16] H. Hoekstra and B. Jain, "Weak Gravitational Lensing and Its Cosmological Applications," *Annual Review of Nuclear and Particle Science*, vol. 58, pp. 99–123, Nov. 2008.

[17] A. Goobar and B. Leibundgut, "Supernova Cosmology: Legacy and Future," *Annual Review of Nuclear and Particle Science*, vol. 61, pp. 251–279, Nov. 2011.

[18] S. Tsujikawa, "Quintessence: a review," *Classical and Quantum Gravity*, vol. 30, p. 214003, Nov. 2013.

[19] T. Clifton, P. G. Ferreira, A. Padilla, and C. Skordis, "Modified gravity and cosmology," Phys. Rept. , vol. 513, pp. 1–189, Mar. 2012.

[20] P. J. E. Peebles, "Recombination of the Primeval Plasma," *Astrophysical Journal*, vol. 153, p. 1, July 1968.

[21] A. A. Penzias and R. W. Wilson, "A Measurement of Excess Antenna Temperature at 4080 Mc/s.," *Astrophysical Journal*, vol. 142, pp. 419–421, July 1965.

[22] R. H. Dicke, P. J. E. Peebles, P. G. Roll, and D. T. Wilkinson, "Cosmic Black-Body Radiation.," *Astrophysical Journal*, vol. 142, pp. 414–419, July 1965.

[23] J. C. Mather, E. S. Cheng, R. E. Eplee, Jr., R. B. Isaacman, S. S. Meyer, R. A. Shafer, R. Weiss, E. L. Wright, C. L. Bennett, N. W. Boggess, E. Dwek, S. Gulkis, M. G. Hauser, M. Janssen, T. Kelsall, P. M. Lubin, S. H. Moseley, Jr., T. L. Murdock, R. F. Silverberg, G. F. Smoot, and D. T. Wilkinson, "A preliminary measurement of the cosmic microwave background spectrum by the Cosmic Background Explorer (COBE) satellite," Astrophys. J. Let. , vol. 354, pp. L37–L40, May 1990.

[24] G. F. Smoot, C. L. Bennett, A. Kogut, E. L. Wright, J. Aymon, N. W. Boggess, E. S. Cheng, G. de Amici, S. Gulkis, M. G. Hauser, G. Hinshaw, P. D. Jackson, M. Janssen, E. Kaita, T. Kelsall, P. Keegstra, C. Lineweaver, K. Loewenstein, P. Lubin, J. Mather, S. S. Meyer, S. H. Moseley, T. Murdock, L. Rokke, R. F. Silverberg, L. Tenorio, R. Weiss, and D. T. Wilkinson, "Structure in the COBE differential microwave radiometer first-year maps," Astrophys. J. Let. , vol. 396, pp. L1–L5, Sept. 1992.

[25] C. L. Bennett, D. Larson, J. L. Weiland, N. Jarosik, G. Hinshaw, N. Odegard, K. M. Smith, R. S. Hill, B. Gold, M. Halpern, E. Komatsu, M. R. Nolta, L. Page, D. N. Spergel, E. Wollack, J. Dunkley, A. Kogut, M. Limon, S. S. Meyer, G. S. Tucker, and E. L. Wright, "Nine-year Wilkinson Microwave Anisotropy Probe (WMAP) Observations: Final Maps and Results," *ApJS*, vol. 208, p. 20, Oct. 2013.

[26] Planck Collaboration, N. Aghanim, M. Arnaud, M. Ashdown, J. Aumont, C. Baccigalupi, A. J. Banday, R. B. Barreiro, J. G. Bartlett, N. Bartolo, and

et al., "Planck 2015 results. XI. CMB power spectra, likelihoods, and robustness of parameters," *ArXiv e-prints*, July 2015.

[27] S. Das, T. Louis, M. R. Nolta, G. E. Addison, E. S. Battistelli, J. R. Bond, E. Calabrese, D. Crichton, M. J. Devlin, S. Dicker, J. Dunkley, R. Dünner, J. W. Fowler, M. Gralla, A. Hajian, M. Halpern, M. Hasselfield, M. Hilton, A. D. Hincks, R. Hlozek, K. M. Huffenberger, J. P. Hughes, K. D. Irwin, A. Kosowsky, R. H. Lupton, T. A. Marriage, D. Marsden, F. Menanteau, K. Moodley, M. D. Niemack, L. A. Page, B. Partridge, E. D. Reese, B. L. Schmitt, N. Sehgal, B. D. Sherwin, J. L. Sievers, D. N. Spergel, S. T. Staggs, D. S. Swetz, E. R. Switzer, R. Thornton, H. Trac, and E. Wollack, "The Atacama Cosmology Telescope: temperature and gravitational lensing power spectrum measurements from three seasons of data," *JCAP*, vol. 4, p. 014, Apr. 2014.

[28] R. Keisler, C. L. Reichardt, K. A. Aird, B. A. Benson, L. E. Bleem, J. E. Carlstrom, C. L. Chang, H. M. Cho, T. M. Crawford, A. T. Crites, T. de Haan, M. A. Dobbs, J. Dudley, E. M. George, N. W. Halverson, G. P. Holder, W. L. Holzapfel, S. Hoover, Z. Hou, J. D. Hrubes, M. Joy, L. Knox, A. T. Lee, E. M. Leitch, M. Lueker, D. Luong-Van, J. J. McMahon, J. Mehl, S. S. Meyer, M. Millea, J. J. Mohr, T. E. Montroy, T. Natoli, S. Padin, T. Plagge, C. Pryke, J. E. Ruhl, K. K. Schaffer, L. Shaw, E. Shirokoff, H. G. Spieler, Z. Staniszewski, A. A. Stark, K. Story, A. van Engelen, K. Vanderlinde, J. D. Vieira, R. Williamson, and O. Zahn, "A Measurement of the Damping Tail

of the Cosmic Microwave Background Power Spectrum with the South Pole Telescope," *Astrophysical Journal*, vol. 743, p. 28, Dec. 2011.

[29] W. C. Jones, P. A. R. Ade, J. J. Bock, J. R. Bond, J. Borrill, A. Boscaleri, P. Cabella, C. R. Contaldi, B. P. Crill, P. de Bernardis, G. De Gasperis, A. de Oliveira-Costa, G. De Troia, and j. . Astrophysical Journal. e. . a. k. . C. y. . . m. . a. v. . . p. . . d. . . a. . h. a. . P. di Stefano, G. and Hivon, E. and Jaffe, A. H. and Kisner, T. S. and Lange, A. E. and MacTavish, C. J. and Masi, S. and Mauskopf, P. D. and Melchiorri, A. and Montroy, T. E. and Natoli, P. and Netterfield, C. B. and Pascale, E. and Piacentini, F. and Pogosyan, D. and Polenta, G. and Prunet, S. and Ricciardi, S. and Romeo, G. and Ruhl, J. E. and Santini, P. and Tegmark, M. and Veneziani, M. and Vittorio, N. , title = "A Measurement of the Angular Power Spectrum of the CMB Temperature Anisotropy from the 2003 Flight of BOOMERANG"

[30] S. Hanany, P. Ade, A. Balbi, J. Bock, J. Borrill, A. Boscaleri, P. de Bernardis, P. G. Ferreira, V. V. Hristov, A. H. Jaffe, A. E. Lange, A. T. Lee, P. D. Mauskopf, C. B. Netterfield, S. Oh, E. Pascale, B. Rabii, P. L. Richards, G. F. Smoot, R. Stompor, C. D. Winant, and J. H. P. Wu, "MAXIMA-1: A Measurement of the Cosmic Microwave Background Anisotropy on Angular Scales of 10'-5 degrees," Astrophys. J. Let. , vol. 545, pp. L5–L9, Dec. 2000.

[31] N. Kaiser, "Small-angle anisotropy of the microwave background radiation in the adiabatic theory," Mon. Not. Roy. Astron. Soc. , vol. 202, pp. 1169–1180, Mar. 1983.

[32] J. M. Kovac, E. M. Leitch, C. Pryke, J. E. Carlstrom, N. W. Halverson, and W. L. Holzapfel, "Detection of polarization in the cosmic microwave background using DASI," *Nature*, vol. 420, pp. 772–787, Dec. 2002.

[33] S. Naess, M. Hasselfield, J. McMahon, M. D. Niemack, G. E. Addison, P. A. R. Ade, R. Allison, M. Amiri, N. Battaglia, J. A. Beall, F. de Bernardis, J. R. Bond, J. Britton, E. Calabrese, H.-m. Cho, K. Coughlin, D. Crichton, S. Das, R. Datta, M. J. Devlin, S. R. Dicker, J. Dunkley, R. Dünner, J. W. Fowler, A. E. Fox, P. Gallardo, E. Grace, M. Gralla, A. Hajian, M. Halpern, S. Henderson, J. C. Hill, G. C. Hilton, M. Hilton, A. D. Hincks, R. Hlozek, P. Ho, J. Hubmayr, K. M. Huffenberger, J. P. Hughes, L. Infante, K. Irwin, R. Jackson, S. Muya Kasanda, J. Klein, B. Koopman, A. Kosowsky, D. Li, T. Louis, M. Lungu, M. Madhavacheril, T. A. Marriage, L. Maurin, F. Menanteau, K. Moodley, C. Munson, L. Newburgh, J. Nibarger, M. R. Nolta, L. A. Page, C. Pappas, B. Partridge, F. Rojas, B. L. Schmitt, N. Sehgal, B. D. Sherwin, J. Sievers, S. Simon, D. N. Spergel, S. T. Staggs, E. R. Switzer, R. Thornton, H. Trac, C. Tucker, M. Uehara, A. Van Engelen, J. T. Ward, and E. J. Wollack, "The Atacama Cosmology Telescope: CMB polarization at $200 < \mathrm{l} < 9000$," *JCAP*, vol. 10, p. 007, Oct. 2014.

[34] R. Keisler, S. Hoover, N. Harrington, J. W. Henning, P. A. R. Ade, K. A. Aird, J. E. Austermann, J. A. Beall, A. N. Bender, B. A. Benson, L. E. Bleem, J. E. Carlstrom, C. L. Chang, H. C. Chiang, H.-M. Cho, R. Citron, T. M. Crawford, A. T. Crites, T. de Haan, M. A. Dobbs, W. Everett, J. Gallicchio, J. Gao, E. M. George, A. Gilbert, N. W. Halverson, D. Hanson, G. C. Hilton,

G. P. Holder, W. L. Holzapfel, Z. Hou, J. D. Hrubes, N. Huang, J. Hubmayr, K. D. Irwin, L. Knox, A. T. Lee, E. M. Leitch, D. Li, D. Luong-Van, D. P. Marrone, J. J. McMahon, J. Mehl, S. S. Meyer, L. Mocanu, T. Natoli, J. P. Nibarger, V. Novosad, S. Padin, C. Pryke, C. L. Reichardt, J. E. Ruhl, B. R. Saliwanchik, J. T. Sayre, K. K. Schaffer, E. Shirokoff, G. Smecher, A. A. Stark, K. T. Story, C. Tucker, K. Vanderlinde, J. D. Vieira, G. Wang, N. Whitehorn, V. Yefremenko, and O. Zahn, "Measurements of Sub-degree B-mode Polarization in the Cosmic Microwave Background from 100 Square Degrees of SPTpol Data," *Astrophysical Journal*, vol. 807, p. 151, July 2015.

[35] W. Hu and M. White, "A CMB polarization primer," *New Astronomy*, vol. 2, pp. 323–344, Oct. 1997.

[36] B. W. Lee and S. Weinberg, "Cosmological lower bound on heavy-neutrino masses," *Physical Review Letters*, vol. 39, pp. 165–168, July 1977.

[37] G. Jungman, M. Kamionkowski, and K. Griest, "Supersymmetric dark matter," Phys. Rept. , vol. 267, pp. 195–373, Mar. 1996.

[38] P. J. Fox, R. Harnik, J. Kopp, and Y. Tsai, "Missing energy signatures of dark matter at the LHC," Phys. Rev. **D** , vol. 85, p. 056011, Mar. 2012.

[39] R. Bernabei, P. Belli, A. Di Marco, F. Cappella, A. d'Angelo, A. Incicchitti, V. Caracciolo, R. Cerulli, C. J. Dai, H. L. He, X. H. Ma, X. D. Sheng, R. G. Wang, F. Montecchia, and Z. P. Ye, "DAMA/LIBRA results and perspectives," *ArXiv e-prints*, Jan. 2013.

[40] CDMS Collaboration, Agnese et al., "Dark Matter Search Results Using the Silicon Detectors of CDMS II," *ArXiv e-prints*, Apr. 2013.

[41] C. E. Aalseth, P. S. Barbeau, J. Colaresi, J. I. Collar, J. Diaz Leon, J. E. Fast, N. Fields, T. W. Hossbach, M. E. Keillor, J. D. Kephart, A. Knecht, M. G. Marino, H. S. Miley, M. L. Miller, J. L. Orrell, D. C. Radford, J. F. Wilkerson, and K. M. Yocum, "Search for an Annual Modulation in a p-Type Point Contact Germanium Dark Matter Detector," *Physical Review Letters*, vol. 107, p. 141301, Sept. 2011.

[42] G. Angloher, M. Bauer, I. Bavykina, A. Bento, C. Bucci, C. Ciemniak, G. Deuter, F. Feilitzsch, D. Hauff, P. Huff, C. Isaila, J. Jochum, M. Kiefer, M. Kimmerle, J.-C. Lanfranchi, F. Petricca, S. Pfister, W. Potzel, F. Pröbst, F. Reindl, S. Roth, K. Rottler, C. Sailer, K. Schäffner, J. Schmaler, S. Scholl, W. Seidel, M. Sivers, L. Stodolsky, C. Strandhagen, R. Strauß, A. Tanzke, I. Usherov, S. Wawoczny, M. Willers, and A. Zöller, "Results from 730 kg days of the cresst-ii dark matter search," *The European Physical Journal C*, vol. 72, no. 4, pp. 1–22, 2012.

[43] O. Adriani, G. C. Barbarino, G. A. Bazilevskaya, R. Bellotti, A. Bianco, M. Boezio, E. A. Bogomolov, M. Bongi, V. Bonvicini, S. Bottai, A. Bruno, F. Cafagna, D. Campana, R. Carbone, P. Carlson, M. Casolino, G. Castellini, C. De Donato, C. De Santis, N. De Simone, V. Di Felice, V. Formato, A. M. Galper, A. V. Karelin, S. V. Koldashov, S. A. Koldobskiy, S. Y. Krutkov, A. N. Kvashnin, A. Leonov, V. Malakhov, L. Marcelli, M. Martucci, A. G. Mayorov,

W. Menn, M. Mergé, V. V. Mikhailov, E. Mocchiutti, A. Monaco, N. Mori, R. Munini, G. Osteria, F. Palma, P. Papini, M. Pearce, P. Picozza, C. Pizzolotto, M. Ricci, S. B. Ricciarini, L. Rossetto, R. Sarkar, V. Scotti, M. Simon, R. Sparvoli, P. Spillantini, S. J. Stochaj, J. C. Stockton, Y. I. Stozhkov, A. Vacchi, E. Vannuccini, G. I. Vasilyev, S. A. Voronov, Y. T. Yurkin, G. Zampa, N. Zampa, and V. G. Zverev, "Cosmic-ray positron energy spectrum measured by pamela," *Phys. Rev. Lett.*, vol. 111, p. 081102, Aug 2013.

[44] M. e. a. Aguilar, "First result from the alpha magnetic spectrometer on the international space station: Precision measurement of the positron fraction in primary cosmic rays of 0.5˘350 gev," *Phys. Rev. Lett.*, vol. 110, p. 141102, Apr 2013.

[45] M. Ackermann, M. Ajello, A. Allafort, W. B. Atwood, L. Baldini, G. Barbiellini, D. Bastieri, K. Bechtol, R. Bellazzini, B. Berenji, R. D. Blandford, E. D. Bloom, E. Bonamente, A. W. Borgland, A. Bouvier, J. Bregeon, M. Brigida, P. Bruel, R. Buehler, S. Buson, G. A. Caliandro, R. A. Cameron, P. A. Caraveo, J. M. Casandjian, C. Cecchi, E. Charles, A. Chekhtman, C. C. Cheung, J. Chiang, S. Ciprini, R. Claus, J. Cohen-Tanugi, J. Conrad, S. Cutini, A. de Angelis, F. de Palma, C. D. Dermer, S. W. Digel, E. Do Couto E Silva, P. S. Drell, A. Drlica-Wagner, C. Favuzzi, S. J. Fegan, E. C. Ferrara, W. B. Focke, P. Fortin, Y. Fukazawa, S. Funk, P. Fusco, F. Gargano, D. Gasparrini, S. Germani, N. Giglietto, P. Giommi, F. Giordano, M. Giroletti, T. Glanzman, G. Godfrey, I. A. Grenier, J. E. Grove, S. Guiriec, M. Gustafsson, D. Hadasch, A. K. Harding, M. Hayashida, R. E. Hughes, G. Jóhannesson, A. S. Johnson,

T. Kamae, H. Katagiri, J. Kataoka, J. Knödlseder, M. Kuss, J. Lande, L. Latronico, M. Lemoine-Goumard, M. Llena Garde, F. Longo, F. Loparco, M. N. Lovellette, P. Lubrano, G. M. Madejski, M. N. Mazziotta, J. E. McEnery, P. F. Michelson, W. Mitthumsiri, T. Mizuno, A. A. Moiseev, C. Monte, M. E. Monzani, A. Morselli, I. V. Moskalenko, S. Murgia, T. Nakamori, P. L. Nolan, J. P. Norris, E. Nuss, M. Ohno, T. Ohsugi, A. Okumura, N. Omodei, E. Orlando, J. F. Ormes, M. Ozaki, D. Paneque, D. Parent, M. Pesce-Rollins, M. Pierbattista, F. Piron, G. Pivato, T. A. Porter, S. Rainò, R. Rando, M. Razzano, S. Razzaque, A. Reimer, O. Reimer, T. Reposeur, S. Ritz, R. W. Romani, M. Roth, H. F.-W. Sadrozinski, C. Sbarra, T. L. Schalk, C. Sgrò, E. J. Siskind, G. Spandre, P. Spinelli, A. W. Strong, H. Takahashi, T. Takahashi, T. Tanaka, J. G. Thayer, J. B. Thayer, L. Tibaldo, M. Tinivella, D. F. Torres, G. Tosti, E. Troja, Y. Uchiyama, T. L. Usher, J. Vandenbroucke, V. Vasileiou, G. Vianello, V. Vitale, A. P. Waite, B. L. Winer, K. S. Wood, M. Wood, Z. Yang, and S. Zimmer, "Measurement of Separate Cosmic-Ray Electron and Positron Spectra with the Fermi Large Area Telescope," *Physical Review Letters*, vol. 108, p. 011103, Jan. 2012.

[46] J. Diemand, M. Kuhlen, and P. Madau, "Dark Matter Substructure and Gamma-Ray Annihilation in the Milky Way Halo," *Astrophysical Journal*, vol. 657, pp. 262–270, Mar. 2007.

[47] M. Ackermann, A. Albert, B. Anderson, W. B. Atwood, L. Baldini, G. Barbiellini, D. Bastieri, K. Bechtol, R. Bellazzini, E. Bissaldi, R. D. Blandford, E. D. Bloom, R. Bonino, E. Bottacini, T. J. Brandt, J. Bregeon, P. Bruel, R. Buehler,

G. A. Caliandro, R. A. Cameron, R. Caputo, M. Caragiulo, P. A. Caraveo, C. Cecchi, E. Charles, A. Chekhtman, J. Chiang, G. Chiaro, S. Ciprini, R. Claus, J. Cohen-Tanugi, J. Conrad, A. Cuoco, S. Cutini, F. D'Ammando, A. de Angelis, F. de Palma, R. Desiante, S. W. Digel, L. Di Venere, P. S. Drell, A. Drlica-Wagner, R. Essig, C. Favuzzi, S. J. Fegan, E. C. Ferrara, W. B. Focke, A. Franckowiak, Y. Fukazawa, S. Funk, P. Fusco, F. Gargano, D. Gasparrini, N. Giglietto, F. Giordano, M. Giroletti, T. Glanzman, G. Godfrey, G. A. Gomez-Vargas, I. A. Grenier, S. Guiriec, M. Gustafsson, E. Hays, J. W. Hewitt, D. Horan, T. Jogler, G. Jóhannesson, M. Kuss, S. Larsson, L. Latronico, J. Li, L. Li, M. Llena Garde, F. Longo, F. Loparco, P. Lubrano, D. Malyshev, M. Mayer, M. N. Mazziotta, J. E. McEnery, M. Meyer, P. F. Michelson, T. Mizuno, A. A. Moiseev, M. E. Monzani, A. Morselli, S. Murgia, E. Nuss, T. Ohsugi, M. Orienti, E. Orlando, J. F. Ormes, D. Paneque, J. S. Perkins, M. Pesce-Rollins, F. Piron, G. Pivato, T. A. Porter, S. Rainò, R. Rando, M. Razzano, A. Reimer, O. Reimer, S. Ritz, M. Sánchez-Conde, A. Schulz, N. Sehgal, C. Sgrò, E. J. Siskind, F. Spada, G. Spandre, P. Spinelli, L. Strigari, H. Tajima, H. Takahashi, J. B. Thayer, L. Tibaldo, D. F. Torres, E. Troja, G. Vianello, M. Werner, B. L. Winer, K. S. Wood, M. Wood, G. Zaharijas, S. Zimmer, and Fermi-LAT Collaboration, "Searching for Dark Matter Annihilation from Milky Way Dwarf Spheroidal Galaxies with Six Years of Fermi Large Area Telescope Data," *Physical Review Letters*, vol. 115, p. 231301, Dec. 2015.

[48] N. Padmanabhan and D. P. Finkbeiner, "Detecting dark matter annihilation

with CMB polarization: Signatures and experimental prospects," Phys. Rev. **D** , vol. 72, p. 023508, July 2005.

[49] S. Galli, F. Iocco, G. Bertone, and A. Melchiorri, "CMB constraints on dark matter models with large annihilation cross section," Phys. Rev. **D** , vol. 80, p. 023505, July 2009.

[50] T. R. Slatyer, N. Padmanabhan, and D. P. Finkbeiner, "Cmb constraints on wimp annihilation: Energy absorption during the recombination epoch," *Phys. Rev. D*, vol. 80, p. 043526, Aug 2009.

[51] S. Galli, F. Iocco, G. Bertone, and A. Melchiorri, "Updated CMB constraints on dark matter annihilation cross sections," Phys. Rev. **D** , vol. 84, p. 027302, July 2011.

[52] D. P. Finkbeiner, S. Galli, T. Lin, and T. R. Slatyer, "Searching for dark matter in the cmb: A compact parametrization of energy injection from new physics," *Phys. Rev. D*, vol. 85, p. 043522, Feb 2012.

[53] D. Huterer, D. Kirkby, R. Bean, A. Connolly, K. Dawson, S. Dodelson, A. Evrard, B. Jain, M. Jarvis, E. Linder, R. Mandelbaum, M. May, A. Raccanelli, B. Reid, E. Rozo, F. Schmidt, N. Sehgal, A. Slosar, A. van Engelen, H.-Y. Wu, and G. Zhao, "Growth of cosmic structure: Probing dark energy beyond expansion," *Astroparticle Physics*, vol. 63, pp. 23–41, Mar. 2015.

[54] R. A. Sunyaev and I. B. Zeldovich, "Microwave background radiation as a probe of the contemporary structure and history of the universe," *Annual Review of Astronomy and Astrophysics*, vol. 18, pp. 537–560, 1980.

[55] A. Lewis and A. Challinor, "Weak gravitational lensing of the CMB," *Physics Reports*, vol. 429, pp. 1–65, June 2006.

[56] C. Shapiro, S. Dodelson, B. Hoyle, L. Samushia, and B. Flaugher, "Will multiple probes of dark energy find modified gravity?," Phys. Rev. **D** , vol. 82, p. 043520, Aug. 2010.

[57] K. M. Smith, O. Zahn, and O. Doré, "Detection of gravitational lensing in the cosmic microwave background," Phys. Rev. **D** , vol. 76, p. 043510, Aug. 2007.

[58] S. Das, B. D. Sherwin, P. Aguirre, J. W. Appel, J. R. Bond, C. S. Carvalho, M. J. Devlin, J. Dunkley, R. Dünner, T. Essinger-Hileman, J. W. Fowler, A. Hajian, M. Halpern, M. Hasselfield, A. D. Hincks, R. Hlozek, K. M. Huffenberger, J. P. Hughes, K. D. Irwin, J. Klein, A. Kosowsky, R. H. Lupton, T. A. Marriage, D. Marsden, F. Menanteau, K. Moodley, M. D. Niemack, M. R. Nolta, L. A. Page, L. Parker, E. D. Reese, B. L. Schmitt, N. Sehgal, J. Sievers, D. N. Spergel, S. T. Staggs, D. S. Swetz, E. R. Switzer, R. Thornton, K. Visnjic, and E. Wollack, "Detection of the Power Spectrum of Cosmic Microwave Background Lensing by the Atacama Cosmology Telescope," *Physical Review Letters*, vol. 107, p. 021301, July 2011.

[59] A. van Engelen, R. Keisler, O. Zahn, K. A. Aird, B. A. Benson, L. E. Bleem, J. E. Carlstrom, C. L. Chang, H. M. Cho, T. M. Crawford, A. T. Crites, T. de

Haan, M. A. Dobbs, J. Dudley, E. M. George, N. W. Halverson, G. P. Holder, W. L. Holzapfel, S. Hoover, Z. Hou, J. D. Hrubes, M. Joy, L. Knox, A. T. Lee, E. M. Leitch, M. Lueker, D. Luong-Van, J. J. McMahon, J. Mehl, S. S. Meyer, M. Millea, J. J. Mohr, T. E. Montroy, T. Natoli, S. Padin, T. Plagge, C. Pryke, C. L. Reichardt, J. E. Ruhl, J. T. Sayre, K. K. Schaffer, L. Shaw, E. Shirokoff, H. G. Spieler, Z. Staniszewski, A. A. Stark, K. Story, K. Vanderlinde, J. D. Vieira, and R. Williamson, "A Measurement of Gravitational Lensing of the Microwave Background Using South Pole Telescope Data," *Astrophysical Journal*, vol. 756, p. 142, Sept. 2012.

[60] K. T. Story, D. Hanson, P. A. R. Ade, K. A. Aird, J. E. Austermann, J. A. Beall, A. N. Bender, B. A. Benson, L. E. Bleem, J. E. Carlstrom, C. L. Chang, H. C. Chiang, H.-M. Cho, R. Citron, T. M. Crawford, A. T. Crites, T. de Haan, M. A. Dobbs, W. Everett, J. Gallicchio, J. Gao, E. M. George, A. Gilbert, N. W. Halverson, N. Harrington, J. W. Henning, G. C. Hilton, G. P. Holder, W. L. Holzapfel, S. Hoover, Z. Hou, J. D. Hrubes, N. Huang, J. Hubmayr, K. D. Irwin, R. Keisler, L. Knox, A. T. Lee, E. M. Leitch, D. Li, C. Liang, D. Luong-Van, J. J. McMahon, J. Mehl, S. S. Meyer, L. Mocanu, T. E. Montroy, T. Natoli, J. P. Nibarger, V. Novosad, S. Padin, C. Pryke, C. L. Reichardt, J. E. Ruhl, B. R. Saliwanchik, J. T. Sayre, K. K. Schaffer, G. Smecher, A. A. Stark, C. Tucker, K. Vanderlinde, J. D. Vieira, G. Wang, N. Whitehorn, V. Yefremenko, and O. Zahn, "A Measurement of the Cosmic Microwave Background Gravitational Lensing Potential from 100 Square Degrees of SPTpol Data," *Astrophysical Journal*, vol. 810, p. 50, Sept. 2015.

[61] Planck Collaboration, P. A. R. Ade, N. Aghanim, C. Armitage-Caplan, M. Arnaud, M. Ashdown, F. Atrio-Barandela, J. Aumont, C. Baccigalupi, A. J. Banday, and et al., "Planck 2013 results. XVII. Gravitational lensing by large-scale structure," Astron. Astrophys. , vol. 571, p. A17, Nov. 2014.

[62] Planck Collaboration, P. A. R. Ade, N. Aghanim, M. Arnaud, M. Ashdown, J. Aumont, C. Baccigalupi, A. J. Banday, R. B. Barreiro, J. G. Bartlett, and et al., "Planck 2015 results. XV. Gravitational lensing," *ArXiv e-prints*, Feb. 2015.

[63] P. A. R. Ade, Y. Akiba, A. E. Anthony, K. Arnold, M. Atlas, D. Barron, D. Boettger, J. Borrill, S. Chapman, Y. Chinone, M. Dobbs, T. Elleflot, J. Errard, G. Fabbian, C. Feng, D. Flanigan, A. Gilbert, W. Grainger, N. W. Halverson, M. Hasegawa, K. Hattori, M. Hazumi, W. L. Holzapfel, Y. Hori, J. Howard, P. Hyland, Y. Inoue, G. C. Jaehnig, A. Jaffe, B. Keating, Z. Kermish, R. Keskitalo, T. Kisner, M. Le Jeune, A. T. Lee, E. Linder, E. M. Leitch, M. Lungu, F. Matsuda, T. Matsumura, X. Meng, N. J. Miller, H. Morii, S. Moyerman, M. J. Myers, M. Navaroli, H. Nishino, H. Paar, J. Peloton, E. Quealy, G. Rebeiz, C. L. Reichardt, P. L. Richards, C. Ross, I. Schanning, D. E. Schenck, B. Sherwin, A. Shimizu, C. Shimmin, M. Shimon, P. Siritanasak, G. Smecher, H. Spieler, N. Stebor, B. Steinbach, R. Stompor, A. Suzuki, S. Takakura, T. Tomaru, B. Wilson, A. Yadav, O. Zahn, and Polarbear Collaboration, "Measurement of the Cosmic Microwave Background Polarization Lensing Power Spectrum with the POLARBEAR Experiment," *Physical Review Letters*, vol. 113, p. 021301, July 2014.

[64] T. Keck Array, BICEP2 Collaborations, :, P. A. R. Ade, Z. Ahmed, R. W. Aikin, K. D. Alexander, D. Barkats, S. J. Benton, C. A. Bischoff, J. J. Bock, R. Bowens-Rubin, J. A. Brevik, I. Buder, E. Bullock, V. Buza, J. Connors, B. P. Crill, L. Duband, C. Dvorkin, J. P. Filippin, S. Fliescher, J. Grayson, M. Halpern, S. Harrison, S. R. Hildebrandt, G. C. Hilton, H. Hui, K. D. Irwin, J. Kang, K. S. Karkare, E. Karpel, J. P. Kaufman, B. G. Keating, S. Kefeli, S. A. Kernasovskiy, J. M. Kovac, C. L. Kuo, E. M. Leitch, M. Lueker, K. G. Megerian, T. Namikawa, C. B. Netterfield, H. T. Nguyen, R. O'Brient, R. W. Ogburn, IV, A. Orlando, C. Pryke, S. Richter, R. Schwarz, C. D. Sheehy, Z. K. Staniszewski, B. Steinbach, R. V. Sudiwala, G. P. Teply, K. L. Thompson, J. E. Tolan, C. Tucker, A. D. Turner, A. G. Vieregg, A. C. Weber, D. V. Wiebe, J. Willmert, C. L. Wong, W. L. K. Wu, and K. W. Yoon, "BICEP2 / Keck Array VIII: Measurement of gravitational lensing from large-scale B-mode polarization," *ArXiv e-prints*, June 2016.

[65] M. Madhavacheril, N. Sehgal, R. Allison, N. Battaglia, J. R. Bond, E. Calabrese, J. Caliguiri, K. Coughlin, D. Crichton, R. Datta, M. J. Devlin, J. Dunkley, R. Dünner, K. Fogarty, E. Grace, A. Hajian, M. Hasselfield, J. C. Hill, M. Hilton, A. D. Hincks, R. Hlozek, J. P. Hughes, A. Kosowsky, T. Louis, M. Lungu, J. McMahon, K. Moodley, C. Munson, S. Naess, F. Nati, L. Newburgh, M. D. Niemack, L. A. Page, B. Partridge, B. Schmitt, B. D. Sherwin, J. Sievers, D. N. Spergel, S. T. Staggs, R. Thornton, A. Van Engelen, J. T. Ward, E. J. Wollack, and Atacama Cosmology Telescope Collaboration, "Evidence of Lensing of the Cosmic Microwave Background by Dark Matter Halos,"

Physical Review Letters, vol. 114, p. 151302, Apr. 2015.

[66] E. J. Baxter, R. Keisler, S. Dodelson, K. A. Aird, S. W. Allen, M. L. N. Ashby, M. Bautz, M. Bayliss, B. A. Benson, L. E. Bleem, S. Bocquet, M. Brodwin, J. E. Carlstrom, C. L. Chang, I. Chiu, H.-M. Cho, A. Clocchiatti, T. M. Crawford, A. T. Crites, S. Desai, J. P. Dietrich, T. de Haan, M. A. Dobbs, R. J. Foley, W. R. Forman, E. M. George, M. D. Gladders, A. H. Gonzalez, N. W. Halverson, N. L. Harrington, C. Hennig, H. Hoekstra, G. P. Holder, W. L. Holzapfel, Z. Hou, J. D. Hrubes, C. Jones, L. Knox, A. T. Lee, E. M. Leitch, J. Liu, M. Lueker, D. Luong-Van, A. Mantz, D. P. Marrone, M. McDonald, J. J. McMahon, S. S. Meyer, M. Millea, L. M. Mocanu, S. S. Murray, S. Padin, C. Pryke, C. L. Reichardt, A. Rest, J. E. Ruhl, B. R. Saliwanchik, A. Saro, J. T. Sayre, K. K. Schaffer, E. Shirokoff, J. Song, H. G. Spieler, B. Stalder, S. A. Stanford, Z. Staniszewski, A. A. Stark, K. T. Story, A. van Engelen, K. Vanderlinde, J. D. Vieira, A. Vikhlinin, R. Williamson, O. Zahn, and A. Zenteno, "A Measurement of Gravitational Lensing of the Cosmic Microwave Background by Galaxy Clusters Using Data from the South Pole Telescope," *Astrophysical Journal*, vol. 806, p. 247, June 2015.

[67] Planck Collaboration, P. A. R. Ade, N. Aghanim, M. Arnaud, M. Ashdown, J. Aumont, C. Baccigalupi, A. J. Banday, R. B. Barreiro, J. G. Bartlett, and et al., "Planck 2015 results. XXIV. Cosmology from Sunyaev-Zeldovich cluster counts," *ArXiv e-prints*, Feb. 2015.

[68] J. A. Tyson, F. Valdes, and R. A. Wenk, "Detection of systematic gravitational

lens galaxy image alignments - Mapping dark matter in galaxy clusters," Astrophys. J. Let. , vol. 349, pp. L1–L4, Jan. 1990.

[69] G. Fahlman, N. Kaiser, G. Squires, and D. Woods, "Dark matter in MS 1224 from distortion of background galaxies," *Astrophysical Journal*, vol. 437, pp. 56–62, Dec. 1994.

[70] D. J. Bacon, A. R. Refregier, and R. S. Ellis, "Detection of weak gravitational lensing by large-scale structure," Mon. Not. Roy. Astron. Soc. , vol. 318, pp. 625–640, Oct. 2000.

[71] N. Kaiser, G. Wilson, and G. A. Luppino, "Large-Scale Cosmic Shear Measurements," *ArXiv Astrophysics e-prints*, Mar. 2000.

[72] L. Van Waerbeke, Y. Mellier, T. Erben, J. C. Cuillandre, F. Bernardeau, R. Maoli, E. Bertin, H. J. McCracken, O. Le Fèvre, B. Fort, M. Dantel-Fort, B. Jain, and P. Schneider, "Detection of correlated galaxy ellipticities from CFHT data: first evidence for gravitational lensing by large-scale structures," Astron. Astrophys. , vol. 358, pp. 30–44, June 2000.

[73] D. M. Wittman, J. A. Tyson, D. Kirkman, I. Dell'Antonio, and G. Bernstein, "Detection of weak gravitational lensing distortions of distant galaxies by cosmic dark matter at large scales," *Nature*, vol. 405, pp. 143–148, May 2000.

[74] T. D. Kitching, A. F. Heavens, J. Alsing, T. Erben, C. Heymans, H. Hildebrandt, H. Hoekstra, A. Jaffe, A. Kiessling, Y. Mellier, L. Miller, L. van Waerbeke, J. Benjamin, J. Coupon, L. Fu, M. J. Hudson, M. Kilbinger, K. Kuijken,

B. T. P. Rowe, T. Schrabback, E. Semboloni, and M. Velander, “3D cosmic shear: cosmology from CFHTLenS,” Mon. Not. Roy. Astron. Soc. , vol. 442, pp. 1326–1349, Aug. 2014.

[75] M. R. Becker, M. A. Troxel, N. MacCrann, E. Krause, T. F. Eifler, O. Friedrich, A. Nicola, A. Refregier, A. Amara, D. Bacon, G. M. Bernstein, C. Bonnett, S. L. Bridle, M. T. Busha, C. Chang, S. Dodelson, B. Erickson, A. E. Evrard, J. Frieman, E. Gaztanaga, D. Gruen, W. Hartley, B. Jain, M. Jarvis, T. Kacprzak, D. Kirk, A. Kravtsov, B. Leistedt, E. S. Rykoff, C. Sabiu, C. Sanchez, H. Seo, E. Sheldon, R. H. Wechsler, J. Zuntz, T. Abbott, F. B. Abdalla, S. Allam, R. Armstrong, M. Banerji, A. H. Bauer, A. Benoit-Levy, E. Bertin, D. Brooks, E. Buckley-Geer, D. L. Burke, D. Capozzi, A. Carnero Rosell, M. Carrasco Kind, J. Carretero, F. J. Castander, M. Crocce, C. E. Cunha, C. B. D’Andrea, L. N. da Costa, D. L. DePoy, S. Desai, H. T. Diehl, J. P. Dietrich, P. Doel, A. Fausti Neto, E. Fernandez, D. A. Finley, B. Flaugher, P. Fosalba, D. W. Gerdes, R. A. Gruendl, G. Gutierrez, K. Honscheid, D. J. James, K. Kuehn, N. Kuropatkin, O. Lahav, T. S. Li, M. Lima, M. A. G. Maia, M. March, P. Martini, P. Melchior, C. J. Miller, R. Miquel, J. J. Mohr, R. C. Nichol, B. Nord, R. Ogando, A. A. Plazas, K. Reil, A. K. Romer, A. Roodman, M. Sako, E. Sanchez, V. Scarpine, M. Schubnell, I. Sevilla-Noarbe, R. C. Smith, M. Soares-Santos, F. Sobreira, E. Suchyta, M. E. C. Swanson, G. Tarle, J. Thaler, D. Thomas, V. Vikram, A. R. Walker, and The DES Collaboration, “Cosmic Shear Measurements with DES Science Verification Data,” *ArXiv e-prints*, July 2015.

[76] M. Takada, "Subaru Hyper Suprime-Cam Project," in *American Institute of Physics Conference Series* (N. Kawai and S. Nagataki, eds.), vol. 1279 of *American Institute of Physics Conference Series*, pp. 120–127, Oct. 2010.

[77] J. T. A. de Jong, K. Kuijken, D. Applegate, K. Begeman, A. Belikov, C. Blake, J. Bout, D. Boxhoorn, H. Buddelmeijer, A. Buddendiek, M. Cacciato, M. Capaccioli, A. Choi, O. Cordes, G. Covone, M. Dall'Ora, A. Edge, T. Erben, J. Franse, F. Getman, A. Grado, J. Harnois-Deraps, E. Helmich, R. Herbonnet, C. Heymans, H. Hildebrandt, H. Hoekstra, Z. Huang, N. Irisarri, B. Joachimi, F. Köhlinger, T. Kitching, F. La Barbera, P. Lacerda, J. McFarland, L. Miller, R. Nakajima, N. R. Napolitano, M. Paolillo, J. Peacock, B. Pila-Diez, E. Puddu, M. Radovich, A. Rifatto, P. Schneider, T. Schrabback, C. Sifon, G. Sikkema, P. Simon, W. Sutherland, A. Tudorica, E. Valentijn, R. van der Burg, E. van Uitert, L. van Waerbeke, M. Velander, G. V. Kleijn, M. Viola, and W.-J. Vriend, "The Kilo-Degree Survey," *The Messenger*, vol. 154, pp. 44–46, Dec. 2013.

[78] H. Hildebrandt, A. Choi, C. Heymans, C. Blake, T. Erben, L. Miller, R. Nakajima, L. van Waerbeke, M. Viola, A. Buddendiek, J. Harnois-Déraps, A. Hojjati, B. Joachimi, S. Joudaki, T. D. Kitching, C. Wolf, S. Gwyn, K. Kuijken, Z. Sheikhbahaee, A. Tudorica, and H. K. C. Yee, "RCSLenS: The Red Cluster Sequence Lensing Survey," *ArXiv e-prints*, Mar. 2016.

[79] J. A. Tyson, "Large Synoptic Survey Telescope: Overview," in *Survey and Other Telescope Technologies and Discoveries* (J. A. Tyson and S. Wolff, eds.),

vol. 4836 of *SPIE Proceedings*, pp. 10–20, Dec. 2002.

[80] R. Laureijs, J. Amiaux, S. Arduini, J. . Augueres, J. Brinchmann, R. Cole, M. Cropper, C. Dabin, L. Duvet, A. Ealet, and et al., "Euclid Definition Study Report," *ArXiv e-prints*, Oct. 2011.

[81] D. Spergel, N. Gehrels, J. Breckinridge, M. Donahue, A. Dressler, B. S. Gaudi, T. Greene, O. Guyon, C. Hirata, J. Kalirai, N. J. Kasdin, W. Moos, S. Perlmutter, M. Postman, B. Rauscher, J. Rhodes, Y. Wang, D. Weinberg, J. Centrella, W. Traub, C. Baltay, J. Colbert, D. Bennett, A. Kiessling, B. Macintosh, J. Merten, M. Mortonson, M. Penny, E. Rozo, D. Savransky, K. Stapelfeldt, Y. Zu, C. Baker, E. Cheng, D. Content, J. Dooley, M. Foote, R. Goullioud, K. Grady, C. Jackson, J. Kruk, M. Levine, M. Melton, C. Peddie, J. Ruffa, and S. Shaklan, "Wide-Field InfraRed Survey Telescope-Astrophysics Focused Telescope Assets WFIRST-AFTA Final Report," *ArXiv e-prints*, May 2013.

[82] G. M. Bernstein and M. Jarvis, "Shapes and Shears, Stars and Smears: Optimal Measurements for Weak Lensing," *The Astronomical Journal*, vol. 123, pp. 583–618, Feb. 2002.

[83] T. Kacprzak, S. Bridle, B. Rowe, L. Voigt, J. Zuntz, M. Hirsch, and N. MacCrann, "Sérsic galaxy models in weak lensing shape measurement: model bias, noise bias and their interaction," Mon. Not. Roy. Astron. Soc. , vol. 441, pp. 2528–2538, July 2014.

[84] J. Hartlap, S. Hilbert, P. Schneider, and H. Hildebrandt, "A bias in cosmic shear from galaxy selection: results from ray-tracing simulations," Astron. Astrophys. , vol. 528, p. A51, Apr. 2011.

[85] G. M. Bernstein and R. Armstrong, "Bayesian lensing shear measurement," Mon. Not. Roy. Astron. Soc. , vol. 438, pp. 1880–1893, Feb. 2014.

[86] T. Kacprzak, J. Zuntz, B. Rowe, S. Bridle, A. Refregier, A. Amara, L. Voigt, and M. Hirsch, "Measurement and calibration of noise bias in weak lensing galaxy shape estimation," Mon. Not. Roy. Astron. Soc. , vol. 427, pp. 2711–2722, Dec. 2012.

[87] A. Vallinotto, "Using Cosmic Microwave Background Lensing to Constrain the Multiplicative Bias of Cosmic Shear," *Astrophysical Journal*, vol. 759, p. 32, Nov. 2012.

[88] S. Das, J. Errard, and D. Spergel, "Can CMB Lensing Help Cosmic Shear Surveys?," *ArXiv e-prints*, Nov. 2013.

[89] E. J. Baxter, J. Clampitt, T. Giannantonio, S. Dodelson, B. Jain, D. Huterer, L. E. Bleem, T. M. Crawford, G. Efstathiou, P. Fosalba, D. Kirk, J. Kwan, C. Sánchez, K. T. Story, M. A. Troxel, T. M. C. Abbott, F. B. Abdalla, R. Armstrong, A. Benoit-Lévy, B. A. Benson, G. M. Bernstein, R. A. Bernstein, E. Bertin, D. Brooks, J. E. Carlstrom, A. Carnero Rosell, M. Carrasco Kind, J. Carretero, R. Chown, M. Crocce, C. E. Cunha, C. B. D'Andrea, L. N. da Costa, S. Desai, H. T. Diehl, J. P. Dietrich, P. Doel, A. E. Evrard,

A. Fausti Neto, B. Flaugher, J. Frieman, D. Gruen, R. A. Gruendl, G. Gutierrez, T. de Haan, G. P. Holder, K. Honscheid, Z. Hou, D. J. James, K. Kuehn, N. Kuropatkin, M. Lima, M. March, J. L. Marshall, P. Martini, P. Melchior, C. J. Miller, R. Miquel, J. J. Mohr, B. Nord, Y. Omori, A. A. Plazas, C. L. Reichardt, A. K. Romer, E. S. Rykoff, E. Sanchez, I. Sevilla-Noarbe, E. Sheldon, R. C. Smith, M. Soares-Santos, F. Sobreira, E. Suchyta, A. A. Stark, M. E. C. Swanson, G. Tarle, D. Thomas, A. R. Walker, and R. H. Wechsler, "Joint Measurement of Lensing-Galaxy Correlations Using SPT and DES SV Data," *ArXiv e-prints*, Feb. 2016.

[90] J. Liu, A. Ortiz-Vazquez, and J. C. Hill, "Constraining Multiplicative Bias in CFHTLenS Weak Lensing Shear Data," *ArXiv e-prints*, Jan. 2016.

[91] B. Jain and A. Taylor, "Cross-Correlation Tomography: Measuring Dark Energy Evolution with Weak Lensing," *Physical Review Letters*, vol. 91, p. 141302, Oct. 2003.

[92] W. Hu, D. E. Holz, and C. Vale, "CMB cluster lensing: Cosmography with the longest lever arm," Phys. Rev. **D** , vol. 76, p. 127301, Dec. 2007.

[93] S. Das and D. N. Spergel, "Measuring distance ratios with CMB-galaxy lensing cross-correlations," Phys. Rev. **D** , vol. 79, p. 043509, Feb. 2009.

[94] M. S. Madhavacheril, N. Sehgal, and T. R. Slatyer, "Current dark matter annihilation constraints from CMB and low-redshift data," Phys. Rev. **D** , vol. 89, p. 103508, May 2014.

[95] J. M. Cline and P. Scott, “Dark matter CMB constraints and likelihoods for poor particle physicists,” *Journal of Cosmology and Astroparticle Physics*, vol. 3, p. 44, Mar. 2013.

[96] R. Diamanti, L. Lopez-Honorez, O. Mena, S. Palomares-Ruiz, and A. C. Vincent, “Constraining dark matter late-time energy injection: decays and p-wave annihilations,” *ArXiv e-prints*, Aug. 2013.

[97] S. Galli, T. R. Slatyer, M. Valdes, and F. Iocco, “Systematic Uncertainties In Constraining Dark Matter Annihilation From The Cosmic Microwave Background,” *ArXiv*, June 2013.

[98] L. Lopez-Honorez, O. Mena, S. Palomares-Ruiz, and A. C. Vincent, “Constraints on dark matter annihilation from CMB observations before Planck,” *Journal of Cosmology and Astroparticle Physics*, vol. 7, p. 46, July 2013.

[99] C. Weniger, P. D. Serpico, F. Iocco, and G. Bertone, “CMB bounds on dark matter annihilation: Nucleon energy losses after recombination,” Phys. Rev. **D** , vol. 87, p. 123008, June 2013.

[100] A. Natarajan, “Closer look at CMB constraints on WIMP dark matter,” Phys. Rev. **D** , vol. 85, p. 083517, Apr. 2012.

[101] P. J. E. Peebles, “Recombination of the Primeval Plasma,” *Astrophysical Journal*, vol. 153, p. 1, July 1968.

[102] R. Bean, A. Melchiorri, and J. Silk, "Cosmological constraints in the presence of ionizing and resonance radiation at recombination," Phys. Rev. **D** , vol. 75, p. 063505, Mar. 2007.

[103] S. Galli, R. Bean, A. Melchiorri, and J. Silk, "Delayed recombination and cosmic parameters," Phys. Rev. **D** , vol. 78, p. 063532, Sept. 2008.

[104] G. Hütsi, J. Chluba, A. Hektor, and M. Raidal, "WMAP7 and future CMB constraints on annihilating dark matter: implications for GeV-scale WIMPs," *Astronomy and Astrophysics*, vol. 535, p. A26, Nov. 2011.

[105] A. Natarajan and D. J. Schwarz, "Dark matter annihilation and its effect on CMB and hydrogen 21cm observations," Phys. Rev. **D** , vol. 80, p. 043529, Aug. 2009.

[106] G. Giesen, J. Lesgourgues, B. Audren, and Y. Ali-Haïmoud, "CMB photons shedding light on dark matter," *Journal of Cosmology and Astroparticle Physics*, vol. 12, p. 8, Dec. 2012.

[107] J. Shull and M. Van Steenberg, "X-ray secondary heating and ionization in quasar emission-line clouds," *Journal Name: Astrophys. J.*, Nov 1985.

[108] X. Chen and M. Kamionkowski, "Particle decays during the cosmic dark ages," Phys. Rev. **D** , vol. 70, p. 043502, Aug. 2004.

[109] M. Valdés and A. Ferrara, "The energy cascade from warm dark matter decays," *Monthly Notices of the Royal Astronomical Society*, vol. 387, pp. L8–L12, June 2008.

[110] S. R. Furlanetto and S. J. Stoever, "Secondary ionization and heating by fast electrons," *Monthly Notices of the Royal Astronomical Society*, vol. 404, pp. 1869–1878, June 2010.

[111] M. Valdés, C. Evoli, and A. Ferrara, "Particle energy cascade in the intergalactic medium," *Monthly Notices of the Royal Astronomical Society*, vol. 404, pp. 1569–1582, May 2010.

[112] C. Evoli, S. Pandolfi, and A. Ferrara, "Cosmic microwave background constraints on light dark matter candidates," *Monthly Notices of the Royal Astronomical Society*, vol. 433, pp. 1736–1744, Aug. 2013.

[113] T. R. Slatyer, "Energy injection and absorption in the cosmic dark ages," Phys. Rev. **D** , vol. 87, p. 123513, June 2013.

[114] The Planck Collaboration, "The Scientific Programme of Planck," *ArXiv Astrophysics e-prints*, Apr. 2006.

[115] A. Lewis and S. Bridle, "Cosmological parameters from CMB and other data: A Monte Carlo approach," Phys. Rev. **D** , vol. 66, p. 103511, Nov. 2002.

[116] Planck Collaboration, P. A. R. Ade, N. Aghanim, C. Armitage-Caplan, M. Arnaud, M. Ashdown, F. Atrio-Barandela, J. Aumont, C. Baccigalupi, A. J. Banday, and et al., "Planck 2013 results. XVI. Cosmological parameters," *ArXiv e-prints*, Mar. 2013.

[117] C. L. Bennett, D. Larson, J. L. Weiland, N. Jarosik, G. Hinshaw, N. Odegard, K. M. Smith, R. S. Hill, B. Gold, M. Halpern, E. Komatsu, M. R.

Nolta, L. Page, D. N. Spergel, E. Wollack, J. Dunkley, A. Kogut, M. Limon, S. S. Meyer, G. S. Tucker, and E. L. Wright, "Nine-year Wilkinson Microwave Anisotropy Probe (WMAP) Observations: Final Maps and Results," *The Astrophysical Journal*, vol. 208, p. 20, Oct. 2013.

[118] S. Das et al., "The Atacama Cosmology Telescope: Temperature and Gravitational Lensing Power Spectrum Measurements from Three Seasons of Data," *ArXiv e-prints*, Jan. 2013.

[119] K. K. Schaffer et al., "The First Public Release of South Pole Telescope Data: Maps of a 95 $\deg^2$ Field from 2008 Observations," *Astrophysical Journal*, vol. 743, p. 90, Dec. 2011.

[120] Planck collaboration, P. A. R. Ade, N. Aghanim, C. Armitage-Caplan, M. Arnaud, M. Ashdown, F. Atrio-Barandela, J. Aumont, C. Baccigalupi, A. J. Banday, and et al., "Planck 2013 results. XV. CMB power spectra and likelihood," *ArXiv e-prints*, Mar. 2013.

[121] K. S. Dawson et al., "The Baryon Oscillation Spectroscopic Survey of SDSS-III," *The Astronomical Journal*, vol. 145, p. 10, Jan. 2013.

[122] A. G. Riess et al., "A 3% Solution: Determination of the Hubble Constant with the Hubble Space Telescope and Wide Field Camera 3," *Astrophysical Journal*, vol. 730, p. 119, Apr. 2011.

[123] N. Suzuki et al., "The Hubble Space Telescope Cluster Supernova Survey. V. Improving the Dark-energy Constraints above $z > 1$ and Building an Early-

type-hosted Supernova Sample," *Astrophysical Journal*, vol. 746, p. 85, Feb. 2012.

[124] D. Hooper, P. Blasi, and P. Dario Serpico, "Pulsars as the sources of high energy cosmic ray positrons," *Journal of Cosmology and Astroparticle Physics*, vol. 1, p. 25, Jan. 2009.

[125] H. Yüksel, M. D. Kistler, and T. Stanev, "TeV Gamma Rays from Geminga and the Origin of the GeV Positron Excess," *Physical Review Letters*, vol. 103, p. 051101, July 2009.

[126] S. Profumo, "Dissecting cosmic-ray electron-positron data with Occam's razor: the role of known pulsars," *Central European Journal of Physics*, vol. 10, pp. 1–31, Feb. 2012.

[127] D. Malyshev, I. Cholis, and J. Gelfand, "Pulsars versus dark matter interpretation of ATIC/PAMELA," Phys. Rev. **D** , vol. 80, p. 063005, Sept. 2009.

[128] D. Grasso, S. Profumo, A. W. Strong, L. Baldini, R. Bellazzini, E. D. Bloom, J. Bregeon, G. Di Bernardo, D. Gaggero, N. Giglietto, T. Kamae, L. Latronico, F. Longo, M. N. Mazziotta, A. A. Moiseev, A. Morselli, J. F. Ormes, M. Pesce-Rollins, M. Pohl, M. Razzano, C. Sgro, G. Spandre, and T. E. Stephens, "On possible interpretations of the high energy electron-positron spectrum measured by the Fermi Large Area Telescope," *Astroparticle Physics*, vol. 32, pp. 140–151, Sept. 2009.

[129] H.-B. Jin, Y.-L. Wu, and Y.-F. Zhou, "Implications of the first AMS-02 measurement for dark matter annihilation and decay," *ArXiv e-prints*, Apr. 2013.

[130] I. Cholis and D. Hooper, "Dark matter and pulsar origins of the rising cosmic ray positron fraction in light of new data from the ams," *Phys. Rev. D*, vol. 88, p. 023013, Jul 2013.

[131] L. Bergstrom, T. Bringmann, I. Cholis, D. Hooper, and C. Weniger, "New limits on dark matter annihilation from AMS cosmic ray positron data," *ArXiv e-prints*, June 2013.

[132] J. Kopp, "Constraints on dark matter annihilation from AMS-02 results," *ArXiv e-prints*, Apr. 2013.

[133] O. Adriani, G. C. Barbarino, G. A. Bazilevskaya, R. Bellotti, M. Boezio, E. A. Bogomolov, L. Bonechi, M. Bongi, V. Bonvicini, S. Borisov, S. Bottai, A. Bruno, F. Cafagna, D. Campana, R. Carbone, P. Carlson, M. Casolino, G. Castellini, L. Consiglio, M. P. de Pascale, C. de Santis, N. de Simone, V. di Felice, A. M. Galper, W. Gillard, L. Grishantseva, P. Hofverberg, G. Jerse, A. V. Karelin, S. V. Koldashov, S. Y. Krutkov, A. N. Kvashnin, A. Leonov, V. Malvezzi, L. Marcelli, A. G. Mayorov, W. Menn, V. V. Mikhailov, E. Mocchiutti, A. Monaco, N. Mori, N. Nikonov, G. Osteria, P. Papini, M. Pearce, P. Picozza, C. Pizzolotto, M. Ricci, S. B. Ricciarini, L. Rossetto, M. Simon, R. Sparvoli, P. Spillantini, Y. I. Stozhkov, A. Vacchi, E. Vannuccini, G. Vasilyev, S. A. Voronov, J. Wu, Y. T. Yurkin, G. Zampa, N. Zampa, V. G. Zverev, and PAMELA Collaboration, "PAMELA Results on the Cosmic-Ray Antipro-

ton Flux from 60 MeV to 180 GeV in Kinetic Energy," *Physical Review Letters*, vol. 105, p. 121101, Sept. 2010.

[134] A. A. Abdo, M. Ackermann, M. Ajello, W. B. Atwood, M. Axelsson, L. Baldini, J. Ballet, G. Barbiellini, D. Bastieri, M. Battelino, B. M. Baughman, K. Bechtol, R. Bellazzini, B. Berenji, R. D. Blandford, E. D. Bloom, G. Bogaert, E. Bonamente, A. W. Borgland, J. Bregeon, A. Brez, M. Brigida, P. Bruel, T. H. Burnett, G. A. Caliandro, R. A. Cameron, P. A. Caraveo, P. Carlson, J. M. Casandjian, C. Cecchi, E. Charles, A. Chekhtman, C. C. Cheung, J. Chiang, S. Ciprini, R. Claus, J. Cohen-Tanugi, L. R. Cominsky, J. Conrad, S. Cutini, C. D. Dermer, A. de Angelis, F. de Palma, S. W. Digel, G. di Bernardo, E. Do Couto E Silva, P. S. Drell, R. Dubois, D. Dumora, Y. Edmonds, C. Farnier, C. Favuzzi, W. B. Focke, M. Frailis, Y. Fukazawa, S. Funk, P. Fusco, D. Gaggero, F. Gargano, D. Gasparrini, N. Gehrels, S. Germani, B. Giebels, N. Giglietto, F. Giordano, T. Glanzman, G. Godfrey, D. Grasso, I. A. Grenier, M.-H. Grondin, J. E. Grove, L. Guillemot, S. Guiriec, Y. Hanabata, A. K. Harding, R. C. Hartman, M. Hayashida, E. Hays, R. E. Hughes, G. Jóhannesson, A. S. Johnson, R. P. Johnson, W. N. Johnson, T. Kamae, H. Katagiri, J. Kataoka, N. Kawai, M. Kerr, J. Knödlseder, D. Kocevski, F. Kuehn, M. Kuss, J. Lande, L. Latronico, M. Lemoine-Goumard, F. Longo, F. Loparco, B. Lott, M. N. Lovellette, P. Lubrano, G. M. Madejski, A. Makeev, M. M. Massai, M. N. Mazziotta, W. McConville, J. E. McEnery, C. Meurer, P. F. Michelson, W. Mitthumsiri, T. Mizuno, A. A. Moiseev, C. Monte, M. E. Monzani, E. Moretti, A. Morselli, I. V. Moskalenko, S. Murgia, P. L. Nolan,

J. P. Norris, E. Nuss, T. Ohsugi, N. Omodei, E. Orlando, J. F. Ormes, M. Ozaki, D. Paneque, J. H. Panetta, D. Parent, V. Pelassa, M. Pepe, M. Pesce-Rollins, F. Piron, M. Pohl, T. A. Porter, S. Profumo, S. Rainò, R. Rando, M. Razzano, A. Reimer, O. Reimer, T. Reposeur, S. Ritz, L. S. Rochester, A. Y. Rodriguez, R. W. Romani, M. Roth, F. Ryde, H. F.-W. Sadrozinski, D. Sanchez, A. Sander, P. M. Saz Parkinson, J. D. Scargle, T. L. Schalk, A. Sellerholm, C. Sgrò, D. A. Smith, P. D. Smith, G. Spandre, P. Spinelli, J.-L. Starck, T. E. Stephens, M. S. Strickman, A. W. Strong, D. J. Suson, H. Tajima, H. Takahashi, T. Takahashi, T. Tanaka, J. B. Thayer, J. G. Thayer, D. J. Thompson, L. Tibaldo, O. Tibolla, D. F. Torres, G. Tosti, A. Tramacere, Y. Uchiyama, T. L. Usher, A. van Etten, V. Vasileiou, N. Vilchez, V. Vitale, A. P. Waite, E. Wallace, P. Wang, B. L. Winer, K. S. Wood, T. Ylinen, and M. Ziegler, "Measurement of the Cosmic Ray $e^{+}+e^{-}$ Spectrum from 20GeV to 1TeV with the Fermi Large Area Telescope," *Physical Review Letters*, vol. 102, p. 181101, May 2009.

[135] M. Ackermann, M. Ajello, W. B. Atwood, L. Baldini, J. Ballet, G. Barbiellini, D. Bastieri, B. M. Baughman, K. Bechtol, F. Bellardi, R. Bellazzini, F. Belli, B. Berenji, R. D. Blandford, E. D. Bloom, J. R. Bogart, E. Bonamente, A. W. Borgland, T. J. Brandt, J. Bregeon, A. Brez, M. Brigida, P. Bruel, R. Buehler, T. H. Burnett, G. Busetto, S. Buson, G. A. Caliandro, R. A. Cameron, P. A. Caraveo, P. Carlson, S. Carrigan, J. M. Casandjian, M. Ceccanti, C. Cecchi, Ö. Çelik, E. Charles, A. Chekhtman, C. C. Cheung, J. Chiang, A. N. Cillis, S. Ciprini, R. Claus, J. Cohen-Tanugi, J. Conrad,

R. Corbet, M. Deklotz, C. D. Dermer, A. de Angelis, F. de Palma, S. W. Digel, G. di Bernardo, E. Do Couto E Silva, P. S. Drell, A. Drlica-Wagner, R. Dubois, D. Fabiani, C. Favuzzi, S. J. Fegan, P. Fortin, Y. Fukazawa, S. Funk, P. Fusco, D. Gaggero, F. Gargano, D. Gasparrini, N. Gehrels, S. Germani, N. Giglietto, P. Giommi, F. Giordano, M. Giroletti, T. Glanzman, G. Godfrey, D. Grasso, I. A. Grenier, M.-H. Grondin, J. E. Grove, S. Guiriec, M. Gustafsson, D. Hadasch, A. K. Harding, M. Hayashida, E. Hays, D. Horan, R. E. Hughes, G. Jóhannesson, A. S. Johnson, R. P. Johnson, W. N. Johnson, T. Kamae, H. Katagiri, J. Kataoka, M. Kerr, J. Knödlseder, M. Kuss, J. Lande, L. Latronico, M. Lemoine-Goumard, M. Llena Garde, F. Longo, F. Loparco, B. Lott, M. N. Lovellette, P. Lubrano, A. Makeev, M. N. Mazziotta, J. E. McEnery, J. Mehault, P. F. Michelson, M. Minuti, W. Mitthumsiri, T. Mizuno, A. A. Moiseev, C. Monte, M. E. Monzani, E. Moretti, A. Morselli, I. V. Moskalenko, S. Murgia, T. Nakamori, M. Naumann-Godo, P. L. Nolan, J. P. Norris, E. Nuss, T. Ohsugi, A. Okumura, N. Omodei, E. Orlando, J. F. Ormes, M. Ozaki, D. Paneque, J. H. Panetta, D. Parent, V. Pelassa, M. Pepe, M. Pesce-Rollins, V. Petrosian, M. Pinchera, F. Piron, T. A. Porter, S. Profumo, S. Rainò, R. Rando, E. Rapposelli, M. Razzano, A. Reimer, O. Reimer, T. Reposeur, J. Ripken, S. Ritz, L. S. Rochester, R. W. Romani, M. Roth, H. F.-W. Sadrozinski, N. Saggini, D. Sanchez, A. Sander, C. Sgrò, E. J. Siskind, P. D. Smith, G. Spandre, P. Spinelli, Ł. Stawarz, T. E. Stephens, M. S. Strickman, A. W. Strong, D. J. Suson, H. Tajima, H. Takahashi, T. Takahashi, T. Tanaka, J. B. Thayer, J. G. Thayer, D. J. Thompson, L. Tibaldo, O. Ti-

bolla, D. F. Torres, G. Tosti, A. Tramacere, M. Turri, Y. Uchiyama, T. L. Usher, J. Vandenbroucke, V. Vasileiou, N. Vilchez, V. Vitale, A. P. Waite, E. Wallace, P. Wang, B. L. Winer, K. S. Wood, Z. Yang, T. Ylinen, and M. Ziegler, "Fermi LAT observations of cosmic-ray electrons from 7 GeV to 1 TeV," Phys. Rev. **D** , vol. 82, p. 092004, Nov. 2010.

[136] M. Pospelov and A. Ritz, "Astrophysical Signatures of Secluded Dark Matter," *Phys. Lett.*, vol. B671, pp. 391–397, 2009.

[137] N. Arkani-Hamed, D. P. Finkbeiner, T. R. Slatyer, and N. Weiner, "A theory of dark matter," *Phys. Rev. D*, vol. 79, p. 015014, Jan 2009.

[138] K. N. Abazajian, K. Arnold, J. Austermann, B. A. Benson, C. Bischoff, J. Bock, J. R. Bond, J. Borrill, I. Buder, D. L. Burke, E. Calabrese, J. E. Carlstrom, C. S. Carvalho, C. L. Chang, H. C. Chiang, S. Church, A. Cooray, T. M. Crawford, B. P. Crill, K. S. Dawson, S. Das, M. J. Devlin, M. Dobbs, S. Dodelson, O. Doré, J. Dunkley, J. L. Feng, A. Fraisse, J. Gallicchio, S. B. Giddings, D. Green, N. W. Halverson, S. Hanany, D. Hanson, S. R. Hildebrandt, A. Hincks, R. Hlozek, G. Holder, W. L. Holzapfel, K. Honscheid, G. Horowitz, W. Hu, J. Hubmayr, K. Irwin, M. Jackson, W. C. Jones, R. Kallosh, M. Kamionkowski, B. Keating, R. Keisler, W. Kinney, L. Knox, E. Komatsu, J. Kovac, C.-L. Kuo, A. Kusaka, C. Lawrence, A. T. Lee, E. Leitch, A. Linde, E. Linder, P. Lubin, J. Maldacena, E. Martinec, J. McMahon, A. Miller, L. Newburgh, M. D. Niemack, H. Nguyen, H. T. Nguyen, L. Page, C. Pryke, C. L. Reichardt, J. E. Ruhl, N. Sehgal, U. Seljak,

L. Senatore, J. Sievers, E. Silverstein, A. Slosar, K. M. Smith, D. Spergel, S. T. Staggs, A. Stark, R. Stompor, A. G. Vieregg, G. Wang, S. Watson, E. J. Wollack, W. L. K. Wu, K. W. Yoon, O. Zahn, and M. Zaldarriaga, "Inflation Physics from the Cosmic Microwave Background and Large Scale Structure," *ArXiv e-prints*, Sept. 2013.

[139] K. N. Abazajian, K. Arnold, J. Austermann, B. A. Benson, C. Bischoff, J. Bock, J. R. Bond, J. Borrill, E. Calabrese, J. E. Carlstrom, C. S. Carvalho, C. L. Chang, H. C. Chiang, S. Church, A. Cooray, T. M. Crawford, K. S. Dawson, S. Das, M. J. Devlin, M. Dobbs, S. Dodelson, O. Dore, J. Dunkley, J. Errard, A. Fraisse, J. Gallicchio, N. W. Halverson, S. Hanany, S. R. Hildebrandt, A. Hincks, R. Hlozek, G. Holder, W. L. Holzapfel, K. Honscheid, W. Hu, J. Hubmayr, K. Irwin, W. C. Jones, M. Kamionkowski, B. Keating, R. Keisler, L. Knox, E. Komatsu, J. Kovac, C.-L. Kuo, C. Lawrence, A. T. Lee, E. Leitch, E. Linder, P. Lubin, J. McMahon, A. Miller, L. Newburgh, M. D. Niemack, H. Nguyen, H. T. Nguyen, L. Page, C. Pryke, C. L. Reichardt, J. E. Ruhl, N. Sehgal, U. Seljak, J. Sievers, E. Silverstein, A. Slosar, K. M. Smith, D. Spergel, S. T. Staggs, A. Stark, R. Stompor, A. G. Vieregg, G. Wang, S. Watson, E. J. Wollack, W. L. K. Wu, K. W. Yoon, and O. Zahn, "Neutrino Physics from the Cosmic Microwave Background and Large Scale Structure," *ArXiv e-prints*, Sept. 2013.

[140] D. Hooper, I. Cholis, T. Linden, J. Siegal-Gaskins, and T. Slatyer, "Pulsars Cannot Account for the Inner Galaxy's GeV Excess," *ArXiv e-prints*, May 2013.

[141] D. Hooper and T. Linden, "Origin of the gamma rays from the Galactic Center," Phys. Rev. **D** , vol. 84, p. 123005, Dec. 2011.

[142] Dan Hooper and Lisa Goodenough, "Dark matter annihilation in the galactic center as seen by the fermi gamma ray space telescope," *Physics Letters B*, vol. 697, no. 5, pp. 412 – 428, 2011.

[143] D. Hooper, C. Kelso, and F. S. Queiroz, "Stringent constraints on the dark matter annihilation cross section from the region of the Galactic Center," *Astroparticle Physics*, vol. 46, pp. 55–70, June 2013.

[144] C. Gordon and O. Macias, "Dark Matter and Pulsar Model Constraints from Galactic Center Fermi-LAT Gamma Ray Observations," *ArXiv e-prints*, June 2013.

[145] M. S. Madhavacheril, P. McDonald, N. Sehgal, and A. Slosar, "Building unbiased estimators from non-Gaussian likelihoods with application to shear estimation," *JCAP*, vol. 1, p. 022, Jan. 2015.

[146] E. S. Sheldon, "An Implementation of Bayesian Lensing Shear Measurement," *ArXiv e-prints*, Mar. 2014.

[147] J. R. Bond, A. H. Jaffe, and L. Knox, "Estimating the power spectrum of the cosmic microwave background," Phys. Rev. **D** , vol. 57, pp. 2117–2137, Feb. 1998.

[148] U. Seljak, "Cosmography and Power Spectrum Estimation: A Unified Approach," *Astrophysical Journal*, vol. 503, pp. 492–+, Aug. 1998.

[149] J. R. Bond, A. H. Jaffe, and L. Knox, "Radical Compression of Cosmic Microwave Background Data," *Astrophysical Journal*, vol. 533, pp. 19–37, Apr. 2000.

[150] S. Dodelson, *Modern cosmology*. 2003.

[151] D. M. Goldberg and D. J. Bacon, "Galaxy-Galaxy Flexion: Weak Lensing to Second Order," *Astrophysical Journal*, vol. 619, pp. 741–748, Feb. 2005.

[152] LSST Science Collaboration, P. A. Abell, J. Allison, S. F. Anderson, J. R. Andrew, J. R. P. Angel, L. Armus, D. Arnett, S. J. Asztalos, T. S. Axelrod, and et al., "LSST Science Book, Version 2.0," *ArXiv e-prints*, Dec. 2009.

[153] L. Miller, T. D. Kitching, C. Heymans, A. F. Heavens, and L. van Waerbeke, "Bayesian galaxy shape measurement for weak lensing surveys - I. Methodology and a fast-fitting algorithm," Mon. Not. Roy. Astron. Soc. , vol. 382, pp. 315–324, Nov. 2007.

[154] A. Refregier and A. Amara, "A Way Forward for Cosmic Shear: Monte-Carlo Control Loops," *ArXiv e-prints*, Mar. 2013.

[155] K. M. Smith, O. Zahn, and O. Doré, "Detection of gravitational lensing in the cosmic microwave background," Phys. Rev. **D** , vol. 76, pp. 043510–+, Aug. 2007.

[156] C. M. Hirata, S. Ho, N. Padmanabhan, U. Seljak, and N. A. Bahcall, "Correlation of CMB with large-scale structure. II. Weak lensing," Phys. Rev. **D** , vol. 78, p. 043520, Aug. 2008.

[157] S. Das, T. A. Marriage, P. A. R. Ade, P. Aguirre, M. Amiri, J. W. Appel, L. F. Barrientos, E. S. Battistelli, J. R. Bond, B. Brown, B. Burger, J. Chervenak, M. J. Devlin, S. R. Dicker, W. Bertrand Doriese, J. Dunkley, R. Dünner, T. Essinger-Hileman, R. P. Fisher, J. W. Fowler, A. Hajian, M. Halpern, M. Hasselfield, C. Hernández-Monteagudo, G. C. Hilton, M. Hilton, A. D. Hincks, R. Hlozek, K. M. Huffenberger, D. H. Hughes, J. P. Hughes, L. Infante, K. D. Irwin, J. Baptiste Juin, M. Kaul, J. Klein, A. Kosowsky, J. M. Lau, M. Limon, Y.-T. Lin, R. H. Lupton, D. Marsden, K. Martocci, P. Mauskopf, F. Menanteau, K. Moodley, H. Moseley, C. B. Netterfield, M. D. Niemack, M. R. Nolta, L. A. Page, L. Parker, B. Partridge, B. Reid, N. Sehgal, B. D. Sherwin, J. Sievers, D. N. Spergel, S. T. Staggs, D. S. Swetz, E. R. Switzer, R. Thornton, H. Trac, C. Tucker, R. Warne, E. Wollack, and Y. Zhao, "The Atacama Cosmology Telescope: A Measurement of the Cosmic Microwave Background Power Spectrum at 148 and 218 GHz from the 2008 Southern Survey," *Astrophysical Journal*, vol. 729, p. 62, Mar. 2011.

[158] A. van Engelen, R. Keisler, O. Zahn, K. A. Aird, B. A. Benson, L. E. Bleem, J. E. Carlstrom, C. L. Chang, H. M. Cho, T. M. Crawford, A. T. Crites, T. de Haan, M. A. Dobbs, J. Dudley, E. M. George, N. W. Halverson, G. P. Holder, W. L. Holzapfel, S. Hoover, Z. Hou, J. D. Hrubes, M. Joy, L. Knox, A. T. Lee, E. M. Leitch, M. Lueker, D. Luong-Van, J. J. McMahon, J. Mehl, S. S. Meyer, M. Millea, J. J. Mohr, T. E. Montroy, T. Natoli, S. Padin, T. Plagge, C. Pryke, C. L. Reichardt, J. E. Ruhl, J. T. Sayre, K. K. Schaffer, L. Shaw, E. Shirokoff, H. G. Spieler, Z. Staniszewski, A. A. Stark, K. Story, K. Vanderlinde, J. D.

Vieira, and R. Williamson, “A Measurement of Gravitational Lensing of the Microwave Background Using South Pole Telescope Data,” *Astrophysical Journal*, vol. 756, p. 142, Sept. 2012.

[159] Planck Collaboration, “Planck 2013 results. XVII. Gravitational lensing by large-scale structure,” Astron. Astrophys. , vol. 571, p. A17, Nov. 2014.

[160] B. D. Sherwin, S. Das, A. Hajian, G. Addison, J. R. Bond, D. Crichton, M. J. Devlin, J. Dunkley, M. B. Gralla, M. Halpern, J. C. Hill, A. D. Hincks, J. P. Hughes, K. Huffenberger, R. Hlozek, A. Kosowsky, T. Louis, T. A. Marriage, D. Marsden, F. Menanteau, K. Moodley, M. D. Niemack, L. A. Page, E. D. Reese, N. Sehgal, J. Sievers, C. Sifón, D. N. Spergel, S. T. Staggs, E. R. Switzer, and E. Wollack, “The Atacama Cosmology Telescope: Cross-correlation of cosmic microwave background lensing and quasars,” Phys. Rev. **D** , vol. 86, p. 083006, Oct. 2012.

[161] L. E. Bleem, A. van Engelen, G. P. Holder, K. A. Aird, R. Armstrong, M. L. N. Ashby, M. R. Becker, B. A. Benson, T. Biesiadzinski, M. Brodwin, M. T. Busha, J. E. Carlstrom, C. L. Chang, H. M. Cho, T. M. Crawford, A. T. Crites, T. de Haan, S. Desai, M. A. Dobbs, O. Doré, J. Dudley, J. E. Geach, E. M. George, M. D. Gladders, A. H. Gonzalez, N. W. Halverson, N. Harrington, F. W. High, B. P. Holden, W. L. Holzapfel, S. Hoover, J. D. Hrubes, M. Joy, R. Keisler, L. Knox, A. T. Lee, E. M. Leitch, M. Lueker, D. Luong-Van, D. P. Marrone, J. Martinez-Manso, J. J. McMahon, J. Mehl, S. S. Meyer, J. J. Mohr, T. E. Montroy, T. Natoli, S. Padin, T. Plagge, C. Pryke, C. L. Reichardt,

A. Rest, J. E. Ruhl, B. R. Saliwanchik, J. T. Sayre, K. K. Schaffer, L. Shaw, E. Shirokoff, H. G. Spieler, B. Stalder, S. A. Stanford, Z. Staniszewski, A. A. Stark, D. Stern, K. Story, A. Vallinotto, K. Vanderlinde, J. D. Vieira, R. H. Wechsler, R. Williamson, and O. Zahn, "A Measurement of the Correlation of Galaxy Surveys with CMB Lensing Convergence Maps from the South Pole Telescope," *Astrophysical Journal*, vol. 753, p. L9, June 2012.

[162] J. E. Geach, R. C. Hickox, L. E. Bleem, M. Brodwin, G. P. Holder, K. A. Aird, B. A. Benson, S. Bhattacharya, J. E. Carlstrom, C. L. Chang, H.-M. Cho, T. M. Crawford, A. T. Crites, T. de Haan, M. A. Dobbs, J. Dudley, E. M. George, K. N. Hainline, N. W. Halverson, W. L. Holzapfel, S. Hoover, Z. Hou, J. D. Hrubes, R. Keisler, L. Knox, A. T. Lee, E. M. Leitch, M. Lueker, D. Luong-Van, D. P. Marrone, J. J. McMahon, J. Mehl, S. S. Meyer, M. Millea, J. J. Mohr, T. E. Montroy, A. D. Myers, S. Padin, T. Plagge, C. Pryke, C. L. Reichardt, J. E. Ruhl, J. T. Sayre, K. K. Schaffer, L. Shaw, E. Shirokoff, H. G. Spieler, Z. Staniszewski, A. A. Stark, K. T. Story, A. van Engelen, K. Vanderlinde, J. D. Vieira, R. Williamson, and O. Zahn, "A Direct Measurement of the Linear Bias of Mid-infrared-selected Quasars at $z \approx 1$ Using Cosmic Microwave Background Lensing," Astrophys. J. Let. , vol. 776, p. L41, Oct. 2013.

[163] G. P. Holder, M. P. Viero, O. Zahn, K. A. Aird, B. A. Benson, S. Bhattacharya, L. E. Bleem, J. Bock, M. Brodwin, J. E. Carlstrom, C. L. Chang, H.-M. Cho, A. Conley, T. M. Crawford, A. T. Crites, T. de Haan, M. A. Dobbs, J. Dudley, E. M. George, N. W. Halverson, W. L. Holzapfel, S. Hoover, Z. Hou, J. D. Hrubes, R. Keisler, L. Knox, A. T. Lee, E. M. Leitch, M. Lueker, D. Luong-Van,

G. Marsden, D. P. Marrone, J. J. McMahon, J. Mehl, S. S. Meyer, M. Millea, J. J. Mohr, T. E. Montroy, S. Padin, T. Plagge, C. Pryke, C. L. Reichardt, J. E. Ruhl, J. T. Sayre, K. K. Schaffer, B. Schulz, L. Shaw, E. Shirokoff, H. G. Spieler, Z. Staniszewski, A. A. Stark, K. T. Story, A. van Engelen, K. Vanderlinde, J. D. Vieira, R. Williamson, and M. Zemcov, "A Cosmic Microwave Background Lensing Mass Map and Its Correlation with the Cosmic Infrared Background," Astrophys. J. Let. , vol. 771, p. L16, July 2013.

[164] Planck Collaboration, "Planck 2013 results. XVIII. The gravitational lensing-infrared background correlation," Astron. Astrophys. , vol. 571, p. A18, Nov. 2014.

[165] D. Hanson, S. Hoover, A. Crites, P. A. R. Ade, K. A. Aird, J. E. Austermann, J. A. Beall, A. N. Bender, B. A. Benson, L. E. Bleem, J. J. Bock, J. E. Carlstrom, C. L. Chang, H. C. Chiang, H.-M. Cho, A. Conley, T. M. Crawford, T. de Haan, M. A. Dobbs, W. Everett, J. Gallicchio, J. Gao, E. M. George, N. W. Halverson, N. Harrington, J. W. Henning, G. C. Hilton, G. P. Holder, W. L. Holzapfel, J. D. Hrubes, N. Huang, J. Hubmayr, K. D. Irwin, R. Keisler, L. Knox, A. T. Lee, E. Leitch, D. Li, C. Liang, D. Luong-Van, G. Marsden, J. J. McMahon, J. Mehl, S. S. Meyer, L. Mocanu, T. E. Montroy, T. Natoli, J. P. Nibarger, V. Novosad, S. Padin, C. Pryke, C. L. Reichardt, J. E. Ruhl, B. R. Saliwanchik, J. T. Sayre, K. K. Schaffer, B. Schulz, G. Smecher, A. A. Stark, K. T. Story, C. Tucker, K. Vanderlinde, J. D. Vieira, M. P. Viero, G. Wang, V. Yefremenko, O. Zahn, and M. Zemcov, "Detection of B-Mode

Polarization in the Cosmic Microwave Background with Data from the South Pole Telescope," *Physical Review Letters*, vol. 111, p. 141301, Oct. 2013.

[166] P. A. R. Ade, Y. Akiba, A. E. Anthony, K. Arnold, M. Atlas, D. Barron, D. Boettger, J. Borrill, C. Borys, S. Chapman, Y. Chinone, M. Dobbs, T. Elleflot, J. Errard, G. Fabbian, C. Feng, D. Flanigan, A. Gilbert, W. Grainger, N. W. Halverson, M. Hasegawa, K. Hattori, M. Hazumi, W. L. Holzapfel, Y. Hori, J. Howard, P. Hyland, Y. Inoue, G. C. Jaehnig, A. Jaffe, B. Keating, Z. Kermish, R. Keskitalo, T. Kisner, M. Le Jeune, A. T. Lee, E. M. Leitch, E. Linder, M. Lungu, F. Matsuda, T. Matsumura, X. Meng, N. J. Miller, H. Morii, S. Moyerman, M. J. Myers, M. Navaroli, H. Nishino, H. Paar, J. Peloton, D. Poletti, E. Quealy, G. Rebeiz, C. L. Reichardt, P. L. Richards, C. Ross, K. Rotermund, I. Schanning, D. E. Schenck, B. D. Sherwin, A. Shimizu, C. Shimmin, M. Shimon, P. Siritanasak, G. Smecher, H. Spieler, N. Stebor, B. Steinbach, R. Stompor, A. Suzuki, S. Takakura, A. Tikhomirov, T. Tomaru, B. Wilson, A. Yadav, O. Zahn, and Polarbear Collaboration, "Evidence for Gravitational Lensing of the Cosmic Microwave Background Polarization from Cross-Correlation with the Cosmic Infrared Background," *Physical Review Letters*, vol. 112, p. 131302, Apr. 2014.

[167] P. A. R. Ade, Y. Akiba, A. E. Anthony, K. Arnold, D. Barron, D. Boettger, J. Borrill, S. Chapman, Y. Chinone, M. Dobbs, T. Elleflot, J. Errard, G. Fabbian, C. Feng, D. Flanigan, A. Gilbert, W. Grainger, N. W. Halverson, M. Hasegawa, K. Hattori, M. Hazumi, W. L. Holzapfel, Y. Hori, J. Howard, P. Hyland, Y. Inoue, G. C. Jaehnig, A. Jaffe, B. Keating, Z. Kermish, R. Keski-

talo, T. Kisner, M. Le Jeune, A. T. Lee, E. Linder, M. Lungu, F. Matsuda, T. Matsumura, X. Meng, N. J. Miller, H. Morii, S. Moyerman, M. J. Myers, M. Navaroli, H. Nishino, H. Paar, J. Peloton, E. Quealy, G. Rebeiz, C. L. Reichardt, P. L. Richards, C. Ross, I. Schanning, D. E. Schenck, B. Sherwin, A. Shimizu, C. Shimmin, M. Shimon, P. Siritanasak, G. Smecher, H. Spieler, N. Stebor, B. Steinbach, R. Stompor, A. Suzuki, S. Takakura, T. Tomaru, B. Wilson, A. Yadav, and O. Zahn, "Gravitational Lensing of Cosmic Microwave Background Polarization," Dec. 2013.

[168] N. Hand, A. Leauthaud, S. Das, B. D. Sherwin, G. E. Addison, J. R. Bond, E. Calabrese, A. Charbonnier, M. J. Devlin, J. Dunkley, T. Erben, A. Hajian, M. Halpern, J. Harnois-Déraps, C. Heymans, H. Hildebrandt, A. D. Hincks, J.-P. Kneib, A. Kosowsky, M. Makler, L. Miller, K. Moodley, B. Moraes, M. D. Niemack, L. A. Page, B. Partridge, N. Sehgal, H. Shan, J. L. Sievers, D. N. Spergel, S. T. Staggs, E. R. Switzer, J. E. Taylor, L. Van Waerbeke, and E. J. Wollack, "First Measurement of the Cross-Correlation of CMB Lensing and Galaxy Lensing," Nov. 2013.

[169] F. Bianchini, P. Bielewicz, A. Lapi, J. Gonzalez-Nuevo, C. Baccigalupi, G. de Zotti, L. Danese, N. Bourne, A. Cooray, L. Dunne, S. Dye, S. Eales, R. Ivison, S. Maddox, M. Negrello, D. Scott, and E. Valiante, "Cross-correlation between the CMB lensing potential measured by Planck and high-z sub-mm galaxies detected by the Herschel-ATLAS survey," *ArXiv e-prints*, Oct. 2014.

[170] M. A. DiPompeo, A. D. Myers, R. C. Hickox, J. E. Geach, G. Holder, K. N.

Hainline, and S. W. Hall, "Weighing obscured and unobscured quasar hosts with the CMB," *ArXiv e-prints*, Nov. 2014.

[171] N. Fornengo, L. Perotto, M. Regis, and S. Camera, "Evidence of cross-correlation between the CMB lensing and the gamma-ray sky," *ArXiv e-prints*, Oct. 2014.

[172] J. C. Hill and D. N. Spergel, "Detection of thermal SZ-CMB lensing cross-correlation in Planck nominal mission data," *JCAP*, vol. 2, p. 30, Feb. 2014.

[173] Planck Collaboration, "Planck 2013 results. XVI. Cosmological parameters," Astron. Astrophys. , vol. 571, p. A16, Nov. 2014.

[174] K. N. Abazajian, K. Arnold, J. Austermann, B. A. Benson, C. Bischoff, J. Bock, J. R. Bond, J. Borrill, E. Calabrese, J. E. Carlstrom, C. S. Carvalho, C. L. Chang, H. C. Chiang, S. Church, A. Cooray, T. M. Crawford, K. S. Dawson, S. Das, M. J. Devlin, M. Dobbs, S. Dodelson, O. Dore, J. Dunkley, J. Errard, A. Fraisse, J. Gallicchio, N. W. Halverson, S. Hanany, S. R. Hildebrandt, A. Hincks, R. Hlozek, G. Holder, W. L. Holzapfel, K. Honscheid, W. Hu, J. Hubmayr, K. Irwin, W. C. Jones, M. Kamionkowski, B. Keating, R. Keisler, L. Knox, E. Komatsu, J. Kovac, C.-L. Kuo, C. Lawrence, A. T. Lee, E. Leitch, E. Linder, P. Lubin, J. McMahon, A. Miller, L. Newburgh, M. D. Niemack, H. Nguyen, H. T. Nguyen, L. Page, C. Pryke, C. L. Reichardt, J. E. Ruhl, N. Sehgal, U. Seljak, J. Sievers, E. Silverstein, A. Slosar, K. M. Smith, D. Spergel, S. T. Staggs, A. Stark, R. Stompor, A. G. Vieregg, G. Wang, S. Watson, E. J. Wollack, W. L. K. Wu, K. W. Yoon, and O. Zahn, "Neutrino Physics from the

Cosmic Microwave Background and Large Scale Structure," *ArXiv e-prints*, Sept. 2013.

[175] K. N. Abazajian, K. Arnold, J. Austermann, B. A. Benson, C. Bischoff, J. Bock, J. R. Bond, J. Borrill, I. Buder, D. L. Burke, E. Calabrese, J. E. Carlstrom, C. S. Carvalho, C. L. Chang, H. C. Chiang, S. Church, A. Cooray, T. M. Crawford, B. P. Crill, K. S. Dawson, S. Das, M. J. Devlin, M. Dobbs, S. Dodelson, O. Doré, J. Dunkley, J. L. Feng, A. Fraisse, J. Gallicchio, S. B. Giddings, D. Green, N. W. Halverson, S. Hanany, D. Hanson, S. R. Hildebrandt, A. Hincks, R. Hlozek, G. Holder, W. L. Holzapfel, K. Honscheid, G. Horowitz, W. Hu, J. Hubmayr, K. Irwin, M. Jackson, W. C. Jones, R. Kallosh, M. Kamionkowski, B. Keating, R. Keisler, W. Kinney, L. Knox, E. Komatsu, J. Kovac, C.-L. Kuo, A. Kusaka, C. Lawrence, A. T. Lee, E. Leitch, A. Linde, E. Linder, P. Lubin, J. Maldacena, E. Martinec, J. McMahon, A. Miller, V. Mukhanov, L. Newburgh, M. D. Niemack, H. Nguyen, H. T. Nguyen, L. Page, C. Pryke, C. L. Reichardt, J. E. Ruhl, N. Sehgal, U. Seljak, L. Senatore, J. Sievers, E. Silverstein, A. Slosar, K. M. Smith, D. Spergel, S. T. Staggs, A. Stark, R. Stompor, A. G. Vieregg, G. Wang, S. Watson, E. J. Wollack, W. L. K. Wu, K. W. Yoon, O. Zahn, and M. Zaldarriaga, "Inflation Physics from the Cosmic Microwave Background and Large Scale Structure," *ArXiv e-prints*, Sept. 2013.

[176] E. Calabrese, R. Hložek, N. Battaglia, J. R. Bond, F. de Bernardis, M. J. Devlin, A. Hajian, S. Henderson, J. C. Hil, A. Kosowsky, *et al.*, "Precision

epoch of reionization studies with next-generation cmb experiments," *Journal of Cosmology and Astroparticle Physics*, vol. 2014, no. 08, p. 010, 2014.

[177] U. Seljak and M. Zaldarriaga, "Lensing-induced cluster signatures in the cosmic microwave background," *The Astrophysical Journal*, vol. 538, no. 1, p. 57, 2000.

[178] M. Zaldarriaga, "Lensing of the cmb: Non-gaussian aspects," *Physical Review D*, vol. 62, no. 6, p. 063510, 2000.

[179] S. Dodelson and G. D. Starkman, "Galaxy-CMB Lensing," *ArXiv Astrophysics e-prints*, May 2003.

[180] G. Holder and A. Kosowsky, "Gravitational lensing of the microwave background by galaxy clusters," *The Astrophysical Journal*, vol. 616, no. 1, p. 8, 2004.

[181] S. Dodelson, "Cmb-cluster lensing," *Physical Review D*, vol. 70, no. 2, p. 023009, 2004.

[182] C. Vale, A. Amblard, and M. White, "Cluster lensing of the CMB," *New Astronomy*, vol. 10, pp. 1–15, Nov. 2004.

[183] M. Maturi, M. Bartelmann, M. Meneghetti, and L. Moscardini, "Gravitational lensing of the CMB by galaxy clusters," Astron. Astrophys. , vol. 436, pp. 37–46, June 2005.

[184] A. Lewis and L. King, "Cluster masses from CMB and galaxy weak lensing," Phys. Rev. **D** , vol. 73, p. 063006, Mar. 2006.

[185] W. Hu, D. E. Holz, and C. Vale, "CMB cluster lensing: Cosmography with the longest lever arm," Phys. Rev. **D** , vol. 76, p. 127301, Dec. 2007.

[186] W. Hu, S. DeDeo, and C. Vale, "Cluster mass estimators from cmb temperature and polarization lensing," *New Journal of Physics*, vol. 9, no. 12, p. 441, 2007.

[187] J. Yoo and M. Zaldarriaga, "Improved estimation of cluster mass profiles from the cosmic microwave background," Phys. Rev. **D** , vol. 78, p. 083002, Oct. 2008.

[188] J. Yoo, M. Zaldarriaga, and L. Hernquist, "Lensing reconstruction of cluster-mass cross correlation with cosmic microwave background polarization," Phys. Rev. **D** , vol. 81, p. 123006, June 2010.

[189] J.-B. Melin and J. G. Bartlett, "Measuring cluster masses with CMB lensing: a statistical approach," *ArXiv e-prints*, Aug. 2014.

[190] D. J. Eisenstein, D. H. Weinberg, E. Agol, H. Aihara, C. A. Prieto, S. F. Anderson, J. A. Arns, É. Aubourg, S. Bailey, E. Balbinot, *et al.*, "Sdss-iii: Massive spectroscopic surveys of the distant universe, the milky way, and extra-solar planetary systems," *The Astronomical Journal*, vol. 142, no. 3, p. 72, 2011.

[191] K. S. Dawson, D. J. Schlegel, C. P. Ahn, S. F. Anderson, É. Aubourg, S. Bailey, R. H. Barkhouser, J. E. Bautista, A. Beifiori, A. A. Berlind, *et al.*, "The baryon oscillation spectroscopic survey of sdss-iii," *The Astronomical Journal*, vol. 145, no. 1, p. 10, 2013.

[192] C. P. Ahn, R. Alexandroff, C. Allende Prieto, F. Anders, S. F. Anderson, T. Anderton, B. H. Andrews, É. Aubourg, S. Bailey, F. A. Bastien, *et al.*, "The tenth data release of the sloan digital sky survey: First spectroscopic data from the sdss-iii apache point observatory galactic evolution experiment," *The Astrophysical Journal Supplement Series*, vol. 211, p. 17, 2014.

[193] M. D. Niemack, P. A. R. Ade, J. Aguirre, F. Barrientos, J. A. Beall, J. R. Bond, J. Britton, H. M. Cho, S. Das, M. J. Devlin, S. Dicker, J. Dunkley, R. Dünner, J. W. Fowler, A. Hajian, M. Halpern, M. Hasselfield, G. C. Hilton, M. Hilton, J. Hubmayr, J. P. Hughes, L. Infante, K. D. Irwin, N. Jarosik, J. Klein, A. Kosowsky, T. A. Marriage, J. McMahon, F. Menanteau, K. Moodley, J. P. Nibarger, M. R. Nolta, L. A. Page, B. Partridge, E. D. Reese, J. Sievers, D. N. Spergel, S. T. Staggs, R. Thornton, C. Tucker, E. Wollack, and K. W. Yoon, "ACTPol: a polarization-sensitive receiver for the Atacama Cosmology Telescope," in *Society of Photo-Optical Instrumentation Engineers (SPIE) Conference Series*, vol. 7741, July 2010.

[194] S. Naess, M. Hasselfield, J. McMahon, M. D. Niemack, G. E. Addison, P. A. R. Ade, R. Allison, M. Amiri, N. Battaglia, J. A. Beall, F. de Bernardis, J. R. Bond, J. Britton, E. Calabrese, H.-m. Cho, K. Coughlin, D. Crichton, S. Das, R. Datta, M. J. Devlin, S. R. Dicker, J. Dunkley, R. Dünner, J. W. Fowler, A. E. Fox, P. Gallardo, E. Grace, M. Gralla, A. Hajian, M. Halpern, S. Henderson, J. C. Hill, G. C. Hilton, M. Hilton, A. D. Hincks, R. Hlozek, P. Ho, J. Hubmayr, K. M. Huffenberger, J. P. Hughes, L. Infante, K. Irwin, R. Jackson, S. Muya Kasanda, J. Klein, B. Koopman, A. Kosowsky, D. Li, T. Louis, M. Lungu,

M. Madhavacheril, T. A. Marriage, L. Maurin, F. Menanteau, K. Moodley, C. Munson, L. Newburgh, J. Nibarger, M. R. Nolta, L. A. Page, C. Pappas, B. Partridge, F. Rojas, B. L. Schmitt, N. Sehgal, B. D. Sherwin, J. Sievers, S. Simon, D. N. Spergel, S. T. Staggs, E. R. Switzer, R. Thornton, H. Trac, C. Tucker, M. Uehara, A. Van Engelen, J. T. Ward, and E. J. Wollack, "The Atacama Cosmology Telescope: CMB polarization at 200 ¡ l ¡ 9000," *JCAP*, vol. 10, p. 7, Oct. 2014.

[195] Planck Collaboration, "Planck 2013 results. I. Overview of products and scientific results," Mar. 2013.

[196] T. Louis, G. E. Addison, M. Hasselfield, J. R. Bond, E. Calabrese, S. Das, M. J. Devlin, J. Dunkley, R. Dünner, M. Gralla, A. Hajian, A. D. Hincks, R. Hlozek, K. Huffenberger, L. Infante, A. Kosowsky, T. A. Marriage, K. Moodley, S. Næss, M. D. Niemack, M. R. Nolta, L. A. Page, B. Partridge, N. Sehgal, J. L. Sievers, D. N. Spergel, S. T. Staggs, B. Z. Walter, and E. J. Wollack, "The Atacama Cosmology Telescope: cross correlation with Planck maps," *JCAP*, vol. 7, p. 16, July 2014.

[197] D. G. York, J. Adelman, J. E. Anderson Jr, S. F. Anderson, J. Annis, N. A. Bahcall, J. Bakken, R. Barkhouser, S. Bastian, E. Berman, *et al.*, "The sloan digital sky survey: Technical summary," *The Astronomical Journal*, vol. 120, no. 3, p. 1579, 2000.

[198] J. E. Gunn, W. A. Siegmund, E. J. Mannery, R. E. Owen, C. L. Hull, R. F. Leger, L. N. Carey, G. R. Knapp, D. G. York, W. N. Boroski, *et al.*, "The 2.5 m

telescope of the sloan digital sky survey," *The Astronomical Journal*, vol. 131, no. 4, p. 2332, 2006.

[199] D. J. Eisenstein, J. Annis, J. E. Gunn, A. S. Szalay, A. J. Connolly, R. C. Nichol, N. A. Bahcall, M. Bernardi, S. Burles, F. J. Castander, M. Fukugita, D. W. Hogg, Ž. Ivezić, G. R. Knapp, R. H. Lupton, V. Narayanan, M. Postman, D. E. Reichart, M. Richmond, D. P. Schneider, D. J. Schlegel, M. A. Strauss, M. SubbaRao, D. L. Tucker, D. Vanden Berk, M. S. Vogeley, D. H. Weinberg, and B. Yanny, "Spectroscopic Target Selection for the Sloan Digital Sky Survey: The Luminous Red Galaxy Sample," *AJ*, vol. 122, pp. 2267–2280, Nov. 2001.

[200] L. Anderson, E. Aubourg, S. Bailey, D. Bizyaev, M. Blanton, A. S. Bolton, J. Brinkmann, J. R. Brownstein, A. Burden, A. J. Cuesta, L. A. N. da Costa, K. S. Dawson, R. de Putter, D. J. Eisenstein, J. E. Gunn, H. Guo, J.-C. Hamilton, P. Harding, S. Ho, K. Honscheid, E. Kazin, D. Kirkby, J.-P. Kneib, A. Labatie, C. Loomis, R. H. Lupton, E. Malanushenko, V. Malanushenko, R. Mandelbaum, M. Manera, C. Maraston, C. K. McBride, K. T. Mehta, O. Mena, F. Montesano, D. Muna, R. C. Nichol, S. E. Nuza, M. D. Olmstead, D. Oravetz, N. Padmanabhan, N. Palanque-Delabrouille, K. Pan, J. Parejko, I. Pâris, W. J. Percival, P. Petitjean, F. Prada, B. Reid, N. A. Roe, A. J. Ross, N. P. Ross, L. Samushia, A. G. Sánchez, D. J. Schlegel, D. P. Schneider, C. G. Scóccola, H.-J. Seo, E. S. Sheldon, A. Simmons, R. A. Skibba, M. A. Strauss, M. E. C. Swanson, D. Thomas, J. L. Tinker, R. Tojeiro, M. V. Magaña, L. Verde, C. Wagner, D. A. Wake, B. A. Weaver, D. H. Weinberg, M. White,

X. Xu, C. Yèche, I. Zehavi, and G.-B. Zhao, "The clustering of galaxies in the SDSS-III Baryon Oscillation Spectroscopic Survey: baryon acoustic oscillations in the Data Release 9 spectroscopic galaxy sample," Mon. Not. Roy. Astron. Soc. , vol. 427, pp. 3435–3467, Dec. 2012.

[201] B. A. Reid, L. Samushia, M. White, W. J. Percival, M. Manera, N. Padmanabhan, A. J. Ross, A. G. Sánchez, S. Bailey, D. Bizyaev, A. S. Bolton, H. Brewington, J. Brinkmann, J. R. Brownstein, A. J. Cuesta, D. J. Eisenstein, J. E. Gunn, K. Honscheid, E. Malanushenko, V. Malanushenko, C. Maraston, C. K. McBride, D. Muna, R. C. Nichol, D. Oravetz, K. Pan, R. de Putter, N. A. Roe, N. P. Ross, D. J. Schlegel, D. P. Schneider, H.-J. Seo, A. Shelden, E. S. Sheldon, A. Simmons, R. A. Skibba, S. Snedden, M. E. C. Swanson, D. Thomas, J. Tinker, R. Tojeiro, L. Verde, D. A. Wake, B. A. Weaver, D. H. Weinberg, I. Zehavi, and G.-B. Zhao, "The clustering of galaxies in the SDSS-III Baryon Oscillation Spectroscopic Survey: measurements of the growth of structure and expansion rate at z = 0.57 from anisotropic clustering," Mon. Not. Roy. Astron. Soc. , vol. 426, pp. 2719–2737, Nov. 2012.

[202] H. Miyatake, S. More, R. Mandelbaum, M. Takada, D. Spergel, J.-P. Kneib, D. P. Schneider, J. Brinkmann, J. R. Brownstein, *et al.*, "The weak lensing signal and clustering of sdss-iii cmass galaxies i. probing matter content," *arXiv preprint arXiv:1311.1480*, 2013.

[203] C. Heymans, L. Van Waerbeke, L. Miller, T. Erben, H. Hildebrandt, H. Hoekstra, T. D. Kitching, Y. Mellier, P. Simon, C. Bonnett, J. Coupon, L. Fu,

J. Harnois Déraps, M. J. Hudson, M. Kilbinger, K. Kuijken, B. Rowe, T. Schrabback, E. Semboloni, E. van Uitert, S. Vafaei, and M. Velander, "CFHTLenS: the Canada-France-Hawaii Telescope Lensing Survey," Mon. Not. Roy. Astron. Soc. , vol. 427, pp. 146–166, Nov. 2012.

[204] W. Hu and T. Okamoto, "Mass reconstruction with cosmic microwave background polarization," *The Astrophysical Journal*, vol. 574, no. 2, p. 566, 2002.

[205] D. Hanson, G. Rocha, and K. Górski, "Lensing reconstruction from Planck sky maps: inhomogeneous noise," Mon. Not. Roy. Astron. Soc. , vol. 400, pp. 2169–2173, Dec. 2009.

[206] T. Namikawa, D. Hanson, and R. Takahashi, "Bias-hardened CMB lensing," Mon. Not. Roy. Astron. Soc. , vol. 431, pp. 609–620, May 2013.

[207] J. F. Navarro, C. S. Frenk, and S. D. White, "A universal density profile from hierarchical clustering," *The Astrophysical Journal*, vol. 490, no. 2, p. 493, 1997.

[208] M. Bartelmann, "Arcs from a universal dark-matter halo profile.," Astron. Astrophys. , vol. 313, pp. 697–702, Sept. 1996.

[209] A. V. Macciò, A. A. Dutton, F. C. van den Bosch, B. Moore, D. Potter, and J. Stadel, "Concentration, spin and shape of dark matter haloes: scatter and the dependence on mass and environment," Mon. Not. Roy. Astron. Soc. , vol. 378, pp. 55–71, June 2007.

[210] A. Cooray, M. Kamionkowski, and R. R. Caldwell, "Cosmic shear of the microwave background: The curl diagnostic," *Physical Review D*, vol. 71, no. 12, p. 123527, 2005.

[211] B. D. Sherwin, S. Das, A. Hajian, G. Addison, J. R. Bond, D. Crichton, M. J. Devlin, J. Dunkley, M. B. Gralla, M. Halpern, *et al.*, "The atacama cosmology telescope: Cross-correlation of cosmic microwave background lensing and quasars," *Physical Review D*, vol. 86, no. 8, p. 083006, 2012.

[212] R. A. Sunyaev and Y. B. Zel'dovich, "The Spectrum of Primordial Radiation, its Distortions and their Significance," *Comments on Astrophysics and Space Physics*, vol. 2, pp. 66–+, Mar. 1970.

[213] R. A. Sunyaev and Y. B. Zel'dovich, "The Observations of Relic Radiation as a Test of the Nature of X-Ray Radiation from the Clusters of Galaxies," *Comments on Astrophysics and Space Physics*, vol. 4, pp. 173–+, Nov. 1972.

[214] N. Hand, J. W. Appel, N. Battaglia, J. R. Bond, S. Das, M. J. Devlin, J. Dunkley, R. Dünner, T. Essinger-Hileman, J. W. Fowler, A. Hajian, M. Halpern, M. Hasselfield, M. Hilton, A. D. Hincks, R. Hlozek, J. P. Hughes, K. D. Irwin, J. Klein, A. Kosowsky, Y.-T. Lin, T. A. Marriage, D. Marsden, M. McLaren, F. Menanteau, K. Moodley, M. D. Niemack, M. R. Nolta, L. A. Page, L. Parker, B. Partridge, R. Plimpton, E. D. Reese, F. Rojas, N. Sehgal, B. D. Sherwin, J. L. Sievers, D. N. Spergel, S. T. Staggs, D. S. Swetz, E. R. Switzer, R. Thornton, H. Trac, K. Visnjic, and E. Wollack, "The Atacama Cosmology Telescope:

Detection of Sunyaev-Zel'Dovich Decrement in Groups and Clusters Associated with Luminous Red Galaxies," *Astrophysical Journal*, vol. 736, p. 39, July 2011.

[215] C.-P. Ma and J. N. Fry, "Deriving the Nonlinear Cosmological Power Spectrum and Bispectrum from Analytic Dark Matter Halo Profiles and Mass Functions," *Astrophysical Journal*, vol. 543, pp. 503–513, Nov. 2000.

[216] U. Seljak, "Analytic model for galaxy and dark matter clustering," Mon. Not. Roy. Astron. Soc. , vol. 318, pp. 203–213, Oct. 2000.

[217] H. Miyatake, M. S. Madhavacheril, N. Sehgal, A. Slosar, D. N. Spergel, B. Sherwin, and A. van Engelen, "Measurement of a Cosmographic Distance Ratio with Galaxy and CMB Lensing," *ArXiv e-prints*, May 2016.

[218] W. Hu, "Dark synergy: Gravitational lensing and the CMB," Phys. Rev. **D** , vol. 65, p. 023003, Jan. 2002.

[219] L. Hollenstein, D. Sapone, R. Crittenden, and B. M. Schäfer, "Constraints on early dark energy from CMB lensing and weak lensing tomography," *JCAP*, vol. 4, p. 012, Apr. 2009.

[220] T. Namikawa, S. Saito, and A. Taruya, "Probing dark energy and neutrino mass from upcoming lensing experiments of CMB and galaxies," *JCAP*, vol. 12, p. 027, Dec. 2010.

[221] A. Vallinotto, "The Synergy between the Dark Energy Survey and the South Pole Telescope," *Astrophysical Journal*, vol. 778, p. 108, Dec. 2013.

[222] N. Hand, A. Leauthaud, S. Das, B. D. Sherwin, G. E. Addison, J. R. Bond, E. Calabrese, A. Charbonnier, M. J. Devlin, J. Dunkley, T. Erben, A. Hajian, M. Halpern, J. Harnois-Déraps, C. Heymans, H. Hildebrandt, A. D. Hincks, J.-P. Kneib, A. Kosowsky, M. Makler, L. Miller, K. Moodley, B. Moraes, M. D. Niemack, L. A. Page, B. Partridge, N. Sehgal, H. Shan, J. L. Sievers, D. N. Spergel, S. T. Staggs, E. R. Switzer, J. E. Taylor, L. Van Waerbeke, C. Welker, and E. J. Wollack, "First measurement of the cross-correlation of CMB lensing and galaxy lensing," Phys. Rev. **D** , vol. 91, p. 062001, Mar. 2015.

[223] J. Liu and J. C. Hill, "Cross-correlation of Planck CMB lensing and CFHTLenS galaxy weak lensing maps," Phys. Rev. **D** , vol. 92, p. 063517, Sept. 2015.

[224] Y. Omori and G. Holder, "Cross-Correlation of CFHTLenS Galaxy Number Density and Planck CMB Lensing," *ArXiv e-prints*, Feb. 2015.

[225] T. Giannantonio, P. Fosalba, R. Cawthon, Y. Omori, M. Crocce, F. Elsner, B. Leistedt, S. Dodelson, A. Benoit-Lévy, E. Gaztañaga, G. Holder, H. V. Peiris, W. J. Percival, D. Kirk, A. H. Bauer, B. A. Benson, G. M. Bernstein, J. Carretero, T. M. Crawford, R. Crittenden, D. Huterer, B. Jain, E. Krause, C. L. Reichardt, A. J. Ross, G. Simard, B. Soergel, A. Stark, K. T. Story, J. D. Vieira, J. Weller, T. Abbott, F. B. Abdalla, S. Allam, R. Armstrong, M. Banerji, R. A. Bernstein, E. Bertin, D. Brooks, E. Buckley-Geer, D. L. Burke, D. Capozzi, J. E. Carlstrom, A. Carnero Rosell, M. Carrasco Kind, F. J. Castander, C. L. Chang, C. E. Cunha, L. N. da Costa, C. B. D'Andrea, D. L. DePoy, S. Desai, H. T. Diehl, J. P. Dietrich, P. Doel, T. F. Eifler, A. E. Evrard,

A. F. Neto, E. Fernandez, D. A. Finley, B. Flaugher, J. Frieman, D. Gerdes, D. Gruen, R. A. Gruendl, G. Gutierrez, W. L. Holzapfel, K. Honscheid, D. J. James, K. Kuehn, N. Kuropatkin, O. Lahav, T. S. Li, M. Lima, M. March, J. L. Marshall, P. Martini, P. Melchior, R. Miquel, J. J. Mohr, R. C. Nichol, B. Nord, R. Ogando, A. A. Plazas, A. K. Romer, A. Roodman, E. S. Rykoff, M. Sako, B. R. Saliwanchik, E. Sanchez, M. Schubnell, I. Sevilla-Noarbe, R. C. Smith, M. Soares-Santos, F. Sobreira, E. Suchyta, M. E. C. Swanson, G. Tarle, J. Thaler, D. Thomas, V. Vikram, A. R. Walker, R. H. Wechsler, and J. Zuntz, "CMB lensing tomography with the DES Science Verification galaxies," Mon. Not. Roy. Astron. Soc. , vol. 456, pp. 3213–3244, Mar. 2016.

[226] A. R. Pullen, S. Alam, S. He, and S. Ho, "Constraining Gravity at the Largest Scales through CMB Lensing and Galaxy Velocities," *ArXiv e-prints*, Nov. 2015.

[227] D. Kirk, Y. Omori, A. Benoit-Lévy, R. Cawthon, C. Chang, P. Larsen, A. Amara, D. Bacon, T. M. Crawford, S. Dodelson, P. Fosalba, T. Giannantonio, G. Holder, B. Jain, T. Kacprzak, O. Lahav, N. MacCrann, A. Nicola, A. Refregier, E. Sheldon, K. T. Story, M. A. Troxel, J. D. Vieira, V. Vikram, J. Zuntz, T. M. C. Abbott, F. B. Abdalla, M. R. Becker, B. A. Benson, G. M. Bernstein, R. A. Bernstein, L. E. Bleem, C. Bonnett, S. L. Bridle, D. Brooks, E. Buckley-Geer, D. L. Burke, D. Capozzi, J. E. Carlstrom, A. C. Rosell, M. C. Kind, J. Carretero, M. Crocce, C. E. Cunha, C. B. D'Andrea, L. N. da Costa, S. Desai, H. T. Diehl, J. P. Dietrich, P. Doel, T. F. Eifler, A. E. Evrard, B. Flaugher, J. Frieman, D. W. Gerdes, D. A. Goldstein, D. Gruen,

R. A. Gruendl, K. Honscheid, D. J. James, M. Jarvis, S. Kent, K. Kuehn, N. Kuropatkin, M. Lima, M. March, P. Martini, P. Melchior, C. J. Miller, R. Miquel, R. C. Nichol, R. Ogando, A. A. Plazas, C. L. Reichardt, A. Roodman, E. Rozo, E. S. Rykoff, M. Sako, E. Sanchez, V. Scarpine, M. Schubnell, I. Sevilla-Noarbe, G. Simard, R. C. Smith, M. Soares-Santos, F. Sobreira, E. Suchyta, M. E. C. Swanson, G. Tarle, D. Thomas, R. H. Wechsler, and J. Weller, "Cross-correlation of gravitational lensing from DES Science Verification data with SPT and Planck lensing," Mon. Not. Roy. Astron. Soc. , vol. 459, pp. 21–34, June 2016.

[228] A. N. Taylor, T. D. Kitching, D. J. Bacon, and A. F. Heavens, "Probing dark energy with the shear-ratio geometric test," Mon. Not. Roy. Astron. Soc. , vol. 374, pp. 1377–1403, Feb. 2007.

[229] T. D. Kitching, A. N. Taylor, and A. F. Heavens, "Systematic effects on dark energy from 3D weak shear," Mon. Not. Roy. Astron. Soc. , vol. 389, pp. 173–190, Sept. 2008.

[230] T. E. Collett, M. W. Auger, V. Belokurov, P. J. Marshall, and A. C. Hall, "Constraining the dark energy equation of state with double-source plane strong lenses," Mon. Not. Roy. Astron. Soc. , vol. 424, pp. 2864–2875, Aug. 2012.

[231] E. V. Linder, "Doubling Strong Lensing as a Cosmological Probe," *ArXiv e-prints*, May 2016.

[232] T. D. Kitching, A. F. Heavens, A. N. Taylor, M. L. Brown, K. Meisenheimer, C. Wolf, M. E. Gray, and D. J. Bacon, "Cosmological constraints from

COMBO-17 using 3D weak lensing," Mon. Not. Roy. Astron. Soc. , vol. 376, pp. 771–778, Apr. 2007.

[233] E. Medezinski, T. Broadhurst, K. Umetsu, N. Benítez, and A. Taylor, "A weak lensing detection of the cosmological distance-redshift relation behind three massive clusters," Mon. Not. Roy. Astron. Soc. , vol. 414, pp. 1840–1850, July 2011.

[234] J. E. Taylor, R. J. Massey, A. Leauthaud, M. R. George, J. Rhodes, T. D. Kitching, P. Capak, R. Ellis, A. Finoguenov, O. Ilbert, E. Jullo, J.-P. Kneib, A. M. Koekemoer, N. Scoville, and M. Tanaka, "Measuring the Geometry of the Universe from Weak Gravitational Lensing behind Galaxy Groups in the HST COSMOS Survey," *Astrophysical Journal*, vol. 749, p. 127, Apr. 2012.

[235] T. D. Kitching, M. Viola, H. Hildebrandt, A. Choi, T. Erben, D. G. Gilbank, C. Heymans, L. Miller, R. Nakajima, and E. van Uitert, "RCSLenS: Cosmic Distances from Weak Lensing," *ArXiv e-prints*, Dec. 2015.

[236] T. E. Collett and M. W. Auger, "Cosmological constraints from the double source plane lens SDSSJ0946+1006," Mon. Not. Roy. Astron. Soc. , vol. 443, pp. 969–976, Sept. 2014.

[237] M. White, M. Blanton, A. Bolton, D. Schlegel, J. Tinker, A. Berlind, L. da Costa, E. Kazin, Y.-T. Lin, M. Maia, C. K. McBride, N. Padmanabhan, J. Parejko, W. Percival, F. Prada, B. Ramos, E. Sheldon, F. de Simoni, R. Skibba, D. Thomas, D. Wake, I. Zehavi, Z. Zheng, R. Nichol, D. P. Schneider, M. A. Strauss, B. A. Weaver, and D. H. Weinberg, "The Clustering of

Massive Galaxies at z ˜ 0.5 from the First Semester of BOSS Data," *Astrophysical Journal*, vol. 728, p. 126, Feb. 2011.

[238] H. Miyatake, S. More, R. Mandelbaum, M. Takada, D. N. Spergel, J.-P. Kneib, D. P. Schneider, J. Brinkmann, and J. R. Brownstein, "The Weak Lensing Signal and the Clustering of BOSS Galaxies. I. Measurements," *Astrophysical Journal*, vol. 806, p. 1, June 2015.

[239] A. J. Ross, W. J. Percival, A. G. Sánchez, L. Samushia, S. Ho, E. Kazin, M. Manera, B. Reid, M. White, R. Tojeiro, C. K. McBride, X. Xu, D. A. Wake, M. A. Strauss, F. Montesano, M. E. C. Swanson, S. Bailey, A. S. Bolton, A. M. Dorta, D. J. Eisenstein, H. Guo, J.-C. Hamilton, R. C. Nichol, N. Padmanabhan, F. Prada, D. J. Schlegel, M. V. Magaña, I. Zehavi, M. Blanton, D. Bizyaev, H. Brewington, A. J. Cuesta, E. Malanushenko, V. Malanushenko, D. Oravetz, J. Parejko, K. Pan, D. P. Schneider, A. Shelden, A. Simmons, S. Snedden, and G.-b. Zhao, "The clustering of galaxies in the SDSS-III Baryon Oscillation Spectroscopic Survey: analysis of potential systematics," Mon. Not. Roy. Astron. Soc. , vol. 424, pp. 564–590, July 2012.

[240] C. Heymans, L. Van Waerbeke, L. Miller, T. Erben, H. Hildebrandt, H. Hoekstra, T. D. Kitching, Y. Mellier, P. Simon, C. Bonnett, J. Coupon, L. Fu, J. Harnois Déraps, M. J. Hudson, M. Kilbinger, K. Kuijken, B. Rowe, T. Schrabback, E. Semboloni, E. van Uitert, S. Vafaei, and M. Velander, "CFHTLenS: the Canada-France-Hawaii Telescope Lensing Survey," Mon. Not. Roy. Astron. Soc. , vol. 427, pp. 146–166, Nov. 2012.

[241] T. Erben, H. Hildebrandt, L. Miller, L. van Waerbeke, C. Heymans, H. Hoekstra, T. D. Kitching, Y. Mellier, J. Benjamin, C. Blake, C. Bonnett, O. Cordes, J. Coupon, L. Fu, R. Gavazzi, B. Gillis, E. Grocutt, S. D. J. Gwyn, K. Holhjem, M. J. Hudson, M. Kilbinger, K. Kuijken, M. Milkeraitis, B. T. P. Rowe, T. Schrabback, E. Semboloni, P. Simon, M. Smit, O. Toader, S. Vafaei, E. van Uitert, and M. Velander, "CFHTLenS: the Canada-France-Hawaii Telescope Lensing Survey - imaging data and catalogue products," Mon. Not. Roy. Astron. Soc. , vol. 433, pp. 2545–2563, Aug. 2013.

[242] L. Miller, C. Heymans, T. D. Kitching, L. van Waerbeke, T. Erben, H. Hildebrandt, H. Hoekstra, Y. Mellier, B. T. P. Rowe, J. Coupon, J. P. Dietrich, L. Fu, J. Harnois-Déraps, M. J. Hudson, M. Kilbinger, K. Kuijken, T. Schrabback, E. Semboloni, S. Vafaei, and M. Velander, "Bayesian galaxy shape measurement for weak lensing surveys - III. Application to the Canada-France-Hawaii Telescope Lensing Survey," Mon. Not. Roy. Astron. Soc. , vol. 429, pp. 2858–2880, Mar. 2013.

[243] N. Benítez, "Bayesian Photometric Redshift Estimation," *Astrophysical Journal*, vol. 536, pp. 571–583, June 2000.

[244] D. Coe, N. Benítez, S. F. Sánchez, M. Jee, R. Bouwens, and H. Ford, "Galaxies in the Hubble Ultra Deep Field. I. Detection, Multiband Photometry, Photometric Redshifts, and Morphology," *AJ* , vol. 132, pp. 926–959, Aug. 2006.

[245] H. Hildebrandt, T. Erben, K. Kuijken, L. van Waerbeke, C. Heymans, J. Coupon, J. Benjamin, C. Bonnett, L. Fu, H. Hoekstra, T. D. Kitching,

Y. Mellier, L. Miller, M. Velander, M. J. Hudson, B. T. P. Rowe, T. Schrabback, E. Semboloni, and N. Benítez, "CFHTLenS: improving the quality of photometric redshifts with precision photometry," Mon. Not. Roy. Astron. Soc. , vol. 421, pp. 2355–2367, Apr. 2012.

[246] M. Manera, R. Scoccimarro, W. J. Percival, L. Samushia, C. K. McBride, A. J. Ross, R. K. Sheth, M. White, B. A. Reid, A. G. Sánchez, R. de Putter, X. Xu, A. A. Berlind, J. Brinkmann, C. Maraston, B. Nichol, F. Montesano, N. Padmanabhan, R. A. Skibba, R. Tojeiro, and B. A. Weaver, "The clustering of galaxies in the SDSS-III Baryon Oscillation Spectroscopic Survey: a large sample of mock galaxy catalogues," Mon. Not. Roy. Astron. Soc. , vol. 428, pp. 1036–1054, Jan. 2013.

[247] M. Manera, L. Samushia, R. Tojeiro, C. Howlett, A. J. Ross, W. J. Percival, H. Gil-Marín, J. R. Brownstein, A. Burden, and F. Montesano, "The clustering of galaxies in the SDSS-III Baryon Oscillation Spectroscopic Survey: mock galaxy catalogues for the low-redshift sample," Mon. Not. Roy. Astron. Soc. , vol. 447, pp. 437–445, Feb. 2015.

[248] R. Mandelbaum, C. M. Hirata, U. Seljak, J. Guzik, N. Padmanabhan, C. Blake, M. R. Blanton, R. Lupton, and J. Brinkmann, "Systematic errors in weak lensing: application to SDSS galaxy-galaxy weak lensing," Mon. Not. Roy. Astron. Soc. , vol. 361, pp. 1287–1322, Aug. 2005.

[249] K. M. Górski, E. Hivon, A. J. Banday, B. D. Wandelt, F. K. Hansen, M. Reinecke, and M. Bartelmann, "HEALPix: A Framework for High-Resolution

Discretization and Fast Analysis of Data Distributed on the Sphere," *Astrophysical Journal*, vol. 622, pp. 759–771, Apr. 2005.

[250] Planck Collaboration, P. A. R. Ade, N. Aghanim, M. Arnaud, M. Ashdown, J. Aumont, C. Baccigalupi, A. J. Banday, R. B. Barreiro, J. G. Bartlett, and et al., "Planck 2015 results. XV. Gravitational lensing," *ArXiv e-prints*, Feb. 2015.

[251] A. Challinor and A. Lewis, "Linear power spectrum of observed source number counts," Phys. Rev. **D** , vol. 84, p. 043516, Aug. 2011.

[252] R. E. Smith, J. A. Peacock, A. Jenkins, S. D. M. White, C. S. Frenk, F. R. Pearce, P. A. Thomas, G. Efstathiou, and H. M. P. Couchman, "Stable clustering, the halo model and non-linear cosmological power spectra," Mon. Not. Roy. Astron. Soc. , vol. 341, pp. 1311–1332, June 2003.

[253] R. Takahashi, M. Sato, T. Nishimichi, A. Taruya, and M. Oguri, "Revising the Halofit Model for the Nonlinear Matter Power Spectrum," *Astrophysical Journal*, vol. 761, p. 152, Dec. 2012.

[254] G. Covone, M. Sereno, M. Kilbinger, and V. F. Cardone, "Measurement of the Halo Bias from Stacked Shear Profiles of Galaxy Clusters," Astrophys. J. Let. , vol. 784, p. L25, Apr. 2014.

[255] Planck Collaboration, P. A. R. Ade, N. Aghanim, M. Arnaud, M. Ashdown, J. Aumont, C. Baccigalupi, A. J. Banday, R. B. Barreiro, J. G. Bartlett, and

et al., "Planck 2015 results. XIII. Cosmological parameters," *ArXiv e-prints*, Feb. 2015.

[256] S. W. Henderson, R. Allison, J. Austermann, T. Baildon, N. Battaglia, J. A. Beall, D. Becker, F. De Bernardis, J. R. Bond, E. Calabrese, S. K. Choi, K. P. Coughlin, K. T. Crowley, R. Datta, M. J. Devlin, S. M. Duff, J. Dunkley, R. Dünner, A. van Engelen, P. A. Gallardo, E. Grace, M. Hasselfield, F. Hills, G. C. Hilton, A. D. Hincks, R. Hlozêk, S. P. Ho, J. Hubmayr, K. Huffenberger, J. P. Hughes, K. D. Irwin, B. J. Koopman, A. B. Kosowsky, D. Li, J. McMahon, C. Munson, F. Nati, L. Newburgh, M. D. Niemack, P. Niraula, L. A. Page, C. G. Pappas, M. Salatino, A. Schillaci, B. L. Schmitt, N. Sehgal, B. D. Sherwin, J. L. Sievers, S. M. Simon, D. N. Spergel, S. T. Staggs, J. R. Stevens, R. Thornton, J. Van Lanen, E. M. Vavagiakis, J. T. Ward, and E. J. Wollack, "Advanced ACTPol Cryogenic Detector Arrays and Readout," *Journal of Low Temperature Physics*, Mar. 2016.

[257] Planck Collaboration, P. A. R. Ade, N. Aghanim, M. Arnaud, M. Ashdown, J. Aumont, C. Baccigalupi, A. J. Banday, R. B. Barreiro, J. G. Bartlett, and et al., "Planck 2015 results. XIII. Cosmological parameters," *ArXiv e-prints*, Feb. 2015.

[258] R. Mandelbaum, B. Rowe, R. Armstrong, D. Bard, E. Bertin, J. Bosch, D. Boutigny, F. Courbin, W. A. Dawson, A. Donnarumma, I. Fenech Conti, R. Gavazzi, M. Gentile, M. S. S. Gill, D. W. Hogg, E. M. Huff, M. J. Jee, T. Kacprzak, M. Kilbinger, T. Kuntzer, D. Lang, W. Luo, M. C. March, P. J.

Marshall, J. E. Meyers, L. Miller, H. Miyatake, R. Nakajima, F. M. Ngolé Mboula, G. Nurbaeva, Y. Okura, S. Paulin-Henriksson, J. Rhodes, M. D. Schneider, H. Shan, E. S. Sheldon, M. Simet, J.-L. Starck, F. Sureau, M. Tewes, K. Zarb Adami, J. Zhang, and J. Zuntz, "GREAT3 results - I. Systematic errors in shear estimation and the impact of real galaxy morphology," Mon. Not. Roy. Astron. Soc. , vol. 450, pp. 2963–3007, July 2015.

[259] B. A. Benson, P. A. R. Ade, Z. Ahmed, S. W. Allen, K. Arnold, J. E. Austermann, A. N. Bender, L. E. Bleem, J. E. Carlstrom, C. L. Chang, H. M. Cho, J. F. Cliche, T. M. Crawford, A. Cukierman, T. de Haan, M. A. Dobbs, D. Dutcher, W. Everett, A. Gilbert, N. W. Halverson, D. Hanson, N. L. Harrington, K. Hattori, J. W. Henning, G. C. Hilton, G. P. Holder, W. L. Holzapfel, K. D. Irwin, R. Keisler, L. Knox, D. Kubik, C. L. Kuo, A. T. Lee, E. M. Leitch, D. Li, M. McDonald, S. S. Meyer, J. Montgomery, M. Myers, T. Natoli, H. Nguyen, V. Novosad, S. Padin, Z. Pan, J. Pearson, C. Reichardt, J. E. Ruhl, B. R. Saliwanchik, G. Simard, G. Smecher, J. T. Sayre, E. Shirokoff, A. A. Stark, K. Story, A. Suzuki, K. L. Thompson, C. Tucker, K. Vanderlinde, J. D. Vieira, A. Vikhlinin, G. Wang, V. Yefremenko, and K. W. Yoon, "SPT-3G: a next-generation cosmic microwave background polarization experiment on the South Pole telescope," in *Millimeter, Submillimeter, and Far-Infrared Detectors and Instrumentation for Astronomy VII*, vol. 9153 of *SPIE Proceedings*, p. 91531P, July 2014.

[260] M. Levi, C. Bebek, T. Beers, R. Blum, R. Cahn, D. Eisenstein, B. Flaugher, K. Honscheid, R. Kron, O. Lahav, P. McDonald, N. Roe, D. Schlegel, and

representing the DESI collaboration, "The DESI Experiment, a whitepaper for Snowmass 2013," *ArXiv e-prints*, Aug. 2013.

[261] B. P. Abbott, R. Abbott, T. D. Abbott, M. R. Abernathy, F. Acernese, K. Ackley, C. Adams, T. Adams, P. Addesso, R. X. Adhikari, and et al., "Observation of Gravitational Waves from a Binary Black Hole Merger," *Physical Review Letters*, vol. 116, p. 061102, Feb. 2016.